Pneumatic Tire Performance On Ice

Anudeep Kishore Bhoopalam

Dissertation submitted to the Faculty of the
Virginia Polytechnic Institute and State University
in partial fulfillment of the requirements for the degree of

Doctor of Philosophy
in
Mechanical Engineering

Corina Sandu, Chair
Saied Taheri, Co-Chair
Tomonari Furukawa
Mehdi Ahmadian
Jan Terziyski

July 29, 2015
Blacksburg, Virginia

Keywords: Tire-Ice Friction, Indoor Testing, Outdoor Testing, Tire-Ice Model

Pneumatic Tire Performance On Ice

Anudeep Kishore Bhoopalam

ABSTRACT

The evolution of vehicle safety systems, from the earliest brakes to today's accident avoidance systems, has led vehicles to have very high passenger safety. Driving on ice, though, still happens to be one of the driving conditions of low safety. A multitude of factors were identified by various studies to contribute to the complex frictional mechanism at the tire−ice interface. The tire is only force transmitting element of the vehicle, to the surface. Thus it is very essential to have in depth understanding of the contact phenomena at the tire−ice interface, to improve vehicle safety on icy roads.

This study has led to understanding of the contact phenomena at the tire−ice contact through experimental studies and a semi-empirical based tire−ice contact model. Experimental studies included both indoor testing and outdoor testing, indoor testing was conducted using the Terramechanics Rig at the Advanced Vehicle Dynamics in Virginia Tech and field tests were conducted at the Keweenaw Research Center in Michigan Tech. The simulation results of the tire-ice model were validated against the findings of the indoor test program.

The P225/60R16 97S Standard Reference Test Tire was the candidate tire for this study. The effects of operational parameters, were studied when in driving traction by comparison of the friction− slip ratio curves. The two tests procedures were performed to understand how each test method influences the test results. A comparison of the laboratory and field test method are also presented, with reasons for the differences in the measured values presented.

The experimental study also led to development of a modular structured tire−ice model(TIM). The model computes the temperature rise in the contact patch based on the pressure distribution in the contact patch, thermal properties of the tread compound and of the ice surface. The contact patch is then classified into wet and dry regions based on the ice surface temperature and temperature rise simulations. The principle of thermal balance is then applied to compute the friction level in the contact patch. The tire-ice contact model is validated for two parameters: temperature rise and friction levels. Temperature rise from simulations are validated against temperature measurements at the leading and trailing edge of the contact patch. Friction levels at different conditions of load, inflation pressure, and ice temperatures have been simulated using the tire-ice contact model and compared to the experimental findings.

This study has been partially supported by the Center for Tire Research (CenTiRe), an NSF-I/UCRC at Virginia Tech, and by the Advanced Vehicle Dynamics Laboratory (AVDL).

Dedication

To the Lotus Feet of the Omnipresent Sri Sathya Sai for always holding my hand.

To my beloved Family for all their love, affection, support, advice and prayers.

Acknowledgments

First and foremost my sincerest and deepest gratitude to my advisor Prof. Corina Sandu. I acknowledge all her guidance and the efforts she has taken in molding me. I feel blessed and honored to have gotten the opportunity to work under her guidance. I am also grateful to my co-advisor Prof. Saied Taheri. I am extremely thankful and indebted to him for sharing his expertise, and sincere and valuable guidance and encouragement extended to me, and for bringing me to Virginia Tech .

I take this opportunity to thank all my committee members for serving on my dissertation committee, Prof .Mehdi Ahmadian for all his help and support during the ice testing at CVeSS; Prof. Tomonari Furukawa for all the interactions and his valuable advice. A special thanks to Dr. Jan Terziyski for serving on my committee and also serving as mentor for the project through the Center for Tire Research. I would like to express my thanks to Dr. Terziyski for all his advise and mentoring me all through my doctoral study at Virginia Tech.

Sincerest thanks to the NSF- I/UCRC Centire for Tire Research for supporting this work. I thank all the project mentors and members of the Industrial Advisory Board of the Center for Tire Research for all their valuable feedback and suggestions during the three years. A special thanks to Mr. Peter Lee from Goodyear for all his insights during the course of my study.

To all my colleagues at the Advanced Vehicle Dynamics Laboratory and the Center for Tire Research; Scott Naranjo for teaching me how to use the Terramechnaics Rig; Elizabeth Armstrong, Jeremy Kolansky, Yitao Zhu and Emilio Jimenez for the insightful conversations and help. Yashwanth Siramdasu, Shahyar Taheri, Mehran Motamedi and Karan Khanse from the Center for Tire Research for their company and for all the discussions. Undergraduate students Dan Mead, Yuta Yoshimura and Tyler Dick for all their help during the ice testing on the Terramechanics Rig. I could not have asked a for better team to work with.

Thanks to Mr.Paul Schultz from Mobilty Research Inc. for conducting the outdoor test program at the Kewennaw Research Center. I would also like to thank Hankook Tires Ltd. for providing the pressure maps for development of my tire−ice model. A special thanks to Prof. Brian Lattimer and Dr. Patrick Summers for allowing me to borrow and teaching me how to use their thermal camera; Dr. Tim Rhyne from Michelin for the interactions and

his advice.

At this juncture, I would like thank Prof. Thomas Kurfess and for all his advice and guidance during my time at Clemson and even now. Prof. Harry Law for the inspiring Vehicle Dynamics class at Clemson which made me passionate to do more in the field.

Most important my parents, Anitha Kishore and Dr. B.N. Kishore Kumar for their love, affection, care and support all through which made this possible. Their parenting and guidance has taught me lot. I promise, I will always live up to the values they taught me. I don't think a lifetime is enough to thank them. I humbly bow down and offering salutations at their feet. My grandparents Aswathamma and D. Ramanjeyulu for their love, care and the amazing values they taught me, my salutations at their feet. Thanks to my brother Anirudh Bhoopalam for all the fun we had over the years and more to follow in the coming years. I remember the beautiful and wonderful interactions we always have; thank you for all the love and support.

I would like to express my sincerest gratitude to Nikhita for agreeing to share her life with me. In May of 2015 we became husband and wife. I feel blessed and honored that I have a person with lots of compassion and love to share my life with. I still remember the day when we first met, you were so kind and down to earth. Everyday I thank God for giving me a woman like you. I promise to keep you and the future junior(s) always happy and smiling. To my in−laws Nalini and Venkatesh Kothamachu for believing that I would be a good son in−law and that I will always keep Nikhita happy, my salutations at their feet.

To the omnipresent almighty and my spiritual guru Bhagawan Sri Sathya Sai Baba for making me get here and always holding my hand. Swami, You executed this and it is all Yours. I know You will always take care of everyone. Please give me the strength to always remember You and, eventually to say my life is Your message.

Contents

1 Introduction **1**

1.1 Motivation 1

1.2 Research Objectives 2

1.3 Research Approach 3

1.4 Main Contributions of this Research 4

1.5 Outline of the Dissertation 5

2 Literature Review **7**

2.1 Overview of Tire-Ice Interaction 8

2.2 Factors Contributing to Tire-Ice Friction 9

2.3 Ambient and Ice Conditions 9

2.3.1 Ambient Temperature 9

2.3.2 Effect of Ice Crystal Size 10

2.3.3 Effect of Ice Texture 11

2.3.4 Effect of Impurities in Ice 11

2.3.5 Effect of Ice Surface Temperature 13

2.3.6 Effect of Age of Ice Track 14

2.3.7 Ice Topography 15

2.3.8 Discussion on ice properties affecting tire performance 16

2.4 Tire Specifications 18

2.4.1 Effect of Tread Pattern 18

2.4.2 Effect of Tread Compound . . . 19
2.4.3 Effect of Tire Normal Pressure . . . 20
2.4.4 Effect of tire type- All-Season, Summer, and Winter Tires . . . 21
2.5 Vehicle Specifications . . . 24
2.5.1 Effect of Braking System ABS ON/OFF . . . 24
2.5.2 Effect of Vehicle Type Passenger Car and Truck . . . 25
2.5.3 All Winter Tires versus Two Winter Tires on the Front Axle . . . 25
2.5.4 Driving on Ice with AWD versus RWD . . . 26
2.5.5 Electric Vehicles on Winter Surfaces . . . 26
2.5.6 Discussion on the Influence of the Vehicle on the Friction Coefficient at Tire−Ice Interface . . . 27
2.6 Testing Tires on Ice . . . 28
2.6.1 Indoor Testing . . . 29
2.6.2 Field Testing . . . 34
2.6.3 Comparison of Indoor and Outdoor tests . . . 38
2.7 Tire-Ice Models . . . 39
2.7.1 Relation between Friction Coefficient and Stopping Distance . . . 39
2.7.2 Relation based on Temperature and Winter Aggregate . . . 40
2.7.3 Tire−Ice model by Hayhoe . . . 41
2.7.4 Tire−Ice model by Peng . . . 42
2.7.5 Discussion on Tire−Ice Models . . . 46
2.8 Summary and Conclusions . . . 46

3 Test Facility and Equipment 51

3.1 Indoor Test Setup . . . 51
3.1.1 Terramechanics Rig . . . 52
3.1.2 Ice Making System . . . 54
3.1.3 Thermotron Chamber . . . 56
3.1.4 Tire Enclosure for Temperature Control . . . 56

3.1.5 Tekscan Pressure Mapping System . . . 58
3.1.6 Ice Resurfacing Tools . . . 59
3.1.7 American Slip Meter . . . 59
3.2 Outdoor Test Facility . . . 61
3.2.1 Test Track at Keweenaw Research Center . . . 61
3.2.2 Traction Truck - Mobility Research Inc. . . . 62
3.3 Summary . . . 62

4 Design of Experiment 63
4.1 P225 60/R16 97S Standard Reference Test Tire . . . 63
4.1.1 Terminology . . . 64
4.2 Indoor Test Program . . . 65
4.3 Outdoor Test Program . . . 65

5 Indoor Test Program 67
5.1 AVDL Test Method . . . 67
5.1.1 Terminology . . . 68
5.1.2 Ice Preparation Procedure . . . 68
5.1.3 Initial Test Procedures . . . 69
5.1.4 Test Procedure . . . 70
5.2 Test Results . . . 73
5.2.1 Observations . . . 73
5.2.2 Repeatability of Test Results . . . 75
5.2.3 Effect of Normal Load . . . 78
5.2.4 Effect of Inflation Pressure . . . 79
5.2.5 Effect of Tread Depth . . . 81
5.2.6 Effect of Toe Angle . . . 83
5.2.7 Effect of Camber Angle . . . 85
5.2.8 Effect of Ambient Temperature . . . 87

5.2.9 Effect of Ice Surface Temperature . . . 88
5.2.10 Effect of Aggregate Application on Ice Surface . . . 89
5.3 Summary and Conclusions . . . 90

6 Outdoor Test Program 92
6.1 Test Conditions . . . 93
6.1.1 Terminology . . . 93
6.2 ASTM−1805 . . . 93
6.3 Test Results . . . 95
6.3.1 Repeatabilty of Test Results . . . 95
6.3.2 Effect of Normal Load . . . 95
6.3.3 Effect of Inflation Pressure . . . 97
6.3.4 Effect of Tread Depth . . . 98
6.4 Summary and Conclusions . . . 100

7 Comparison of Indoor and Outdoor Test Programs 101
7.1 Effect of Normal Load . . . 101
7.2 Effect of Inflation Pressure . . . 103
7.3 Reasons for Differences in Friction Measurement − Indoor versus Outdoor Test Methods . . . 105
7.3.1 Ice Resurfacing Procedure . . . 106
7.3.2 Slip Ratio Control . . . 106
7.3.3 Tread Hardness versus Temperature . . . 107
7.3.4 Normal Load Time Histories . . . 108
7.4 Summary and Conclusions . . . 109

8 Simulating Truck Performance on Ice using Experimental Data 110
8.1 TruckSIM® Model . . . 111
8.2 Vehicle Description . . . 112
8.3 Simulation Results . . . 113

8.3.1 Braking Events . . . 113
8.3.2 Acceleration Events . . . 116
8.4 Summary and Conclusions . . . 118

9 Tire-Ice Model (TIM) 121
9.1 Structure of Tire−Ice Model . . . 122
9.2 Module 1: Experimental Pressure Distribution in the Contact Patch . . . 124
9.3 Module 2: Temperature Rise in the Tire Contact . . . 125
9.3.1 Constitutive Model . . . 125
9.3.2 Temperature Rise Simulations . . . 129
9.4 Module 2: Contact Patch Classification . . . 131
9.5 Module 3: Thermal Balance in the Contact Patch . . . 132
9.6 Summary . . . 134

10 Validation TIM: Experimental versus Simulation 138
10.1 Comparison of Temperature Rise . . . 138
10.1.1 Experimental Setup . . . 139
10.1.2 Temperature Rise on Ice . . . 139
10.1.3 Applicability and Limitations of the Temperature Rise Model . . . 142
10.2 Validation of the Tire-Ice Model (TIM) . . . 143
10.2.1 Friction from Experimental Studies . . . 143
10.2.2 Friction from Simulation and Experimental Studies . . . 144
10.3 Summary and Conclusions . . . 145

11 Conclusions and Future Research Directions 148
11.1 Summary of Research Outcomes . . . 148
11.2 Main Contributions of this Research . . . 151
11.2.1 Journals . . . 152
11.2.2 Peer Reviewed Conference Papers . . . 153
11.2.3 Oral Presentations . . . 153

11.2.4 Poster Presentations 154
11.3 Future Research Directions 155

A Terramechanics Rig Operation Checklist for Safety **156**

B Ice Rink Operation Manual **160**
B.1 Terramechanics Rig Preparation 160
B.2 Ice Chiller Preparation 161
B.3 Melting the Ice 164

C Tire-Ice Model Documentation **166**
C.1 Inputs to the tire−ice model 166
C.2 Procedure to predict friction at tire−ice interface 167
C.3 Outputs from tire−ice model 167

Bibliography **168**

List of Figures

1.1 Probability of accident with variation in friction coefficient of the road surface. Adapted from Topp et al. [1] under fair use; Fair use determination attached. 2

2.1 For tractive performance on ice, effect of ambient temperature on maximum force coefficient (same as maximum friction coefficient), after [2]. The authors in [2] define μ_y as the ratio of the lateral to vertical force; and μ_x as the ratio of the longitudinal to vertical force. The authors in [2] mention tire B refers to a winter tire with winter pattern tread block with four sipes, the description of tire C is not mentioned. Adapted from [2] under fair use; Fair use determination attached. 10

2.2 Friction coefficient (μ) as functions of slip ratios (S) at different temperatures (room temperature of test rig) for tires on ice with different texture, after [3]. Ice (a) refers to clear ice with pillar shaped crystals, ice (b) refers to clear ice with very large pillar shaped crystals, and ice (c) refers to cloudy ice with granular structures. Adapted from [3] under fair use; Fair use determination attached. 11

2.3 Effect of ice texture at different temperatures (room temperature of test rig) on cornering characteristics of different tires, after [3]. The ice legend in the fourth graph applies to all four graphs. Ice (b) is clear ice with very large pillar shaped crystals and ice (c) is cloudy ice with granular structures. (Chocolate block refers to tread pattern of the tire. Sipes are the cuts and groves located on the tread to provide increased traction levels. The tread pattern of the studless tire used to evaluate the cornering characteristics are not mentioned in [3].) Adapted from [3] under fair use; Fair use determination attached. . . 12

2.4 Effect of ice temperature and sliding speed on friction coefficient, after [4]. − refers to coefficient of friction computed on wet glass,−− refers to coefficient of friction computed on ice and− · − refers to friction coefficient computed on dry glass. This effect was studied by Roberts [4] using a Rubber Lens which is hemispherical transparent rubber sample, the contact was studied using low power microscopy. Waves refer to observance of Schallamach waves [5], a peeling separation between the ice surface and rubber sample at very low temperatures. At temperatures close to 0 °C, no waves (no peeling separation) were observed. Wear refers to detachment of rubber particles and observance of debris on the ice surface. Adapted from [4] under fair use; Fair use determination attached. 14

2.5 Effect of initial track temperature on force coefficient (same as friction coefficient), after [2]. (The authors in [2] define μ_x as the ratio of longitudinal to vertical force.) An assumption, that no force can be transmitted on a water film in [2] results in a zero force coefficient (μ_x) at 0 °C. Adapted from [2] under fair use; Fair use determination attached. 15

2.6 Effect of age of ice track on friction coefficient, after [4]. This effect was studied by Roberts [4] using a Rubber Lens which is hemispherical transparent rubber sample, the contact was studied using low power microscopy. Waves refer to observance of Schallamach waves [5], a peeling separation between the ice surface and rubber sample at very low temperatures. At temperatures close to 0 °C, no waves (no peeling separation) were observed. Adapted from [4] under fair use; Fair use determination attached. 16

2.7 Effect of surface type on friction coefficient, which is the vertical axis [6]. Tractive surfaces here are described in Table 2.2. (Coefficients for various winter surfaces; data points represent coefficient values obtained from testing and lines indicate average coefficient values.) Copyright © 1993 SAE International. Reprinted with permission from SAE paper 930896; license agreement attached. 17

2.8 Tread pattern of tires used to study effect on braking and lateral friction on ice [7]. Adapted from [7] under fair use; Fair use determination attached. . . 19

2.9 Braking tests-peaked wheel friction, after [7]. Total bar length is two standard deviations. Adapted from [7] under fair use; Fair use determination attached. 20

2.10 Friction coefficient (μ) as functions of slip ratios (S) for tires 1, 7 and 8, after [7]. The tread pattern of the three tires, is as shown in Figure 2.8. Adapted from [7] under fair use; Fair use determination attached. 21

2.11 Effect of glass transition temperature on friction coefficient,studied with polymers of rubber [4]. The rubber polymers used for this study [4] were Silicone type GE RTV 602; isoprenene type Cariflex 305/92% cis; Nitrile type Polysar Krynac 801/38.5% with acetonitrile. This effect was studied Roberts [4] using a Rubber Lens which is hemispherical transparent rubber sample, the contact was studied using low power microscopy. Waves refer to observance of Schallamach waves [5], a peeling separation between the ice surface and rubber sample at very low temperatures. At temperatures close to 0 °C, no waves (no peeling separation) were observed. Adapted from [4] under fair use; Fair use determination attached. 22

2.12 Effect of crosslink density on friction coefficient [4]. This effect was studied Roberts [4] using a Rubber Lens which is hemispherical transparent rubber sample, the contact was studied using low power microscopy. Waves refer to observance of Schallamach waves [5], a peeling separation between the ice surface and rubber sample at very low temperatures. At temperatures close to 0 °C, no waves (no peeling separation) were observed. The first crepe natural rubber lens samples was crosslinked with 0.5% dicumyl peroxide, the second sample was cross linked with 8% dicumyl peroxide. Adapted from [4] under fair use; Fair use determination attached. 22

2.13 Effect of normal pressure on tire−ice friction [11]. μ_d − Dry coefficient of friction, $v = v_s$− sliding speed of tire and Ti ice temperature. Peng et al. [8, 9] compare the results from their model based on the theory of thermal balance and frictional melting, to the model developed on the basis of heat transfer at the tireice interface by Hayhoe and Sahpley [10]. Test [3] and Model in [3] refer to Hayhoe and Sahpley [10] study cited in Peng et al. [9], and Current refers to results from the model developed by Peng et al.[9]. Copyright © 2000 SAE International. Reprinted with permission from SAE paper 2000-01-1640; license agreement attached. 23

2.14 Drum type indoor tire tester for snow and ice [3, 11]. M/G refers to Motor/Generator. Adapted from [3] under fair use; Fair use determination attached. 30

2.15 Ice making system for the drum type tester [11, 11]. Adapted from [3] under fair use; Fair use determination attached. 30

2.16 Test-rig at Swedish Road and Transportation Institute [7]. Adapted from [7] under fair use; Fair use determination attached. 32

2.17 Reciprocating type Bench Tire Tester [9]. Copyright © 2000 SAE International. Reprinted with permission from SAE paper 2000-01-1640; license agreement attached. A−platform; B−tire; C special hub; D−upper guide arm; E−base; F−sector body; G−vertical shaft; H−horizontal pulled bar; I−lower guide arm; J−turntable; 1,3−angle measuring sensor; 2−travel sensor; 4,6 force measuring ring; 5−force measuring bar. 32

2.18 Schematic of Test Bench at Karlsruhe Institute of Technology (Karlsruhe, Germany), after [2, 12]. The upper view is a side view and lower view is a longitudinal view. Adapted from [12] under fair use; Fair use determination attached. 33

2.19 CRREL instrument vehicle. Reprinted from [13] with permission from Elsevier; license agreement attached. 36

2.20 Comparison of experimental and computed tractive performance [14]. − refers to coefficient of friction computed by the model and ·· refers to coefficient of friction computed experimentally. Copyright © 1989 SAE International. Reprinted with permission from SAE paper 890028; license agreement attached. 42

2.21 Comparison of tractive performance between models and test results [9]. Peng et al. [9, 8] compare the results from their model based on the theory of thermal balance and frictional melting, to the model developed on the basis of heat transfer at the tireice interface by Hayhoe and Sahpley [14]. Test [3] and Model in [3] refer to Hayhoe and Sahpley [14] study cited in Peng et al. [9], and Current refers to results from the model developed by Peng et al. [9]. μ_d is the dry coefficient of friction and T_i is the ice temperature. Copyright © 2000 SAE International. Reprinted with permission from SAE paper 2000-01-1640; license agreement attached 45

2.22 Comparison of locked wheel results [9]. Peng et al. [9, 8] compare the results from their model based on the theory of thermal balance and frictional melting, to the model developed on the basis of heat transfer at the tireice interface by Hayhoe and Sahpley [14]. Test [3] and Model in [3] refer to Hayhoe and Sahpley [14] study cited in Peng et al. [9], and Current refers to results from the model developed by Peng et al. [9]. μ_d is the dry coefficient of friction and T_i is the ice temperature. Copyright © 2000 SAE International. Reprinted with permission from SAE paper 2000-01-1640; license agreement attached. . 45

3.1 Terramechanics Rig at the Advanced Vehicle Dynamics Laboratory employed for evaluation of tire performance on ice. 52

3.2 Components of the Terramechnaics Rig. Left- The carriage in the home position on the test chamber of the Terramechnaics Rig; Right- The carriage with a force hub and air springs for load control. 53

3.3 Drive train system of the Terramechnaics Rig. Left- Motor on the carriage to provide torque to the wheel; Middle- Motor used to control the longitudinal movement of the carriage; Right: Belt drive for longitudinal motion of the carriage. 53

3.4 Toe and camber adjustment capability of the Terramechnaics Rig. 54

3.5 Left-Outdoor chiller unit of Terramechnaics Rig. Right-Ethylene glycol expansion tank. 55

3.6 Thermotron environmental chamber. 56

3.7 Design of tire enclosure for temperature control. 57

3.8 Left- ThermoCell from iThermo®. Right- Tire enclosure in operation on the Terramechnaics Rig controlling temperature. 57

3.9 Left- Tekscan ® 3150 pressure pad. Right- Handle to connect the pressure pad to the computer. 58

3.10 Tekscan ® equilibrator for the pressure pad. 59

3.11 Tools used for resurfacing the ice surface in the test chamber of the Terramechnaics Rig. L−floor scrapper and R−water squeegee. 60

3.12 Slip meter employed to measure the static coefficient of friction of ice. 60

3.13 Test track at the Keweenaw Research Center used for studying tire−ice interaction. 61

3.14 Mobility Research Inc.s' traction truck employed to evaluate tire performance on ice. Reprinted with permission from Mobility Research Inc. 62

4.1 Tread pattern of the SRTTs. Left- Buffed SRTT with 1.6 mm tread depth. Right- Treaded SRTT with full tread depth of 7.97 mm. 64

5.1 Steps involved in ice preparation on the Terramechanics Rig. (a) Laying of insulation and plastic sheets. (b) Placing the ice mat on the test chamber. (c) Water spayed in layers after 3 days. (d) 3 inches of ice after 5 days. . . . 69

5.2 Smoothing and polishing of the ice surface by the tire footprint after testing on three parallel tracks. 74

5.3 Internal cracking of the ice in the Terramechanics Rig during the first few weeks of testing. 74

5.4 Variations of normalized drawbar pull from three test runs for the treaded SRTT. Ice surface temperature of $-10\,^{\circ}\mathrm{C}$, 100% inflation pressure of 242 kPa, and 100% load of 7000 N. 75

5.5 Variations of normalized drawbar pull from three test runs for the buffed SRTT. Ice surface temperature of −10 °C, 100% inflation pressure of 242 kPa, and 100% load of 7000 N. 76

5.6 Variations of peak normalized drawbar pull from five test runs for the buffed SRTT. Ice surface temperature of −10 °C, 100% inflation pressure of 242 kPa, and 100% load of 7000 N. 77

5.7 Variations of peak normalized drawbar pull from five test runs for the buffed SRTT. Ice surface temperature of −10 °C, 100% inflation pressure of 242 kPa, and 100% load of 7000 N. 77

5.8 Effect of normal load on drawbar pull for the treaded SRTT on ice with dry friction. 100% inflation pressure of 242 kPa, the temperature indicated on plots is the laboratory temperature when testing was conducted. 78

5.9 Effect of normal load on drawbar pull for the buffed SRTT on ice with dry friction. 100% inflation pressure of 242 kPa, the temperature indicated on plots is the laboratory temperature when testing was conducted. 79

5.10 Effect of inflation pressure on drawbar pull for the treaded SRTT on ice with dry friction, with load of 100% the load index 7000N. 80

5.11 Effect of inflation pressure on drawbar pull for the buffed SRTT on ice with dry friction, with load of 100% the load index 7000N. 81

5.12 Comparison of drawbar pull slip ratio curves for the treaded and buffed SRTT at 60% load index (4000 N) with inflation pressure 242 kPa for dry friction condition. 82

5.13 Comparison of drawbar pull slip ratio curves for the treaded and buffed SRTT at 100% load index (7000 N) with inflation pressure 242 kPa for dry friction condition. 82

5.14 Comparison of drawbar pull slip ratio curves for the treaded and buffed SRTT at 120% load index (8500 N) with inflation pressure 242 kPa for dry friction condition. 83

5.15 Comparison of drawbar pull slip ratio curves for the treaded and buffed SRTT with 60% inflation pressure of 145 kPa with normal load of 100% load index (7000 N) for dry friction condition. 84

5.16 Comparison of drawbar pull slip ratio curves for the treaded and buffed SRTT with 100% inflation pressure of 242 kPa with normal load of 100% load index (7000 N) for dry friction condition. 84

5.17 Comparison of drawbar pull slip ratio curves for the treaded and buffed SRTT with 120% inflation pressure of 276 kPa with normal load of 100% load index (7000 N) for dry friction condition. 85

5.18 Comparison of drawbar pull slip ratio curves for the treaded SRTT with variation in toe angle. 100% inflation pressure of 242 kPa with normal load of 100% load index (7000 N), on ice with wet friction. 86

5.19 Variation of peak drawbar pull with toe angle for the treaded SRTT. 100% inflation pressure of 242 kPa with normal load of 100% load index (7000 N), on ice with wet friction. 86

5.20 Comparison of drawbar pull slip ratio curves for the treaded SRTT with variation of camber angle. 100% inflation pressure of 242 kPa with normal load of 100% load index (7000 N), on ice with wet friction. 87

5.21 Comparison of drawbar pull slip ratio curves for the treaded SRTT with variation of ambient temperature. 100% inflation pressure of 242 kPa with normal load of 100% load index (7000 N), on ice with dry friction. 88

5.22 Comparison of drawbar pull slip ratio curves for the treaded and buffed SRTT at ice temperatures of $-3\,^{\circ}\mathrm{C}$ for wet friction and $-10\,^{\circ}\mathrm{C}$ for dry friction. 100% inflation pressure of 242 kPa with normal load of 100% load index (7000 N). 89

5.23 Comparison of drawbar pull slip ratio curves for the treaded SRTT on different ice surface conditions. 100% inflation pressure of 242 kPa with normal load of 60% load index (4000 N). 90

6.1 Variation in measured driving coefficient from 10 spin ups for the treaded SRTT. 100% inflation pressure of 242 kPa and 100% normal load of 7000 N. 96

6.2 Variation in measured driving coefficient from 10 spin ups for the buffed SRTT. 100% inflation pressure of 242 kPa and 100% normal load of 7000 N. 96

6.3 Effect of normal load on drawbar pull for the treaded SRTT on ice with 100% inflation pressure (242 kPa), from outdoor testing. 97

6.4 Effect of normal load on drawbar pull for the buffed SRTT on ice with 100% inflation pressure (242 kPa), from outdoor testing. 97

6.5 Effect of inflation pressure on drawbar pull for the treaded SRTT on ice with 100% normal load (7000N), from outdoor testing. 98

6.6 Effect of inflation pressure on drawbar pull for the buffed SRTT on ice with 100% normal load (7000N), from outdoor testing. 99

6.7 Comparison of friction slip ratio curves for the treaded and buffed SRTT with 100% inflation pressure of 242 kPa at different normal loads, from outdoor testing. 99

6.8 Comparison of friction slip ratio curves for the treaded and buffed SRTT with 100% normal load of 7000 N with different inflation pressures, from outdoor testing. 100

7.1 Comparison of drawbar pull/friction slip ratio curves for the treaded SRTT with 100% inflation pressure of 242 kPa at different normal loads, from outdoor and indoor test programs. 102

7.2 Comparison of drawbar pull/friction slip ratio curves for the buffed SRTT with 100% inflation pressure of 242 kPa at different normal loads, from outdoor and indoor test programs. 103

7.3 Comparison of drawbar pull/friction slip ratio curves for the treaded SRTT with 100% normal load of 7000 N with different inflation pressures, from outdoor and indoor test programs. 104

7.4 Comparison of drawbar pull/friction slip ratio curves for the buffed SRTT with 100% normal load of 7000 N with different inflation pressures, from outdoor and indoor test programs. 104

7.5 Variation of tread hardness with temperature for the SRTTs. 107

7.6 Variation of tread hardness with temperature for the SRTTs. 108

8.1 Compact utility truck model in TruckSIM® used for simulating tractive and braking performance on ice. 112

8.2 Time history of longitudinal speed (V_x) of the truck C.G traveling at speed of 80 km/h, spike braking at t = 2 sec, on different ice surfaces from TruckSIM® simulations. 114

8.3 Time history of left front wheel speed, travelling at speed of 80 km/h, spike braking at t = 2 s, on different ice surfaces from TruckSIM® simulations. . 115

8.4 Time history of longitudinal speed (V_x) of the truck C.G traveling at speed of 80 km/h, spike braking at t = 2 sec, with different tire inflation pressures with full tread (treaded SRTT) on dry ice from TruckSIM® simulations. . 116

8.5 Time history of longitudinal speed (V_x) of the truck C.G traveling at speed of 80 km/h, spike braking at t = 2 sec, with different tire inflation pressures with tread depth of 1.6 mm (buffed SRTT) on dry ice from TruckSIM® simulations. 117

8.6 Effect of inflation pressure on stopping distance of the truck travelling at a speed of 80 km/h, spike braking at t = 2 sec, for the treaded and buffed SRTT on ice from TruckSIM® simulations. 117

8.7 Effect of inflation pressure on time to complete 50 m from rest for the compact utility truck with treaded and buffed SRTTs on dry ice from TruckSIM® simulations. 119

9.1 Structure of the tire-ice model (TIM). 123

9.2 Flow chat of the tire-ice model (TIM). 123

9.3 Schematic to represent Jaegers [15] temperature rise formulation, based on representation presented by Fujikawa et al. in [16]. 126

9.4 Schematic representation of tire-ice temperature rise prediction model, based on Fujikawa et al. [16]. The contact between the tread block and ice surface occurs at the plane $z_t = z_i = 0$. 128

9.5 Temperature rise simulation from TIM for a 16" SRTT with nominal load and inflation pressure. 130

9.6 Temperature rise simulation for a 16" SRTT with, (a) 60% load index; (b) 100% load index; (c) 120% load index, Simulations parameters: inflation pressure of 35 psi and 0 N−m wheel torque. The right edge of the patch represents the entry and the left edge represents exit of the contact patch. 135

9.7 Temperature rise simulation from TIM for a 16" SRTT with wheel torque of (a) 0 N−m; (b) 448 N−m; (c) 896 N−m. Simulations parameters: inflation pressure of 35 psi and a normal load of 7000 N. The right edge of the patch represents the entry and the left edge represents exit of the contact patch. . 136

9.8 Contact path classification into wet and dry regions according to TIM. The red refers to the wet regions and the blue refers to the dry regions. The right edge of the patch represents the entry and the left edge represents exit of the contact patch. 137

9.9 Heat balance principle employed in the tire-ice interface of TIM to compute the average friction in the contact patch. 137

10.1 Infrared camera mounted onto the carriage of the Terramechanics Rig. . . . 140

10.2 Schematic representation of infrared camera mounted onto the carriage of the Terramechanics Rig, pointing laterally towards the contact of the tire. 140

10.3 Snapshots from the thermal camera from testing conducted on the Terramechanics Rig with different normal loads: Left: 60% load index (LI); Middle: 100% load index (LI); Right: 120% load index (LI). 141

10.4 Comparison of temperature difference between leading edge and trailing edge of the contact patch, from measurements and simulations. 141

10.5 Comparison of the measured and friction vales predicted by TIM for three different loads on the tire: (a) 60% load index (LI); (b) 100% load index (LI); (c) 120% load index (LI). Inflation pressure of 242 kPa, camber angle of 0°, and dry friction conditions. 146

10.6 Comparison of the measured and friction vales predicted by TIM for wet friction conditions: (a) 60% load index and camber angle of 0° on wet friction; (b) 100% load index (LI) and camber angle of 2° on dry friction. Inflation pressure of 35 psi. 147

A.1 Safety switch of the Terramechanics Rig 157

A.2 Emergency Stop switch on controller of the Terramechanics Rig 157

A.3 Winch on the Terramechanics Rig 158

A.4 Light on NI DAQ pad. 159

B.1 Wodden ramp on connecting hoses. 161

B.2 Breaker switch for chiller system. 162

B.3 Expansion tank of the ice making system. 162

B.4 Glycol from Aqua Solutions used in the ice making system. 163

B.5 Pressure gauge of the ice making system. 164

List of Tables

2.1 Friction coefficient comparison between ices created from tap and deionized water for two rubber samples with glass transition temperatures $-50\,^{\circ}\mathrm{C}$ and $-25\,^{\circ}\mathrm{C}$ for A and B respectively, at a particular load, sliding velocity and cold room temperature [17]. (The authors in [17] used rubber samples provided to them by Michelin, the composition of which is not mentioned.) Reprinted from [17] with permission from Elsevier; license agreement attached. 13

2.2 Surface classification by Hunter, after [6]. Copyright © 1993 SAE International. Reprinted with permission from SAE paper 930896; license agreement attached. 17

2.3 Winter tire/surface classification by Martin et al. [18]. Copyright © 1996 SAE International. Reprinted with permission from SAE paper 960657; license agreement attached. 48

2.4 Braking tests on ice by Eddie, after [19]. Copyright © 1994 SAE International. Reprinted with permission from SAE paper 940724; license agreement attached. 49

2.5 Traction and braking tests on ice by Navin et al., after [20]. Copyright © 1996 SAE International. Reprinted with permission from SAE paper 960652; license agreement attached. 50

4.1 Design of experiment matrix for the indoor test program 66

4.2 Design of experiment matrix for the outdoor test program 66

5.1 Parameters controlled during the indoor test program on ice at AVDL. . . . 71

5.2 Repeatabilty analysis of peak normalized drawbar pull. 76

7.1 Design of experiment matrix for the outdoor test program 105

8.1 Stopping distance of the truck traveling at speed of 80 km/h, on different ice surfaces as obtained from TruckSIM® simulations. 114

8.2 Time required by the compact utility truck to complete 50 m from rest on different ice surfaces from TruckSIM® simulations. 118

9.1 Thermal properties of the tread compound and ice surface used for the tire-ice model. 129

Nomenclature

(X, Y, Z)	Coordinates of the point of the heat source
(x, y, z)	Coordinates of the point of the heat rise
α	Thermal diffusivity (m^2/s)
ΔT	Temperature rise (°C)
ω	Angular velocity on the wheel motor (rad/s)
σ	Standard deviation
$AVDL$	Advanced Vehicle Dynamics Laboratory
d	Depth of heat penetration (m)
$D.P$	Drawbar Pull (N)
F_z	Load on the tire (N)
k	Thermal conductivity (W/mK)
KRC	Keweenaw Research Center
Q	Instantaneously generated heat (J)
R_{eff}	Effective rolling radius of the tire (m)
S	Longitudinal slip ratio
$SRTT$	Standard Reference Test Tire
$Subscript - i$	Subscript: Ice
$Subscript - t$	Tire tread
T	Wheel Torque (N−m)

$V_{carriage}$	Longitudinal velocity of carriage of the Terramechanics Rig (m/s)
V_{tire}	Velocity of the tire (m/s)
$V_{vehicle}$	Velocity of the vehicle (m)
Buffed SRTT	Standard Reference Test Tire with reduced tread depth of 1.6 mm
TIM	Tire−Ice Model
Treaded SRTT	Standard Reference Test Tire with full tread depth of 7.97 mm

Chapter 1

Introduction

In this chapter, the reader is introduced to the research conducted as part of this study. Firstly, the motivation for the present study and the specific study objectives are presented, followed by an outline of this document.

1.1 Motivation

The 10 year (2002-2012) average accident data shows that, out of 1.3 billion weather related mishaps, 13% occurred on ice [21]. 580 deaths occurred and 45,133 persons were injured while driving on ice, between 2002-2012 [21]. The probability of accident occurrence increases with the decrease in the value of the surface coefficient of friction, as seen in Figure 1.1. Icy roads are the worst driving conditions, having the least available friction at the tire-ice interface.

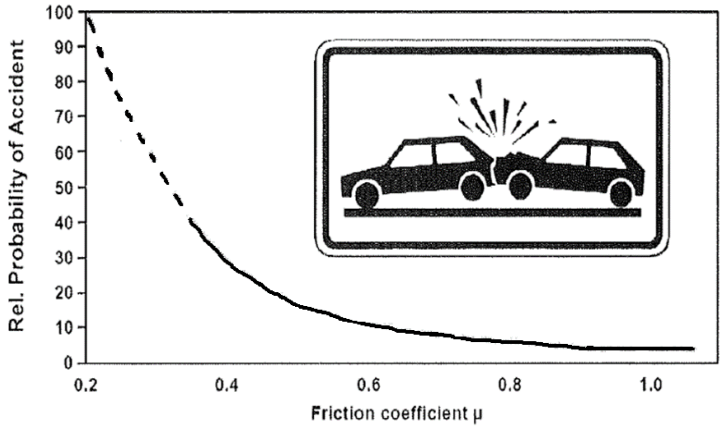

Figure 1.1: Probability of accident with variation in friction coefficient of the road surface. Adapted from Topp et al. [1] under fair use; Fair use determination attached.

1.2 Research Objectives

The tire is the only vehicle's force-transmitting element that contacts the surface. Driving on ice can be totally safe with a clear understanding of the contact phenomenon at tire−ice contact. It is the goal of this research to obtain a clear understanding of the phenomenon at the tire−ice interface, thus laying a strong foundation for improved tire designs and vehicle safety systems for icy roads.

The first objective of this research is to identify the effect of operational parameters on the contact phenomenon and on the forces at the wheel center. Operational parameters include load on the tire, inflation pressure, toe angle, camber angle, ice surface temperature, and ambient temperature studied at different slip ratios.

The second objective is the development of a tire−ice contact model, in order to capture the frictional phenomenon at the tire−ice interface with changes in operational parameters. The forces at the wheel center would then be computed based on the contact conditions, as simulated by the model. The final objective of this research is to validate the tire−ice contact model.

1.3 Research Approach

The first objective of this research was accomplished based on experimental methods; the first step was to design an experiment and to define the different levels of operational parameters. The P 225/60R16 97S Standard Reference Test Tire (SRTT) was the candidate tire for all the test runs. Both indoor and field tests were conducted in order to understand the performance of the SRTT on ice.

The Terramechanics Rig at the Advanced Vehicle Dynamics Lab was employed to conduct indoor studies. The test method was developed; it consisted of the ice preparation procedures, surface resurfacing procedures, test conditions, and slip ratio step time. Field testing was conducted at the Keewenaw Research Center by Mobility Research Inc., as per test procedure outlined in ASTM−1805 [22]. The same levels and values of the operational parameters were maintained in both, the indoor and outdoor test programs.

Accomplishment of the first objective led to the understanding of the effect of operational parameters during operation of the SRTT on ice, and facilitated the fulfillment of the second objective. The contact parameters to be simulated by the model were identified, and the structure of the tire−ice contact model was defined. A semi−analytic approach was decided upon to capture the desired outputs. The contact model was designed to compute the pressure, temperature distribution in the interface, and the dynamic friction coefficient based on tire-ice physics. The final goal of the model was to compute the forces at the wheel center based on the contact conditions.

The final objective of this research will be accomplished by validating the simulations from the tire−ice model using the findings of the experimental studies conducted.

1.4 Main Contributions of this Research

The research conducted in this study was intended to investigate the fundamental behavior of a pneumatic tire on ice, especially regarding its longitudinal traction. Due to the fact that most tire manufacturers conduct standard tests on a Standard Reference Test Tire (SRTT), the industrial partners in this project recommended using it for the experimental and modeling aspects of the project, while developing testing methodologies and modeling procedures generally applicable to other tires. Thus, the research could be of use to a variety of applications, where one may in return have to use the tire of interest to extract the parameters involved in modeling, for example. Thus, the tire used in our research study was the Standard Reference Test Tire (SRTT);data was collected by testing it on ice, via experimental studies conducted at the Advanced Vehicle Dynamics Lab and at the Keweenaw Research Center. The effect of different operational parameters during traction, namely: load on the tire, inflation pressure, ambient temperature, ice surface temperature, toe angle, and camber angle was studied using the indoor and outdoor test methods. A comparison of the friction levels measured by both test methods and reasons for the difference in the measured friction levels are presented. The insight into tire performance on ice also allowed simulations of truck performance on ice using TruckSIM®.

A tire−ice contact model has been developed with consideration of ice surface properties, properties of the tire tread and ambient conditions. After a complete characterization of the tire −ice contact, the friction level at the tire−ice interface is computed and validated against experimental findings.

This research aims at being instrumental in better understanding of tire traction on ice, with the goal of improving tire designs and vehicle safety, to increase the safety potential of vehicles while driving on ice.

1.5 Outline of the Dissertation

Chapter 2 presents a comprehensive literature review on experimental and modeling studies for the behavior of tires on ice from the last half century. The principal topics of the second chapter are factors contributing to the friction mechanism at the tire−ice contact, experimental studies of pneumatic tires on ice and indoor and outdoor test facilities for testing tires on ice, and tire−ice models that predict the tractive and braking performance on ice.

Chapter 3 describes the test setup and all the allied systems that were utilized for this study. The Terramechanics Rig, the ice making system, the cooling chamber, and the slip meter were used for indoor test program. The traction truck used for the outdoor test program is also described.

The design of experiment for the indoor and outdoor test program is described in Chapter 4. In Chapter 5, the results from the indoor test program are presented. The initial test procedures method and the test method are described. The chapter ends with experimental results for the drawbar pull versus slip ratio curves for the different tests conducted on the Terramechanics Rig; the data collected is presented and interpreted.

In Chapter 6, the results from the outdoor indoor test program are presented. The outdoor test method and conditions are detailed. The friction versus slip ratio curves for the different test conditions are presented and interpreted.

Chapter 7 presents the findings of the investigations conducted to understand the reasons for the difference in friction measurement observed between the indoor and the outdoor test programs.

Simulation of the performance of a truck driving on ice using the indoor data collected

in TruckSIM®. is presented in Chapter 8.

The modular structured tire−ice model is described in Chapter 9; the different modules of the model are constructed to simulate the friction levels at the tire−ice interface; the proposed method to compute the friction in the contact patch is detailed.

Chapter 10 details the validation of the tire-ice model based on the findings of the indoor test program.

Finally, Chapter 11 discusses the contribution of this work and recommendations for future research.

Chapter 2

Literature Review

This chapter has been adapted from [23] by A.K. Bhoopalam and C. Sandu. This paper is included in this dissertation with permission from Elsevier. Agreement attached.

In this chapter, the major findings from experimental and modeling studies on the behavior of tires on ice from the last half century are presented in a structured and coherent manner.The principal topics of this chapter are,

- Factors contributing to the friction mechanism at the tire−ice contact
- Experimental studies of pneumatic tires on ice and indoor and outdoor test facilities for testing tires on ice
- Tire−ice models that predict the tractive and braking performance on ice

Finally, after a thorough study of the published work, the key issues of both experimental and modeling studies of tire−ice behavior were identified. The conclusions will serve future investigations as a concise knowledge source to develop improved test facilities and tire−ice models, aiding to the development of better tire designs, and improved vehicle safety

systems.

2.1 Overview of Tire-Ice Interaction

The frictional mechanism at the tire−ice interface is complex with numerous factors affecting it. Tire−ice contact analysis becomes challenging, as the friction-contributing factors keep changing over time, which has a direct effect on the performance of pneumatic tires on ice. These factors could be grouped into three broad areas, namely:

- Ambient conditions and the ice conditions
- Tire specifications
- Vehicle specifications and vehicle type

The prime requirement of experimental studies of tires on ice is maintaining constant test conditions through the entire test run. Correlation of indoor and field test data also happens to be a major challenge considering the differences in ice and ambient conditions. Absence of standard test procedures for tire testing on ice, and new regulations requiring rating of the tires wet grip performance emphasize the need for a better understanding of tire−ice contact leading to improved vehicle safety on icy roads. The review outcomes are organized into different sections. The next section describes various factors that influence the friction mechanism at the tire−ice interface. This section is divided into three subsections that discuss the influence of the ambient conditions and ice conditions, influence of the tire, and influence of the vehicle. The third section examines tire testing on ice, indoor test facilities, and outdoor field tests. Tire−ice models are discussed in the fourth section. Finally, conclusions of this review chapter are presented in the last section.

2.2 Factors Contributing to Tire-Ice Friction

Characterizing the variation of the factors that influence the coefficient of friction at the tire−ice contact is a demanding task. The main reasons are the varying ambient and ice conditions, and differences in the wide variety of tires and cars available today. Often, icy conditions co-occur in the presence of strong winds; blowing wind carries dust and other particles that settle on ice-covered roads. The settling of foreign particles on the ice surface alters the friction coefficient of ice and also enhances melting of the ice. An increase in the ambient temperature and surface impurities on ice aid the melting of ice, leading to the formation of a thin water film on the ice surface where the lowest traction levels are observed. The ice surface becomes rougher as vehicle tires traffic on the ice, due to footprints induced by the tires. Thus increased traction levels are observed for vehicles that pass by at later times. However, if a thin water film is present and a temperature drop is observed, a new thin layer of ice is formed on top. The new ice surface is smooth and a reduced traction will be observed on vehicles that drive over it.

2.3 Ambient and Ice Conditions

2.3.1 Ambient Temperature

The influence of ambient temperature on the tractive performance of tires on ice was studied by Giessler et al. [2]. At low temperatures, higher force transmissibility (traction transmission capability of the tires) was observed; an increase in ambient temperature resulted in reduction of force transmissibility, as seen in Figure 2.1. Winter tires B and C were used for this study. The change in ambient temperature alters properties on the ice surface; ice begins to melt as temperature increases. A water film is formed as ice gets close to 0 °C,

which is a condition of low friction and hence, when ambient temperature varies, the tire performs differently.

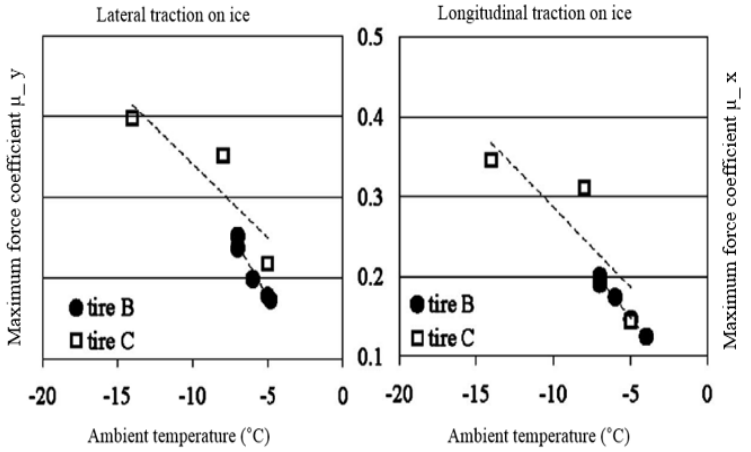

Figure 2.1: For tractive performance on ice, effect of ambient temperature on maximum force coefficient (same as maximum friction coefficient), after [2]. The authors in [2] define μ_y as the ratio of the lateral to vertical force; and μ_x as the ratio of the longitudinal to vertical force. The authors in [2] mention tire B refers to a winter tire with winter pattern tread block with four sipes, the description of tire C is not mentioned. Adapted from [2] under fair use; Fair use determination attached.

2.3.2 Effect of Ice Crystal Size

The variation in ice and ambient conditions has a direct effect on tractive performance of tires on ice. The crystal shape and texture of ice influence the longitudinal coefficient of friction, increased friction coefficient is observed for ice with larger crystal size, but it is dependent on the ambient temperature [3]. The friction coefficient versus slip ratio curves for studies on different ice surfaces from Shimizus study [3], are shown in Figure 2.2, where ice (a) refers to clear ice with pillar shaped crystals, ice (b) refers to clear ice with very large pillar shaped crystals, and ice (c) refers to cloudy ice with granular structures. Ice (b) with large crystals exhibits the highest friction coefficient of the three, whereas ice (c) exhibits the least friction coefficient due to smaller crystal size.

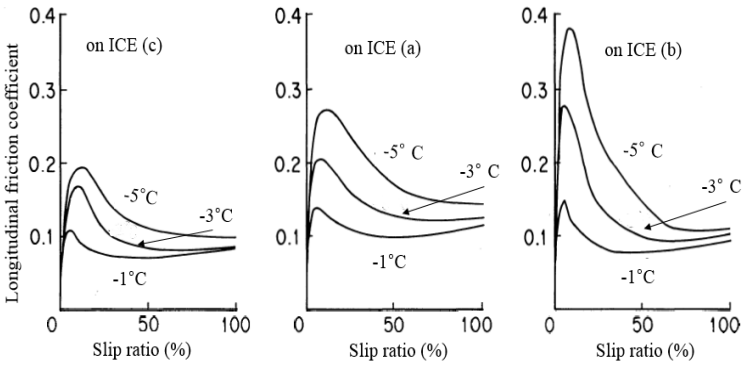

Figure 2.2: Friction coefficient (μ) as functions of slip ratios (S) at different temperatures (room temperature of test rig) for tires on ice with different texture, after [3]. Ice (a) refers to clear ice with pillar shaped crystals, ice (b) refers to clear ice with very large pillar shaped crystals, and ice (c) refers to cloudy ice with granular structures. Adapted from [3] under fair use; Fair use determination attached.

2.3.3 Effect of Ice Texture

Shimizu et al. [3] studied the effect of ice texture on the tire cornering characteristics. The study was conducted with cloudy ice (b) (Figure 2.2) and clear ice (c) (Figure 2.2). The cornering test results with different tires are shown in Figure 2.3, with the tread pattern indicated on the respective plot. Cloudy ice shows poor cornering characteristics at low slips, but stabilizes with increasing slip angle, whereas on clear ice a drop in the lateral friction coefficient is seen at higher slip angles. Ice temperature also influences the cornering characteristics with a greater dependency for clear ice as compared to cloudy ice.

2.3.4 Effect of Impurities in Ice

Impurities, too, affect the friction coefficient of ice; they enhance the rate of melting of the ice and thereby lead to the formation of a water film that reduces traction when compared to traction on dry ice [17]. However, the initial consequences of settlement of impurities on ice would be increasing the friction coefficient and thus improving traction. As

the rate of melting increases, the formation of a water film is observed, leading to a reduction in the friction coefficient and, as a consequence, in traction of the tire. The properties of water used for the creation of ice also affect the static friction coefficient. Skouvaklis et al. [17] demonstrated that ice prepared from tap water exhibits the friction coefficient properties listed in Table 2.1, compared to the properties from when it was created from distilled water for two rubber samples A and B, with glass transition temperatures of 50 °C and 25 °C respectively at two loads and sliding velocities. Glass transition temperature refers to the temperature at which an irreversible transition occurs for rubber, transitioning from a hard to a rubbery state. The glass transition temperature of the rubber compound determines the parameters to be set during the manufacturing process of the tire. The tests in [3] were carried on a linear friction machine installed in a cold room. The study confirmed that ice made from tap water, which contains more salt and a higher impurity content, displays a lower value of the friction coefficient compared with ice created from de−ionized water. The friction coefficient also shows a dependency on normal load and sliding velocity.

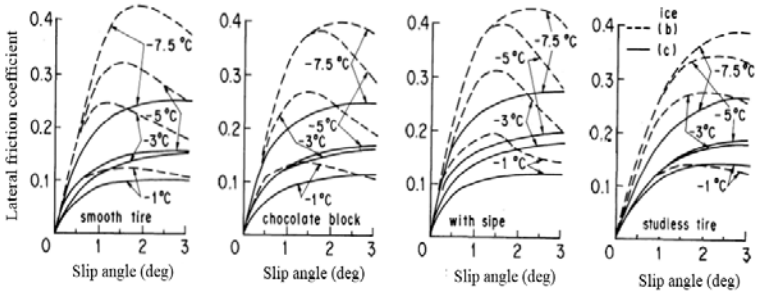

Figure 2.3: Effect of ice texture at different temperatures (room temperature of test rig) on cornering characteristics of different tires, after [3]. The ice legend in the fourth graph applies to all four graphs. Ice (b) is clear ice with very large pillar shaped crystals and ice (c) is cloudy ice with granular structures. (Chocolate block refers to tread pattern of the tire. Sipes are the cuts and groves located on the tread to provide increased traction levels. The tread pattern of the studless tire used to evaluate the cornering characteristics are not mentioned in [3].) Adapted from [3] under fair use; Fair use determination attached.

Table 2.1: Friction coefficient comparison between ices created from tap and deionized water for two rubber samples with glass transition temperatures $-50\,^{\circ}\mathrm{C}$ and $-25\,^{\circ}\mathrm{C}$ for A and B respectively, at a particular load, sliding velocity and cold room temperature [17]. (The authors in [17] used rubber samples provided to them by Michelin, the composition of which is not mentioned.) Reprinted from [17] with permission from Elsevier; license agreement attached.

Rubber samples and type of water used for ice	Friction coefficient	
	$0.45kN, 0.1m/s$ $-13\,^{\circ}\mathrm{C}$	$0.7kN, 1m/s$ $-3.5\,^{\circ}\mathrm{C}$
Rubber A − tap water	0.76	0.1
Rubber A − de−ionized water	0.89	0.11
Rubber B − tap water	0.52	0.1
Rubber B − de−ionized water	0.89	0.12

2.3.5 Effect of Ice Surface Temperature

The effect of ice surface temperature on the friction coefficient was studied in 1981 by Roberts [4], using a transparent rubber hemisphere loaded on ice; the contact area was viewed through a low power microscope. High adhesion levels were observed on cold ice with temperature less than $-10\,^{\circ}\mathrm{C}$. This was also confirmed through visualization of Schallamach waves, named in honor of Adolf Schallamach, who with the aid of microscopy, visualized waves by conducting experiments on rubber abrasion. Detailed information can be found in [5]. The visualization of Schallamach waves at very low temperatures indicates a peel-stick phenomenon and thereby a coefficient of friction greater than 1. At temperatures close to $0\,^{\circ}\mathrm{C}$ no waves are seen, sliding process with friction coefficients less than 1 are observed. The increase in sliding speeds above 10 mm/s saw debris and particles of rubber on the ice, thus the phenomenon of wear was observed. Increase in temperature towards the melting point of ice led to a reduction in adhesion and friction, and both waves and wear were not present. The strong dependency of friction coefficient on ice temperature, as studied by Roberts [4], is shown in Figure 2.4. Martin et al. [18] experiments for studying accidents

on winter surfaces using different vehicle types found a doubling of deceleration rate as ice temperature dropped from 0 °C to −20 °C. This concurred with the observations made by Eddie [19], from his study of the effect of anti-lock brakes (ABS) on ice. This is an indication that ice surface temperature governs the amount to traction available. Giessler et al. [2] studied the influence of initial surface temperature on the friction coefficient at the tire−ice interface. His simulations, shown in Figure 2.4, confirmed the findings of Roberts [4], seen in Figure 2.4. Reduced friction coefficients are observed at the tire−ice interface as the initial track temperature is increased.

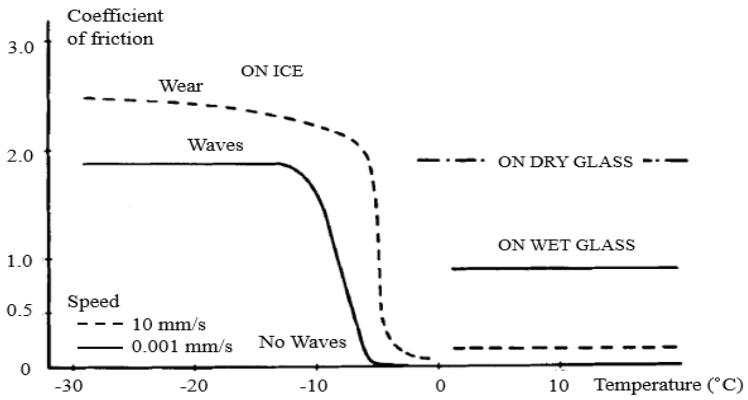

Figure 2.4: Effect of ice temperature and sliding speed on friction coefficient, after [4]. − refers to coefficient of friction computed on wet glass,−− refers to coefficient of friction computed on ice and− · − refers to friction coefficient computed on dry glass. This effect was studied by Roberts [4] using a Rubber Lens which is hemispherical transparent rubber sample, the contact was studied using low power microscopy. Waves refer to observance of Schallamach waves [5], a peeling separation between the ice surface and rubber sample at very low temperatures. At temperatures close to 0 °C, no waves (no peeling separation) were observed. Wear refers to detachment of rubber particles and observance of debris on the ice surface. Adapted from [4] under fair use; Fair use determination attached.

2.3.6 Effect of Age of Ice Track

Roberts [4] extended his study to study the effect of the age of ice track on the friction coefficient. He found that the ionic impurities lead to weakening of the top layers of the ice

track and thereby a reduction in the friction level, as illustrated in Figure 2.6. An additional observation of the study [4], was the separation of the rubber and ice surface which happened by peeling at ice temperatures less than $-15\,^{\circ}\mathrm{C}$. For temperature above $-10\,^{\circ}\mathrm{C}$ both surfaces were seen to pop apart. Wet friction is predominant in the tests conducted at temperatures close to $0\,^{\circ}\mathrm{C}$; the water film drastically reduces the frictional force.

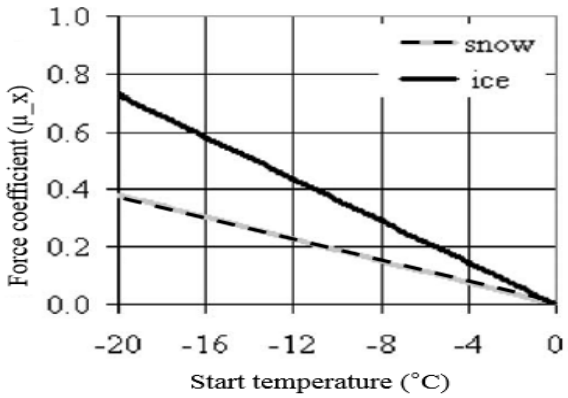

Figure 2.5: Effect of initial track temperature on force coefficient (same as friction coefficient), after [2]. (The authors in [2] define μ_x as the ratio of longitudinal to vertical force.) An assumption, that no force can be transmitted on a water film in [2] results in a zero force coefficient (μ_x) at $0\,^{\circ}\mathrm{C}$. Adapted from [2] under fair use; Fair use determination attached.

2.3.7 Ice Topography

Ice topography still happens to be ambiguous in todays literature. Hunter [6] classified winter surfaces into tent different types, as shown in Table 2.2. From his accident reconstruction studies, friction coefficients reported ranged from a minimum of 0.19 to 0.63 for different ice surfaces. The braking friction coefficients for a passenger car with no ABS on different surfaces are presented in Figure 2.7. Martin et al. [18] defined additional surface classifications compared to Hunter [6], as illustrated in Table 2.3. Both studies classify and characterize winter surfaces. Important outcomes from these studies are their specifications of the conditions of each tractive surface and how tires perform on them. Martin et al.

[18] reports a coefficient of 0.92−0.95 for deep untracked snow, which seems unusually high. These coefficient values were obtained by driving the car into a ditch of snow. Thus the coefficient is a representation of the drag resistance on the vehicle rather than the frictional resistance.

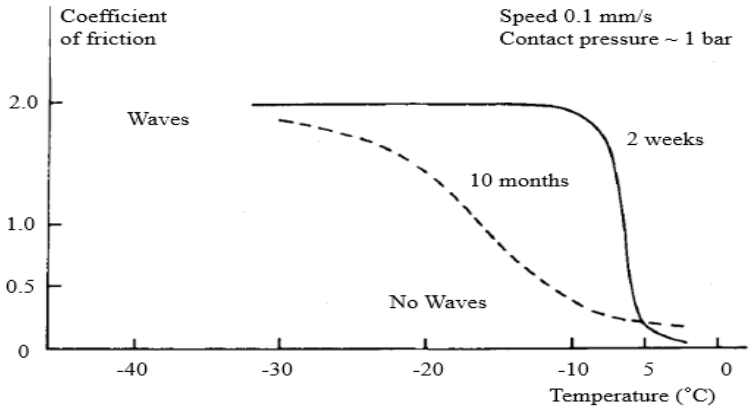

Figure 2.6: Effect of age of ice track on friction coefficient, after [4]. This effect was studied by Roberts [4] using a Rubber Lens which is hemispherical transparent rubber sample, the contact was studied using low power microscopy. Waves refer to observance of Schallamach waves [5], a peeling separation between the ice surface and rubber sample at very low temperatures. At temperatures close to 0 °C, no waves (no peeling separation) were observed. Adapted from [4] under fair use; Fair use determination attached.

2.3.8 Discussion on ice properties affecting tire performance

The first step to understand the performance of tires on ice is to account for all the conditions pertaining to the situation of interest. The conditions to be accounted are:

- salt and the impurity content present in the water from which the ice was formed,
- the size of ice crystals,
- the texture of ice, and
- the age of ice.

Table 2.2: Surface classification by Hunter, after [6]. Copyright © 1993 SAE International. Reprinted with permission from SAE paper 930896; license agreement attached.

Surface classification	Description	Average coefficient of friction
Partial frost	Partial coating surface of frost on road	0.63
Frost	White coating of entire road surface	0.53
Heavy frost	Almost ice conditions	0.39
Tracked snow	Snow compacted by vehicles	0.35
Unpacked snow	Snow not compacted by prior vehicles	0.35
Snow and ice	Compact snow and ice	0.32
Black ice	Icy layer covering asphalt. Difficult to see	0.32
Sunny ice	Ice exposed to heating rays of sun	0.24
Wet ice	Ice covered with a layer of water	0.24
Glare ice	Ice looks like glass	0.19

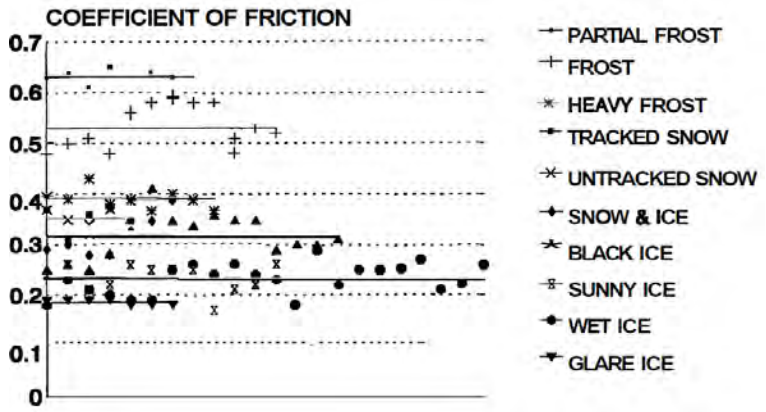

Figure 2.7: Effect of surface type on friction coefficient, which is the vertical axis [6]. Tractive surfaces here are described in Table 2.2. (Coefficients for various winter surfaces; data points represent coefficient values obtained from testing and lines indicate average coefficient values.) Copyright © 1993 SAE International. Reprinted with permission from SAE paper 930896; license agreement attached.

The dependency of the tractive and braking performance on all these ice properties are in turn dependent on the ice surface temperature, which keeps changing with the am-

bient conditions. Investigating of frictional mechanism at the tire−ice interface requires consideration of all the conditions and is challenging with the variation of temperature.

2.4 Tire Specifications

The second major group of factors that influence the tire−ice interaction is the tire itself. The diversity in tires arising from their manufacturing processes, tread compounds, and tread patterns plays an important role in determining tire−ice performance characteristics. The type of tire fitted on the vehicle, the tread depth, and the inflation pressure determine the tire−ice interaction.

2.4.1 Effect of Tread Pattern

The impact of tread patterns on braking and lateral friction on wet ice was studied by the Swedish Road and Transportation Research Institute [7]. Seven commercially available 195/65R15 M+S winter tires from different tire manufactures were used for their study, out of which one of the tires was tested with and without addition of a special undisclosed rubber aggregate (tire 1 and tire 8). The tread patterns for the eight tires tested are as shown in Figure 2.8. It is also important to note that the composition of tread compounds would differ in all seven tires, as they are from different manufacturers. Braking and lateral friction tests were conducted at the Swedish National Road and Transport Research Institute tire test facility with a speed of 30 km/h, ice temperatures of $-3,-5\,^{\circ}\mathrm{C}$ $\pm 1.5\,^{\circ}\mathrm{C}$ and a water film of thickness 0.1 mm. The tires were tested at an inflation pressure of 250 kPa and two normal loads 4 kN and 5 kN. The addition of hard aggregate in the tire−8‘s rubber yielded an increase of the brake and steer friction coefficient, as seen in Figure 2.9. At 13% slip and

an ABS braking situation, the tire−8 with the hard aggregate displayed the highest friction compared to all other tires. A relatively constant friction was observed between 10% and 100% slip from the friction versus slip ratio curves for tire−8, as seen in Figure 2.10, whereas tire−7 exhibited a powerful decrease after the peak friction and for tire−1, a gradual increase before the maximum friction was seen. The advantages of addition of hard aggregate in the tire rubber are evident from the study by VTI [7]; the addition of hard aggregate mimics small studs implanted in the tire and eventually improves the tractive and the braking performance under wet−icy conditions.

Figure 2.8: Tread pattern of tires used to study effect on braking and lateral friction on ice [7]. Adapted from [7] under fair use; Fair use determination attached.

2.4.2 Effect of Tread Compound

The influence of tread compounds was also studied by Roberts [4] by analyzing the effect of glass transition temperature and cross link density on the friction coefficient at

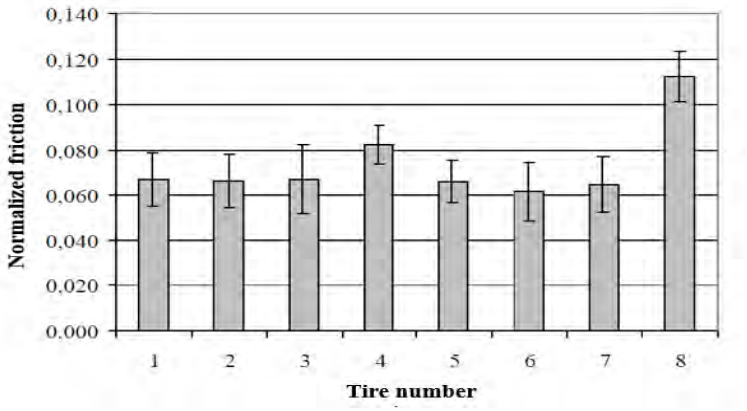

Figure 2.9: Braking tests-peaked wheel friction, after [7]. Total bar length is two standard deviations. Adapted from [7] under fair use; Fair use determination attached.

different ice temperatures. Hemisphere lenses cured with peroxide and made of silicone, cis-polyisoprene, and acrylonitilebutadiene, with glass transition temperatures of $-133\,^{\circ}\mathrm{C}$, $-67\,^{\circ}\mathrm{C}$ and $-25\,^{\circ}\mathrm{C}$, were used for the study. The higher the resilience of the tread compound, the higher is the friction coefficients at low temperatures below $-15\,^{\circ}\mathrm{C}$ and as the ice temperature approached $0\,^{\circ}\mathrm{C}$, the three compounds exhibited low friction values. The silicone compound exhibited the highest friction at low temperatures while the nitrile compound showed the lowest friction (Figure 2.11). Increasing the amount of compound curing agent results in higher levels of hardness and glass transition temperature. An increase in glass transition temperature of the tread compound means higher friction levels at ice temperatures below $-15\,^{\circ}\mathrm{C}$, as illustrated in Figure 2.12.

2.4.3 Effect of Tire Normal Pressure

Tire normal pressure is also a decisive factor to tireice friction at the contact patch, as the normal pressure controls the aspect ratio of the contact patch and thus the shape of the contact patch [8]. Higher friction coefficients were observed for lower normal pressures by Peng et al.[9], as seen in Figure 2.13. Pengs study also demonstrated the advantages of

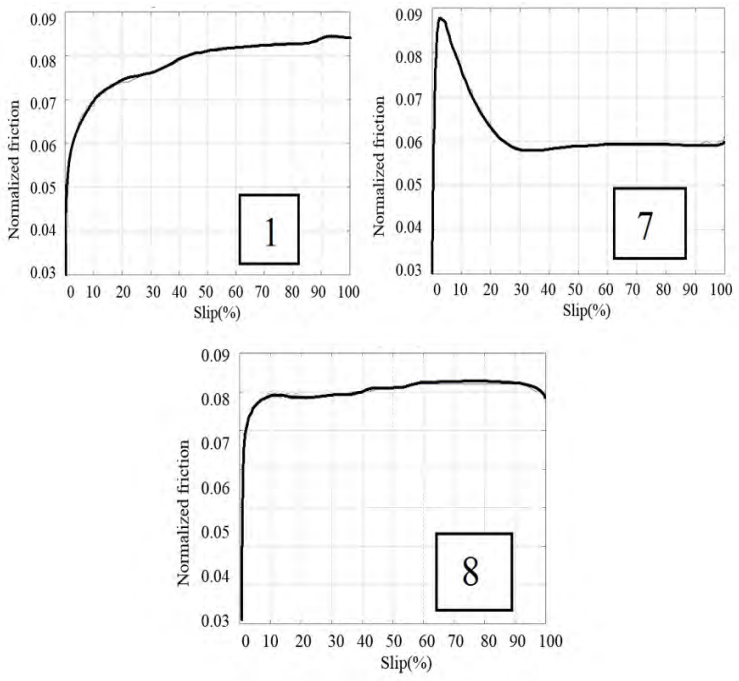

Figure 2.10: Friction coefficient (μ) as functions of slip ratios (S) for tires 1, 7 and 8, after [7]. The tread pattern of the three tires, is as shown in Figure 2.8. Adapted from [7] under fair use; Fair use determination attached.

the Central Tire Inflation Deflation System that adjusts the tire inflation pressure and thus changes the aspect ratio of the contact patch. A rectangular shaped contact patch was found to provide better traction compared to an elliptical shaped interface.

2.4.4 Effect of tire type- All-Season, Summer, and Winter Tires

Winter tires provide better traction and reduced stopping distances compared to summer tires on winter surfaces, but the drawbacks of winter tires when used in summer on bare roads include higher noise and wear. The response of tire type and tire wear was studied by Sumitomo Rubber Industries Ltd. [24], and it was established that the rigidity of tire tread dictates the slope of the $\mu - S$ curve. TyreSafe [25] in their campaign on tire safety conducted braking tests on ice and observed a stopping distance of 8 m on a passenger car

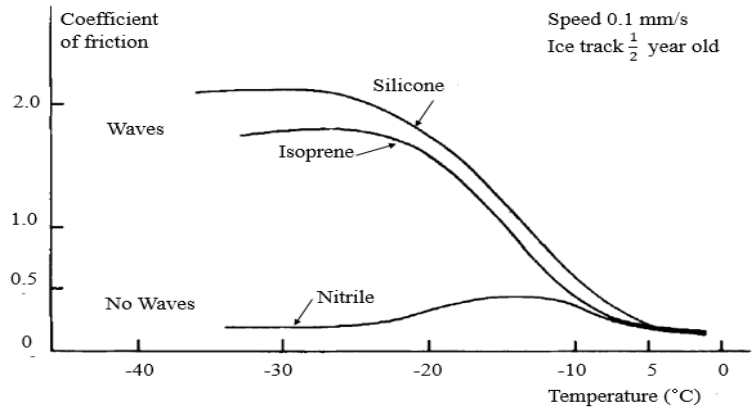

Figure 2.11: Effect of glass transition temperature on friction coefficient,studied with polymers of rubber [4]. The rubber polymers used for this study [4] were Silicone type GE RTV 602; isoprenene type Cariflex 305/92% cis; Nitrile type Polysar Krynac 801/38.5% with acetonitrile. This effect was studied Roberts [4] using a Rubber Lens which is hemispherical transparent rubber sample, the contact was studied using low power microscopy. Waves refer to observance of Schallamach waves [5], a peeling separation between the ice surface and rubber sample at very low temperatures. At temperatures close to 0 °C, no waves (no peeling separation) were observed. Adapted from [4] under fair use; Fair use determination attached.

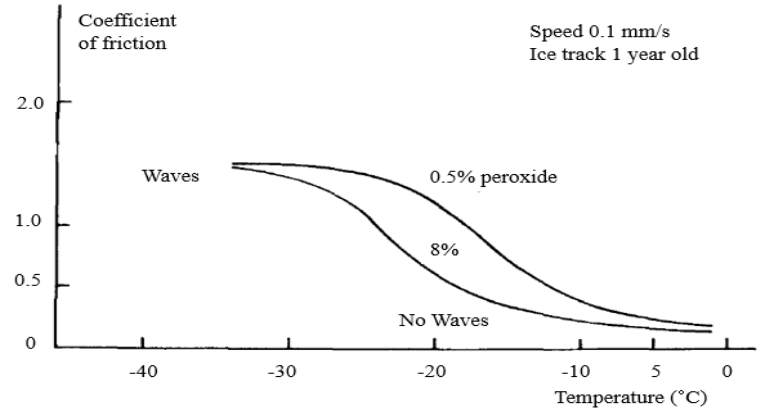

Figure 2.12: Effect of crosslink density on friction coefficient [4]. This effect was studied Roberts [4] using a Rubber Lens which is hemispherical transparent rubber sample, the contact was studied using low power microscopy. Waves refer to observance of Schallamach waves [5], a peeling separation between the ice surface and rubber sample at very low temperatures. At temperatures close to 0 °C, no waves (no peeling separation) were observed. The first crepe natural rubber lens samples was crosslinked with 0.5% dicumyl peroxide, the second sample was cross linked with 8% dicumyl peroxide. Adapted from [4] under fair use; Fair use determination attached.

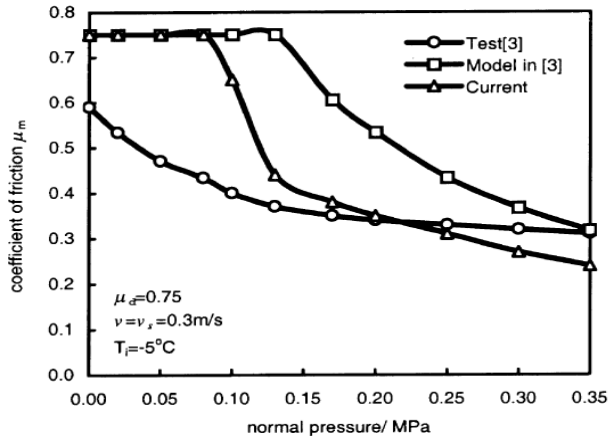

Figure 2.13: Effect of normal pressure on tire−ice friction [11]. μ_d − Dry coefficient of friction, $v = v_s$− sliding speed of tire and Ti ice temperature. Peng et al. [8, 9] compare the results from their model based on the theory of thermal balance and frictional melting, to the model developed on the basis of heat transfer at the tireice interface by Hayhoe and Sahpley [10]. Test [3] and Model in [3] refer to Hayhoe and Sahpley [10] study cited in Peng et al. [9], and Current refers to results from the model developed by Peng et al.[9]. Copyright © 2000 SAE International. Reprinted with permission from SAE paper 2000-01-1640; license agreement attached.

fitted with winter tires when travelling at 24 km/h. In comparison, a 12 m stopping distance was observed when the same vehicle was fitted with summer tires at the same speed of 24 km/h.

Tire-Rack [26], in 2008, compared the performance of winter, summer, and all-season tires on ice with a test vehicle equipped with ABS and traction control. The time to complete 18.3 m was 7.4 s for the summer tire; the all-season tire took 6.5 s. Both tires relied on traction control to complete 18.3 m. The winter tire performed the best taking just 4.5 s to finish and banked minimal on traction control. The braking test observed stopping distances of 14.3 m, 12.1 m, and 6.5 m for the summer, all-season and winter tires respectively. Cornering performance was evaluated by turning a 90 ° corner on ice at around 16 km/h; initial loss of traction was observed in case the summer tire. In case of the all-season tire,

the vehicle lost control towards the exit of the corner. The winter tire outperformed the summer and all-season tires with no loss of control.

2.5 Vehicle Specifications

The type and condition of the vehicle being driven on icy conditions is furthermore an important consideration which decides the friction values at the tire−ice contact. Safety systems such as traction control and ABS are of minimal advantage on ice when the vehicle runs with summer or all-season tires. Winter tires in partnership with safety systems enhance vehicle safety to a great extent. Regulations in several parts of world require replacing summer and all-season tires with winter tires during the winter. Winter driving schools train drivers to drive in snow and icy conditions; in addition, the advantages of winter tires over all-season and summer tires is explained to them.

2.5.1 Effect of Braking System ABS ON/OFF

Cars equipped with ABS enhance passenger safety to a great extent when driven on asphalt roads. On the contrary, the ABS strengthens vehicle safety to a minor degree under certain icy conditions. The braking performance on ice was not primarily governed by the type of tire or braking system, but by the ambient temperature [19]. An increase in the ambient temperature resulted in reduction of traction levels to half of the original levels, as seen in Table 2.4. The ambient temperature regulates the extent of traction available, the texture and roughness of ice surface were also identified as major factors deciding the braking performance, thereby confirming findings of Shimizus [3] study.

2.5.2 Effect of Vehicle Type Passenger Car and Truck

A comparative study to evaluate the tractive performance of a 1993 Pontiac Grand Prix and of a 1985 Ford L9000 truck was carried out by Navin et al. [20]; in addition, the effect of winter aggregate applied on iced roads was also taken into consideration. Winter aggregate usually is mixture which includes different sized particles of gravel chips, sand, concrete and deicing chemicals applied on snow- or ice-covered roads to help in melting of ice or snow and aid to improve traction. Higher braking coefficients and lateral acceleration coefficients were recorded with the g-analyst in passenger cars in comparison to trucks. A g-analyst is a commercially available instrument, from different companies which interfaces through software with a computer. The unit is mounted on a secure location on the vehicle and records the accelerations (1 g = 9.81 m/s^2) during different driving maneuvers. The friction levels, presented in Table 2.5, increase as the application rate of winter aggregate is increased. The role of the winter aggregate in increasing friction levels and hence the vehicle safety is thus a fact to be recognized.

2.5.3 All Winter Tires versus Two Winter Tires on the Front Axle

If only one pair of brand new tires is available, they should definitely replace the old ones on the rear axle. The old tires on the front will hydroplane and lead to understeer which is fairly easy for the driver to control. If the old tires remained in the rear axle, when the rear tires hydroplane, the vehicle would spin, and this would be impossible for the driver to control. It is still a misconception that installing a pair of winter tires on a single axle would improve safety on iced roads.

To disprove this myth, Tire-Rack [27] tested a vehicle with all winter tires and a

vehicle with winter tires just on the front axle, on ice. At a speed of 20 km/h the car with just a pair of winter tires exhibited a stopping distance of 12.2 m compared to 10.7 m for the vehicle with all winter tires. In a 90° turn test, the vehicle with all winter tires was successful in completing the maneuver while the car with just a pair of winter tires spun out, losing control. The stability assist system did not help with contrasting tires on the front and rear axles.

2.5.4 Driving on Ice with AWD versus RWD

Evaluation of an all-wheel drive and a rear wheel drive on ice was conducted by Tire-Rack [28] by accelerating the vehicles and recording time to complete 18.3 m. The traction index, which is a measure of relative performance to the best available in the market, was found to be 67 and 100 for the RWD and AWD vehicle, respectively. The RWD vehicle took 5.945 s to reach 18.3 m while the AWD vehicle took 4.041 s to complete the same distance. Traction and stability control systems aid in increasing traction to a small extent; ultimately the winter tires decide the traction levels.

2.5.5 Electric Vehicles on Winter Surfaces

Shoop [29] studied the rolling resistance and tractive performance of Electric Vehicle (EV) tires in winter conditions, in comparison to winter tires. EV tires are low rolling resistance tires to boost the travel range of an EV or a hybrid vehicle. The rolling resistance of an EV tire is generally 30% lesser in comparison to a conventional tires. High rolling resistance winter tires when fitted onto an EV would decrease the travel range, but provide better traction than EV tires.

Section 2.3.1 reviews the effect of ambient temperature and ice surface temperature on the

coefficient of friction. The influence of ambient temperature on rolling resistance coefficients was also observed in Shoops study [18]. Lower rolling resistance coefficients were measured with higher ambient temperatures, snow tires exhibited higher rolling resistance levels at all temperatures in comparison to EV tires. Peng et al. [9] demonstrated the improvement in traction by lowering the inflation pressure through the Central Tire Inflation Deflation System on a 175/70R13 radial tire as seen in Figure 2.13. On the other hand, no improvement was seen in traction levels for EV tires even with lowering inflation pressure by 40% in [18]. The effect of rolling resistance with lowering was also measured by Shoop [29], lowering inflation pressures resulted in an increase of rolling resistance of EV tires. It is thus crucial to understand the inter-dependence of each of the friction- contributing factors. Shoops study [29] provides a clear understanding of the influence of tire in the raise of vehicle resistance with dropping temperatures. Future research should definitely focus on improving EV performance in winter conditions with improved EV tires.

2.5.6 Discussion on the Influence of the Vehicle on the Friction Coefficient at Tire−Ice Interface

A vast mix of vehicles is noticed on todays roads. Considering this, a comprehensive experimental study was conducted on controlled ice with a number of vehicle types by Macnabb et al. [30]. The vehicles were representing passenger cars with and without ABS, a light van with ABS, and a heavy vehicle tandem axle truck. Braking, tractive, and lateral performance was studied using tires with different tread patterns and inflation pressures in ambient temperatures ranging from $-25\,^{\circ}\mathrm{C}$ to $0\,^{\circ}\mathrm{C}$. The vehicles equipped with ABS experienced 30% higher braking coefficients as compared to locked and sliding wheels; the same was observed in the study conducted by Eddie [19]. Macnabb et al. [30] study also confirmed findings made by Navin et al. [20] that trucks experience lower friction coefficients

compared to passenger cars. Improved vehicle performance was observed with some tires depending on their design, but studded tires were found to perform the best [19], confirming results of the Swedish Road and Transportation Institutes study [7]. Ambient temperature and inflation pressure made a negligible difference on the friction coefficient [19]. On the contrary, significant variations in the friction coefficients were reported in [4, 19, 9] with the variation of inflation pressure and ambient temperature. The reason for this difference in the behavior of the friction coefficient could be the differences due to testing on natural ice [30] compared to testing on artificially created ice [4, 19, 9].

2.6 Testing Tires on Ice

Indoor testing uses test facilities for testing tires on ice while field testing is usually conducted on frozen lakes. Achieving the goal of repeatable testing with reproducible conditions happens to be of prime importance for both indoor and field tests. Testing on ice is done using single tires in indoor test setups using artificial ice, and done using vehicles outdoors on natural ice. Tires are usually tested on ice in two temperature ranges, firstly between $-4\,^{\circ}\mathrm{C}$ to $0\,^{\circ}\mathrm{C}$ which is testing for wet friction where there is a squeezed flow between the tire and road surface with predominant drag force, and between $-10\,^{\circ}\mathrm{C}$ to $-15\,^{\circ}\mathrm{C}$, for dry friction. The principal target of the tire tests on ice are accurate and repeatable tests. The goals of accuracy and repeatability are better accomplished by indoor tests, where climate control helps maintaining constant temperature conditions.

2.6.1 Indoor Testing

Properties of ice created in indoor test facilities depend on different factors; in the first place, the temperature of water used to create the ice directly influences the ice growth rate, which in turn influences the texture of ice. Ice cloudiness increases proportionally with the growth rate of ice [3]. Clearer ice is obtained when hot water is used. The second factor happens to be impurities and salt content present in the water used for ice creation; the salt and impurity content reduce the coefficient of friction of the ice surface [17]. Growth rate of ice is an important factor to prevent ice cracking during the testing. Stronger ice is obtained when created layer by layer with a growth rate of $3-5$ mm/h [3]. Resurfacing the ice surface for a new test run is to be carried out by scrapping a thin layer of ice [11] and then wiping the surface with a clean cloth so as to obtain the same kind of ice surface as the previous test run [9].

Iced Outer Drum Tester

A drum type indoor test setup was developed by Shimizu and Ikeya [11] to evaluate tractive, braking, and cornering characteristics, the schematic of which is shown in Figure 2.14. The setup facilitated creation of 6 cm thickness of ice on the drum and gave the capability to apply a maximum normal load of 5 kN. A double wishbone suspension system with air springs was installed on the setup to simulate a quarter-car; in addition the setup allowed adjustment of toe, camber, and slip angles. A force hub was employed at the wheel center to measure the wheel forces and moments. A DC motor with a maximum power of 15 kW and a maximum torque of 480 N m is used to control the wheel.

Ice is created by spinning the drum at low speeds and the water is sprayed at a rate as to keep the rate of ice growth at 3 mm/h, using a system shown in Figure 2.15. Finally, a

blade is used to scrape a layer of ice to ensure a smooth surface. The slalom procedure was used, which allows automated lateral movement of tire after a revolution of the drum along the width of the drum. This ensures that the tire moves on freshly prepared ice during the entire test run.

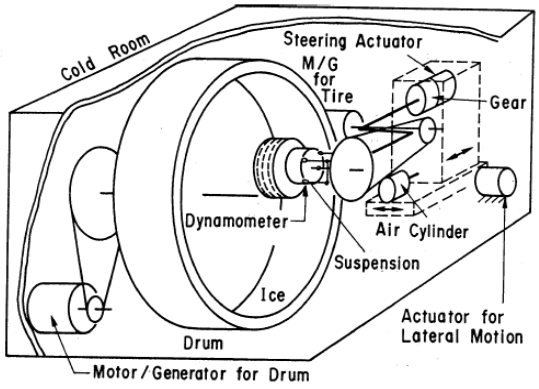

Figure 2.14: Drum type indoor tire tester for snow and ice [3, 11]. M/G refers to Motor/Generator. Adapted from [3] under fair use; Fair use determination attached.

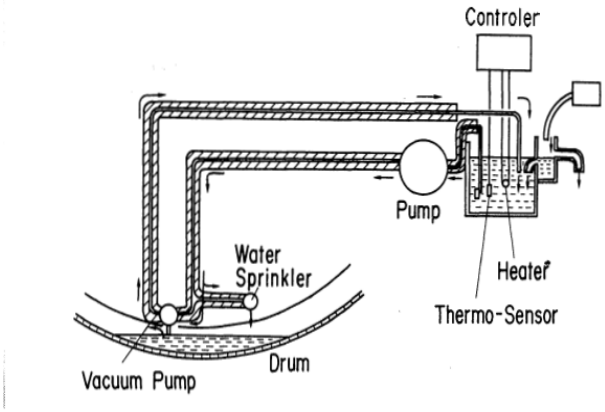

Figure 2.15: Ice making system for the drum type tester [11, 11]. Adapted from [3] under fair use; Fair use determination attached.

VTI Flat Bed Tire Facility

A flat bed tire indoor test rig as seen in Figure 2.16, was developed and installed at the Swedish Road and Transportation Research Institute [31]. The indoor test rig was placed in an environmental chamber to control the ambient conditions; it is capable of evaluating the longitudinal and the cornering characteristics during traction and braking. The test wheel is housed in a stationary rig and it has a moving steel track 55 m long. Applications of the rig include the study of handling properties, braking properties, and friction mechanisms at the tire−ice contact. The setup allows adjustment of camber angle, control of the side-slip angle, and of the wheel load. Braking simulation is carried out with disc brakes on the wheel and a wheel hub is used to measure the forces and moments in the three directions. Ice preparation is done with a refrigeration system that controls ice temperature, with a mixture of water and glycol as the refrigerant. Ice creation is done by an ice laying machine which runs on the rails of the steel track and water is sprayed in layers of 0.1−0.2 mm uni−directionally,at a speed of 0.7 m/s.

Reciprocation Bench Test Facility

A reciprocating test setup for testing tires on ice and compact snow at China FAW Group Corporation RD Center (formerly Changchun Automotive Research Institute, at Changchun, Jilin, P.R. China) as in Figure 2.17, which was described by Peng et al. [9]. An optimal rate of 3 mm/hr. for ice creation on the track is followed to prevent air bubble formation within the ice, after which smoothing of ice is done by blades and an absorbing cloth is used to remove any traces of water on the surface. The adjustment of slip angle is controlled by hydraulic means, platinum thermometers and temperature sensors measure room and ice temperature respectively. Tension bars and rings are employed in measurement

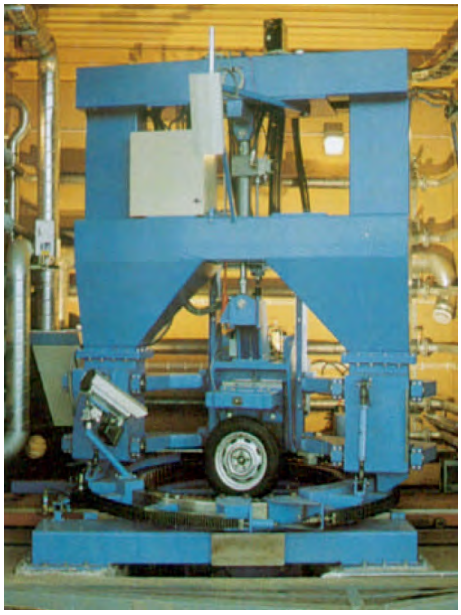

Figure 2.16: Test-rig at Swedish Road and Transportation Institute [7]. Adapted from [7] under fair use; Fair use determination attached.

of forces and moments.

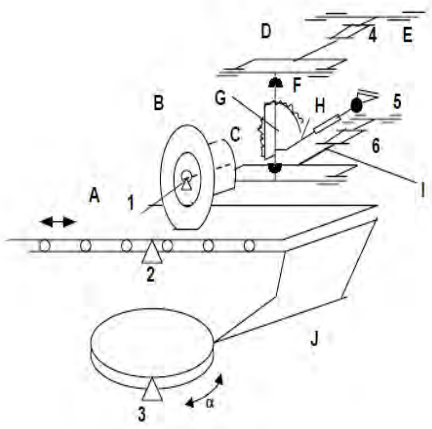

Figure 2.17: Reciprocating type Bench Tire Tester [9]. Copyright © 2000 SAE International. Reprinted with permission from SAE paper 2000-01-1640; license agreement attached. A−platform; B−tire; C special hub; D−upper guide arm; E−base; F−sector body; G−vertical shaft; H−horizontal pulled bar; I−lower guide arm; J−turntable; 1,3−angle measuring sensor; 2−travel sensor; 4,6 force measuring ring; 5−force measuring bar.

Inner Drum Test Bench at Karlsruhe Institute of Technology

Karlsruhe Institute of Technology houses an indoor test rig shown in Figure 2.18, which was described by Giessler et al. [2], with a 3.8 m diameter drum; the track is installed on the inner surface of the drum against which the tire rolls. A measuring hub on which the wheel is mounted measures the tire forces. Hydraulic actuators are employed to modify the slip angle, the camber angle, and the normal load. Tire surface temperature distribution is studied using the infrared images captured by an infrared camera. Ice is created on the internal surface of the drum using tap water.

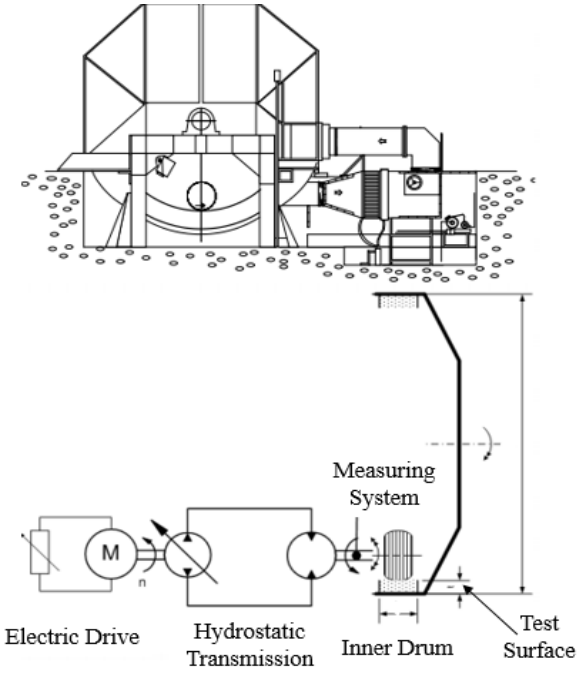

Figure 2.18: Schematic of Test Bench at Karlsruhe Institute of Technology (Karlsruhe, Germany), after [2, 12]. The upper view is a side view and lower view is a longitudinal view. Adapted from [12] under fair use; Fair use determination attached.

High speed linear test Rig-HiLite

The HiLite located at the Institute of Dynamics and Vibrations Research, Leibniz University (Hannover, Lower Saxony-Germany) was described by Ripka et al. [32]. The unique rig is used to study the frictional mechanism between the rubber sample and different surfaces. The rig allows testing up to speeds of 10 m/s, normal load of 100 N, and temperature ranging from $-25\,^{\circ}\mathrm{C}$ to $55\,^{\circ}\mathrm{C}$. A track of 5 m in length allows testing on different surfaces namely concrete, asphalt, snow, and ice. The rubber sample is attached to the carriage that then slides on the track at a defined speed. The forces are measured using 3-D piezoelectric sensors, the ratio of the friction force to the normal force gives the friction coefficient.

2.6.2 Field Testing

Outdoor testing for performance of tires on ice is often carried out on frozen lakes and parking lots; such kind of testing is time consuming for all the desired conditions, as the weather conditions do not remain constant. The changing weather conditions result in different ice surfaces, vehicles behave differently as the surface properties vary [6], testing outdoors with constant conditions is thus cumbersome. Instrumentation on the vehicle being tested outdoor includes a g-analyst to record the g-values during braking and traction at different inflation pressures and vehicle speeds. Thermocouples and thermometers are used to record ice and ambient temperatures.

Testing on frozen lakes is very risky due to uneven ice depth, breaking of ice surface in the middle of the lake during testing is extremely dangerous. Testing on frozen shallow fields is a preferred choice over frozen lakes. Previous studies propose a simple relation to compute the load bearing capacity of a frozen surfaces as,

$$P_{max} = Cz^2 \tag{2.1}$$

where P is the maximum load; C, the constant dependent on Frozen Layer and z is the thickness of the layer. Shoop [33] reports constant C to have a value of 0.23 for weak ice and 0.67 for stronger ice.

Field tests are a must for studies on accident reconstruction. Previous studies have computed the friction coefficients and the variation of deceleration with ambient temperature for the classified ice surfaces [18]. The variation of the friction coefficient is seen from Martins study [18] for different winter surfaces, vehicles, tires, braking configuration (ABS ON/OFF), and vehicle speeds. When testing outdoors each testing condition is unique, so achieving the goal of repeatability is challenging.

Autonomous vehicles could also be used for extensive winter testing. Very high temperature drops will make it difficult for testing with human operation, thus autonomous vehicles with minimal human intervention allow voluminous testing. However, an in-depth understanding of the problems associated with winter operation of vehicles is essential. Diemand et al. [34] identified the temperature related problems associated with vehicle fluids. To avoid cold start problems all machines have to operate with engine heaters and with pan and block heaters. Low temperature lubricants with high viscosity index are to be used, and heavier grade diesel fuels are to be used, as lighter fuels ignite with great difficulty at low temperatures.

Cold Regions Research and Engineering Laboratory (CRREL) instrument vehicle (CIV)

The CIV is a state of the art, all season mobility research vehicle [13], as shown in Figure 2.19. Tractive, resistive and maneuver performance could be studied through various configurations of the CIV. The CIV is backed with different technologies, a GPS to measure position, configurable braking system, velocity sensors for wheel and vehicle speed, and motion sensors for accelerations in three directions.Triaxial load cells at each wheel are used to measure the forces.

The CIV is a useful tool for field tests to study different tires on various winter surfaces. The configurable braking capability of the CIV will help evaluation of braking performance under different configurations. The wide range of winter testing capabilities of the CIV also will serve as validations tools for comprehensive tire−ice models.

Figure 2.19: CRREL instrument vehicle. Reprinted from [13] with permission from Elsevier; license agreement attached.

ASTM-1572 and ASTM-1805

The ASTM 1572 and 1805 standards [35, 22] state standard field test methods for tire performance on snow and ice surfaces. Both ASTM 1572 and 1805 aim at providing a better understanding of influence of ambient temperature, normal load, inflation pressure,

tire wear, vehicle characteristics, surface characteristics, solar load, test driver, rim, and tire temperature on tire ice performance. ASTM 1572 contains test methods for braking and lateral traction. Procedures for carrying out different vehicle maneuvers are outlined within the standard. Different test procedures contained in ASTM 1572 include road circuit handling, winter hill climbing, winter slalom, straight ahead acceleration and braking, and step steer, while ASTM 1805 outlines procedures for longitudinal traction on ice and snow during straight line travel.

preparation procedure, followed by the surface preparation methods. The later sections of the standard state the test procedure for each maneuver, the data analysis and reporting procedure for each of them. However the procedures outlined in these standards are applicable only for evaluation of tire performance and not vehicle performance. ASTM 1572 and 1805 are not be used for ranking vehicle performance or as a specification, the standards are applicable only for research and development purposes [35, 22].

Test Method and its Effect

Field tests were conducted to evaluate tractive performance, using three different test methods. Shoop et al. [36, 37], conducted field tests using three instrumented vehicles namely, CRREL instrument vehicle (CIV), Uniroyal Goodrich (UG) traction tester, and the Saab Friction tester. An aircraft tire was evaluated on the Saab Friction tester and an all season tire on both the CIV and the UG traction tester. On rough ice both the CIV and UG tester yielded the same friction coefficient and the Saab tester measured different traction levels due the difference in tire properties. The test methods although different, resulted in same traction levels on ice. An approximate 11% deviation was observed in traction levels on snow and on a dry asphalt airplane runway surfaces. A comprehensive comparison of test methods on traction measurements of ice will also be significant, with the design of

experiment including all factors stated in Sections 2.3 and 2.4 of this dissertation.

Field Tests for Light Trucks on Winter Surfaces

Pottinger et al. [38] presented a new approach to evaluate force and moment characteristics for truck tires on snow and ice. A test pickup truck was linked to a long wheelbase semi-tractor truck (the tractor element of a semi-trailer truck), which controls the orientation and speed of the test vehicle. The connecting linkages between the two trucks ensured both trucks head at the same angle. The forces and moments were captured using an MTSSWIFTe (Spinning Wheel Integrated Force Transducer by MTS located in Eden Prairie, Minnesota, USA) mounted on left front wheel of the test truck. Lateral performance on ice was evaluated at Smithers Winter Center (Raco, Michigan, USA) and peak traction was observed at $1-2\,^{\circ}$ slip angles, compared to $8-12\,^{\circ}$ on snow. Evaluation of braking performance on ice indicated lesser availability of braking force compared to driving force and wheel lock-up was seen at around -80% to -100% slip. The authors in [38] assume the reduction in braking force and lock-up around -80% to -100% slip occurs as the slowly spinning tire cannot remove water from the tireice contact, whereas a fast spinning tire expels at a faster rate from the contact patch. The strength of this test method will have to be gauged with other test methods through a comparative study to understand the variations of the different test methods, and, finally, adopting a standard test method.

2.6.3 Comparison of Indoor and Outdoor tests

Correlation of data from indoor and field tests should be done with consideration of all the differences in test conditions. The differences in the type of ice, differences in ambient conditions and differences between the test vehicle and the indoor rig have to be

accounted. Deviant longitudinal and cornering characteristics are obtained while testing on outdoors with natural ice and indoors with artificial ice. Good repeatability is the major advantage with indoor tests as they are conducted in a controlled environment while achieving repeatability in outdoor tests is difficult, but they represent more realistic conditions.

2.7 Tire-Ice Models

Tire traction models play a major act in predicting the frictional mechanisms at the tire ice interface taking into account various factors thereby leading to improved vehicle safety on icy road conditions. Various models have been developed to predict the friction coefficient of the tireice interface considering different factors.

2.7.1 Relation between Friction Coefficient and Stopping Distance

Macnabb et al. [30] from his studies on testing on controlled ice and winter roads, developed the relation as in Eq. (2.2) to predict the friction coefficient considering the vehicle speed and stopping distance based on the outdoor tests conducted on different vehicles. The vehicles included passenger cars, a light van and a heavy truck. The tires used for this study included new, used tires and a bald tire. Traction, braking and lateral tests were conducted with some vehicles equipped with ABS and some without. Additional parameters like air temperature, inflation pressure and tread pattern were also studied.

$$\mu = \frac{V^2}{254 * d} \tag{2.2}$$

where μ is the coefficient of friction; V is the vehicle speed in km/h and d is the

stopping distance in m.

Comparing the friction coefficients from experimental studies measured with the g-analyst to the one predicted by Eq. (2.2), an approximate 7% error was observed. The dependency of friction coefficient on speed was also shown by Ripka et al. [32], for different tread compounds on the HiLite Friction Tester. An increase in the coefficient of friction was observed with increase in sliding speed, thereby confirming Eq. (2.2) as friction coefficient is directly proportional to vehicle speed.

2.7.2 Relation based on Temperature and Winter Aggregate

The effect of winter aggregate and ambient temperature on the friction coefficient was expressed through a relation seen in Eqs. (2.3) and (2.4), which was developed by Navin et al. [20] from vehicle traction experiments on ice and snow. Field testing was conducted with a variety of vehicles to represent different vehicle types. Vehicles included passenger cars and light trucks; ones with manual and automatic transmission; with and without ABS. Ice temperature ranged from $-6\,^{\circ}\mathrm{C}$ to $-35\,^{\circ}\mathrm{C}$.

$$f_x(ice, car) = 0.11 - 0:0052T + 0:0002A, A < 1000g/m^2 \tag{2.3}$$

$$f_x(ice, truck) = 0.11 - 0:0052T + 0:00016A, A < 1000g/m^2 \tag{2.4}$$

where *fx (ice, car/truck)* is the average automobile coefficient of friction; A, the aggregate application g/m^2 and T is the temperature in $^{\circ}\mathrm{C}$.

From the above relation it is clear that the addition of winter aggregates increases the friction level. Application of aggregates improves the friction coefficient initially but also enhances the rate of melting, thus leading to water film formation [17]. Hence the relations, Eqns. (2.3) and (2.4) do not hold well in presence of a water film.

2.7.3 Tire−Ice model by Hayhoe

Hayhoe and Sahpley [14] developed a mathematical model based on the principles of heat transfer for the case of wet friction at the tire−ice interface. The contact patch was divided into two regions of wet and dry sliding. The heat generated due to fluid friction is assumed to be used for melting the ice and the remaining heat is conducted into the tire. The location of the beginning of wet sliding in the contact patch was computed from the theory of linear heat flow. The heat balance resulted in the governing equation of the model shown in Eq. (2.5).

$$\frac{dh}{dx} = \frac{A}{h} - \frac{B}{\sqrt{x}} \tag{2.5}$$

$$A = \frac{FrictionFlux}{MeltFlux}.h \tag{2.6}$$

$$B = \frac{ConductionFlux}{FrictionFlux}.\sqrt{x} \tag{2.7}$$

h is the thickness of water film in m and x is the longitudinal distance from front of contact patch m.

The analytical solution of Eq. (2.5) was computed and the force from fluid friction and dry sliding was computed. Validation of the model was conducted through a series of experiments and the model was found to predict the tire performance with a small amount of error, as seen in fig21.

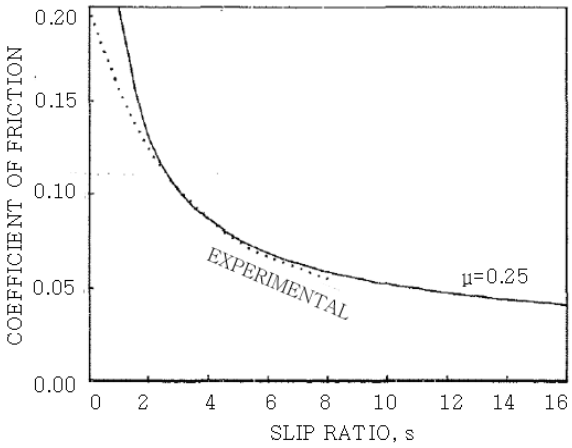

Figure 2.20: Comparison of experimental and computed tractive performance [14]. − refers to coefficient of friction computed by the model and ·· refers to coefficient of friction computed experimentally. Copyright © 1989 SAE International. Reprinted with permission from SAE paper 890028; license agreement attached.

2.7.4 Tire−Ice model by Peng

Based on the model developed by Hayhoe and Sahpley [14], an improved tireice traction model based on thermal balance theory and friction melting was developed by Peng [8]. The model parameters included axle sliding speed, location of phase transition zone in the contact patch, film thickness in the contact patch, pressure across contact patch, and the dry friction coefficient for elliptical and rectangular shapes of the contact patch.
Elliptical and rectangular contact patches were the two shapes considered to setup the model. The mass conservation, energy conservation, and momentum conservation were three basic principal equations used in the model. The model assumed the two distinct regions of the

contact patch namely dry sliding in the forward and wet sliding in the rearward region [8, 9].

$$f_m = \frac{\eta.U_s}{h}.\frac{1}{p_0}.\frac{x_m.y_m2}{\pi.l} + fd.\frac{(\pi - y_m2)(l - x_m)}{\pi.l} \tag{2.8}$$

$$f_m = \frac{\eta.U_s}{h}.\frac{1}{p_0}.\frac{{x_m}^2}{\pi.l} + fd.(1 - \frac{x_m}{\pi.l}) \tag{2.9}$$

$$y_m2 = \theta_m + \frac{\pi}{2} + \frac{l}{2}.\sin 2.\theta_m \tag{2.10}$$

$$\theta_m = \arcsin\frac{x_m - l/2}{l/2} \tag{2.11}$$

where f_m is the average coefficient of friction across the contact patch; f, the coefficient of dry sliding friction; h is the melting film thickness in m; p_0 is the average pressure across the contact patch in Pa; l is the length of contact patch m; U_s, the sliding velocity in m/s and x_m is the length of dry contact patch m.

The first step to predict friction is computing the phase transition location x_m and then calculating the film thickness h and, finally computing the friction coefficient from Eq. (2.8) for an elliptical contact patch and from Eq. (2.9) for a rectangular contact patch. Peng et al. [8] used the same tire and ice parameters from Hayhoe and Sahpley study [14] and the predicted results exhibited an improved accuracy compared to Hayhoe et al. model. Peng et al. [9] improved his original model [8] by considering the length of the contact patch, average contact pressure, thermal conductivity of ice, thermal diffusivity of ice, and surface temperature of ice. The model was validated with experimental studies conducted

on the reciprocating bench indoor test setup [9], using the same parameters from Hayhoe and Sahpley study [14]. The friction coefficient for the rectangular and elliptical shapes of the contact patch are given by Eqs. (2.12) and (2.13).

$$\mu_m = \mu_d.\frac{{x_m}^2}{l} + (C_i + C_t).\Delta T_m.(1 - \frac{x_m}{l})^{\frac{3}{2}}.(\frac{l}{v})^{\frac{-1}{2}}.(p_{av}.v_s)^{-1} \tag{2.12}$$

$$\mu_m = \mu_d.\frac{x_m}{l} + (C_i + C_t).\Delta T_m.(1 - \frac{x_m}{l})^{\frac{1}{2}}.(\frac{l}{v})^{\frac{-1}{2}}.(p_{av}.v_s)^{-1}.y_{2m} \tag{2.13}$$

where l_m is the average friction coefficient in the contact patch; x_m is the length of dry contact patch in m; l, the length of contact patch in m; v is the travelling speed of vehicle in m/s; v_s, the sliding speed of tire in m/s; $p_a v$, the average contact pressure in Pa; $y_m 2$, as defined by Eq. (2.10); l_d, the dry coefficient of friction; l_m is the average coefficient of friction across patch; $\Delta \mathrm{T}_m$ is the difference in melting point temperature and temperature of ice or tire; a is the thermal diffusivity of material in m/s^2; k is the thermal conductivity in W/mK and $C = 2k/(pa)^{1/2}$. Subscript i refers to ice and t refers to tire.

The accuracy of Peng et al. models were compared, it is evident from Figure 2.13, Figure 2.21 and Figure 2.22 that the model [9] predicts the friction coefficient to greater accuracy when studying the influence of sliding velocity under locked wheel conditions compared to the previous model [8]. The influence of normal pressure is better predicted by the later model [9] at low normal pressures; at higher normal pressures Pengs former model [8] is more accurate.

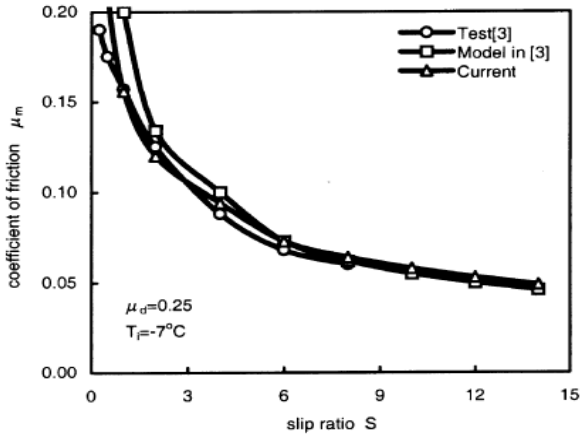

Figure 2.21: Comparison of tractive performance between models and test results [9]. Peng et al. [9, 8] compare the results from their model based on the theory of thermal balance and frictional melting, to the model developed on the basis of heat transfer at the tireice interface by Hayhoe and Sahpley [14]. Test [3] and Model in [3] refer to Hayhoe and Sahpley [14] study cited in Peng et al. [9], and Current refers to results from the model developed by Peng et al. [9]. μ_d is the dry coefficient of friction and T_i is the ice temperature. Copyright © 2000 SAE International. Reprinted with permission from SAE paper 2000-01-1640; license agreement attached

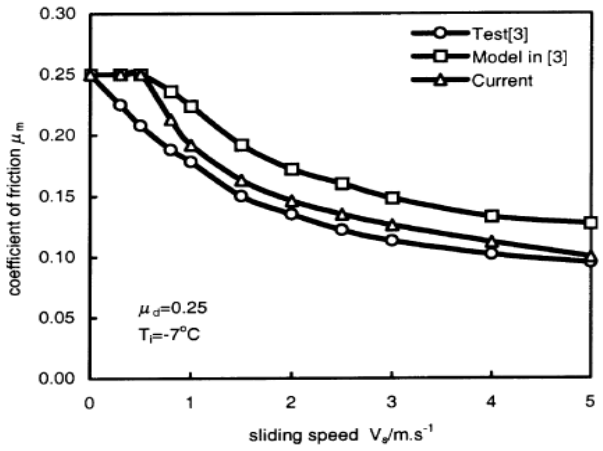

Figure 2.22: Comparison of locked wheel results [9]. Peng et al. [9, 8] compare the results from their model based on the theory of thermal balance and frictional melting, to the model developed on the basis of heat transfer at the tireice interface by Hayhoe and Sahpley [14]. Test [3] and Model in [3] refer to Hayhoe and Sahpley [14] study cited in Peng et al. [9], and Current refers to results from the model developed by Peng et al. [9]. μ_d is the dry coefficient of friction and T_i is the ice temperature. Copyright © 2000 SAE International. Reprinted with permission from SAE paper 2000-01-1640; license agreement attached.

2.7.5 Discussion on Tire−Ice Models

Tire−ice models are based only on a few operating parameters while the experimental studies represent actual conditions. Incorporation of all factors affecting tire−ice friction as discussed in Sections 2.3, 2.4 and 2.5 into the model is vital. A complete model considering all factors will ensure a good design of vehicle safety systems that improve safety on icy conditions. Validation of tire−ice models with experimental studies should still not be expected to yield perfect correlations, as it would be extremely difficult to account for all possible effects.

Tire ice models could be integrated into vehicle models for simulation of vehicle performance on ice. Parker et al. [10] report a winter driving simulator developed by the US Army, their Vehicle Terrain Interaction code helps in evaluation of vehicle performance on any surface, including ice. Tire−ice models in conjunction with simulators will thus act as tools to educate drivers to drive on winter surface. A comparative study on tire−ice models will also lead to development of more comprehensive tire−ice model.

2.8 Summary and Conclusions

In this chapter, the various factors affecting the frictional mechanism at the tire−ice interface are described. These factors are in turn dependent on the ambient temperature; the varying ambient conditions alter the properties of these factors. Hence, different tire−ice behavioral trends are observed with changing temperature. It is very important for experimental studies to take note of all the testing conditions, as the performance results are valid only for those particular conditions.

Test setups must create reproducible testing conditions, namely: ice surface with the same texture, surface roughness, strength, and surface temperature are required. Development of

standard test procedures considering different factors influencing the friction coefficient is the need of the hour. It would also be interesting to conduct a comparative study of different test methods that evaluate braking performance on ice, with varying inflation pressures, normal loads, and ice surfaces. This would lead to creation of a standard test method to evaluate braking performance on ice. Models predicting the friction coefficient during tire braking which take into effect major factors influencing the braking on ice is a vital field of investigation with new regulations requiring the tire manufacturer to rate the braking performance of the tire.

State of the art test facilities and test methods representing the real road and weather conditions to compute the friction coefficient at the tire ice interface are needed to improve vehicle safety. Prediction of the friction coefficient using tire−ice models considering all contributing factors for both traction and braking conditions will lead to better design of the tire, ultimately leading to improved vehicle safety systems and hence enhanced safety while driving on icy road conditions.

Table 2.3: Winter tire/surface classification by Martin et al. [18].

Tire/surface classification	Description	Coefficient of friction range
Ice	Solid sheet of frozen water, thick enough not to be broken by studs	0.054−0.19
Ice with studded snow	Ice as above with studded snow tires at the rear wheels	0.092−0.16
Ice with steel tire chains	Ice and tires with steel chains	0.12−0.18
Ice with low tire pressure	Ice and tire pressure 83−221 kPa	0.13−0.15
Thick black ice	A continuous layer of ice, difficult for driver to see. Thick enough not to be broken by sliding locked tires	0.12−0.26
Thin black ice	A continuous layer of ice, difficult for driver to see. Thin enough to be broken by sliding locked tires	0.17−0.49
Snow and ice glazed at traffic light	Compact ice and snow at a traffic light where prior vehicles have passed by, with warmth from engines and exhaust	0.09−0.22
Snow and ice with sand	Compact snow and ice with a spread of 'sand', almost gravel, particles 3−6 mm in diameter	0.15−0.45
Snow and ice with sand in ruts	Compact snow and ice with worn ruts and rivulets with spread of 3−6 mm diameter sand migrated into ruts	0.20−0.29
Snow and ice with an overlay of fresh snow	Compact snow and ice onto which has fallen a fresh layer of snow 3− 100 mm which has not been tracked	0.18−0.45
Snow and ice with an overlay of old snow	Compact snow and ice onto which has accumulated a layer of rough old snow 100−200 mm which has not been tracked	0.43−0.45

Tire/surface classification	Description	Coefficient of friction range
Snow and ice with 20% exposed ruts	Compact snow and ice which has been worn at the tire tracks to expose 20% of asphalt raving in the ruts	0.20
Tracked snow	Snow which has fallen onto bare pavement and compacted by vehicles	0.24−0.37
Untracked snow	Fresh snow fallen onto bare pavement and not compacted by prior vehicles	0.15−0.42
Deep untracked snow	Snow so deep that vehicle is not supported on its tires	0.92−0.95
Heavy frost	Almost ice conditions. Heavy white coating and very visible to the driver	0.37−0.48
Frost	General white coating covering entire lane. Visible to the driver and completely recognizable as frost	0.48−0.58
Partial frost	Light or partial coating of frost on the road surface. Visible to the driver as intermittent frost appearance	0.61−0.64
Bare	Completely bare dry asphalt road surface. Data was taken to observe effects of low temperature on the friction coefficient of tires on this commonly tested surface	0.59−0.72

Table 2.4: Braking tests on ice by Eddie, after [19]. Copyright © 1994 SAE International. Reprinted with permission from SAE paper 940724; license agreement attached.

Tire type	ABS	Ice temperature(°C)	Air temperature(°C)	Average deceleration (g)
Snow	ON	−5.4	−5.9	0.20
Snow	OFF	− 5.4	−5.9	0.18
Summer	ON	−5.2	−3.1	0.18
Summer	OFF	−5.2	−3.1	0.16
All−season	ON	−3.6	+0.0	0.15
All−season	OFF	−3.6	+0.0	0.13
Snow	ON	−1.9	+2.0	0.13
Snow	OFF	−1.9	+2.0	0.10

Table 2.5: Traction and braking tests on ice by Navin et al., after [20]. Copyright © 1996 SAE International. Reprinted with permission from SAE paper 960652; license agreement attached.

Vehicle	Surface	Application rate (g/m^2)	Temperature (°C)		Acceleration (g)
			Surface	Air	
Braking coefficients					
Passenger car	Bare		−11	−13	0.10
	9.5 mm aggregate	205	−7	−11	0.17
		604	−9	−10	0.26
Tandem axle truck	Bare		−17	−19	0.07
	9.5 mm aggregate	205	−8	−10	0.08
		604	−9	−10	0.12
Lateral acceleration coefficients					
Passenger car	Bare		−31	−35	0.10
	9.5 mm aggregate	244	−14	−22	0.17
		525	−11	−15	0.26
Truck drive tandem	Bare		−14	−22	0.07
	9.5 mm aggregate	244	−14	−22	0.08
		525	−13	−15	0.12

Chapter 3

Test Facility and Equipment

This chapter has been adapted from [39, 40] by A.K. Bhoopalam, C. Sandu and S. Taheri. These papers are included in this dissertation with permission from Elsevier. Agreement attached.

This chapter presents the the test setup, equipment and instruments utilized for the experimental investigations to understand the tire-ice contact and frictional mechanism. The indoor investigations were carried using the Terramechnics Rig at the Advanced Vehicle Dynamics Laboratory, Virginia Tech and the outdoor tests were conducted using a traction truck by Mobility Research Inc. at the Keweenaw Research Center, Michigan Tech in Calumet,MI.

3.1 Indoor Test Setup

All the indoor tests were conducted using the Terramechnaics Rig and the its allied systems. The allied systems include the Custom Ice® ice rink used to create ice,

the Tekscan® pressure mapping system and the American Slip Meter®. The following sub−sections describe in detail everything about the test equipment.

3.1.1 Terramechanics Rig

The Terramechnaics Rig, as seen in Figure 3.1, at the Advanced Vehicle Dynamics Laboratory, is a unique test facility used to study the interaction between tires or metal wheels and different road/off-road surfaces.

Figure 3.1: Terramechanics Rig at the Advanced Vehicle Dynamics Laboratory employed for evaluation of tire performance on ice.

The Terramechnaics Rig was designed and built at the Advanced Vehicle Dynamics Laboratory [41]; the main components of the Rig are a test chamber, the carriage that moves on the test chamber, and the drive train system as shown in Figure 3.2

The test chamber is a 25 ft. (long) X 6 ft. (wide) X 4 ft. (high) container, with a capability of installing a false ceiling at two height levels of 10 inches and 3.5 feet. The test chamber can be filled with different media such as soil, sand, ice etc. Rails installed along the length of the carriage guide the movement of the carriage. The carriage of the wheel assembly supports a stationary motor to provide torque to the wheel. The wheel assembly

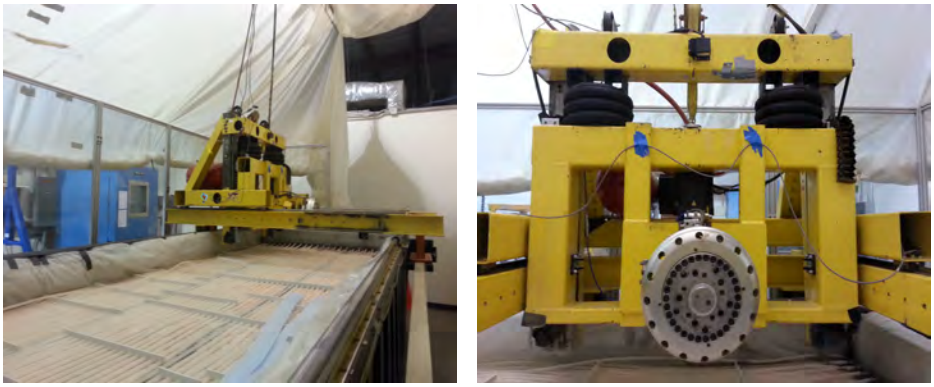

Figure 3.2: Components of the Terramechnaics Rig. Left- The carriage in the home position on the test chamber of the Terramechnaics Rig; Right- The carriage with a force hub and air springs for load control.

is equipped with Kistler®P650 RoaDyn, a wheel force transducer to measure the forces and moments in the three principal directions. The second motor of the drive train system is installed on the test chamber, as shown in Figure 3.3, and controls the movement of the carriage along on the length of the carriage. Thus, a desired slip ratio can be achieved by controlling the speeds of the two motors and based on the estimated value of the effective rolling radius of the tire/wheel.

Figure 3.3: Drive train system of the Terramechnaics Rig. Left- Motor on the carriage to provide torque to the wheel; Middle- Motor used to control the longitudinal movement of the carriage; Right: Belt drive for longitudinal motion of the carriage.

Naranjo [42] developed a *Wireless Internal Tire Sensor (WITS)* system, consisting of eight infrared based measurement sensors mounted on the tire rim in the circumferential

direction. The control algorithm of the WITS chooses the sensor above the contact patch and calculates the deflected rolling radius of the tire. The WITS system was utilized for this study to estimate the effective rolling radius and for calculating the slip ratio. The carriage of the Terramechnaics Rig is also equipped with a *Active Normal Load Control System* consisting of a air−springs and a pneumatic flow control valve. This system was developed by Naranjo [42]; it is a closed loop control system and gets the feedback from the wheel force transducer.

The most recent enhancement of the Terramehanics Rig, is the toe and camber angle adjustment capability. This system has been designed for robustness and accuracy. The system consists on linkages of different lengths to change the toe and camber angle, as seen in Figure 3.4. The camber angle can be adjusted from -8° to $+8^\circ$ in steps of 2° and the toe angle can be adjusted from -25° to $+25^\circ$ in steps of 5°. Additional toe configurations include $\pm 0.5^\circ, 1^\circ, 1.5^\circ, 2^\circ, 4^\circ$ and 6°.

Figure 3.4: Toe and camber adjustment capability of the Terramechnaics Rig.

3.1.2 Ice Making System

The ice making system of the Terramechnaics Rig was purchased from Custom Ice Inc., Burlington, Ontario, Canada. The main components of the system are an ice mat

(roll−out pipe system), custom made for the surface test chamber, as seen Figure 3.2, an outdoor chiller unit and an expansion tank, as seen figure 3.5. The ice mat is a system of pipes that is laid on the surface of the test chamber, the ice mat is then connected to the outdoor unit through a system of hoses. The system works with 50−50 solution of ethylene glycol, which acts as the coolant. The expansion tank, as seen in Figure 3.5, is filled with ethylene glycol and all the air cavities in the system are removed. A constant pressure of 206 kPa in the ice mat indicates all the air entrapped in the system has been removed through the expansion tank.

The ice set point temperature is input in controller and a temperature sensor is placed on the ice mat. Observation of mist on the pipes is an indication to begin spraying water on the ice mat to start ice creation. The outdoor chiller unit cools and circulates the glycol solution to ice set point temperature when the temperature sensor senses an increase in the ice surface temperature.

Figure 3.5: Left-Outdoor chiller unit of Terramechnaics Rig. Right-Ethylene glycol expansion tank.

3.1.3 Thermotron Chamber

The Thermotron® SM4−32 environmental chamber, as seen in Figure 3.6, has a temperature range of −87 °C to 198 °C and an inside capacity of 38 in. X 38 in. X 38 in. The chamber was employed to cool tires before and in between the test runs. The tires were cooled to a low temperature of around −25 °C, as they would reach a temperature close to the ice temperature by the time the tire was removed, fitted onto the Rig,and calibrated for testing.

Figure 3.6: Thermotron environmental chamber.

3.1.4 Tire Enclosure for Temperature Control

A tire enclosure was designed and built during the course of the project to maintain a low temperature around the tire during the test runs. The goal was to mimic winter conditions where both the tire and the surface are at a low temperature. Since due to the space available and budget constraints it was not feasible to create an environmental chamber around the entire Terramechanics Rig, an enclosure was built using cooler bags. The bags were taken apart then stitched to form an enclosure for the tire on the Rig. The design

process is illustrated in Figure 3.7; the enclosure was designed with two openings: one for the drive train and one for the tire−ice interaction.

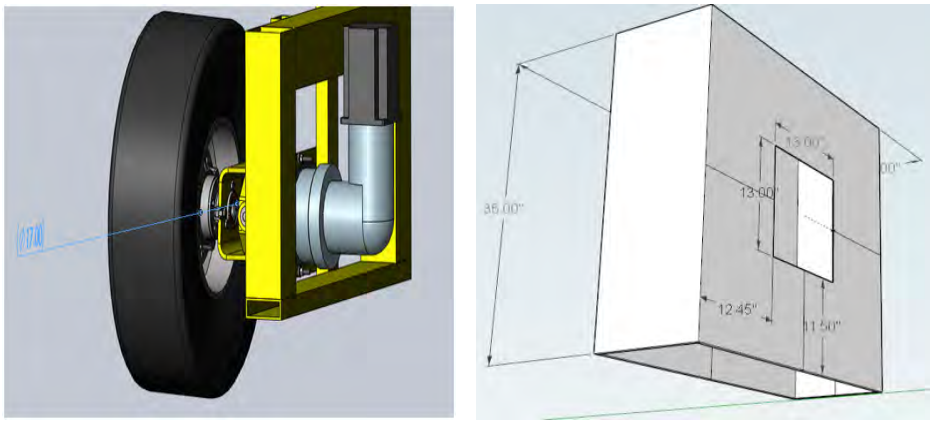

Figure 3.7: Design of tire enclosure for temperature control.

The final enclosure is shown in Figure 3.8; the interior of the enclosure was built with pockets to place iThermo ® cold packs. The iThermo ® cold packs are ice packs with a capacity of delivering frozen power $-10\,^{\circ}\mathrm{C}$ for 10 hours, also having the the advantage of recharge-ability. To avoid any increase in temperature after the tire is fitted onto the Rig, the iThermo ® cold packs placed in the enclosure maintain the tire at a low temperature. The performance of this enclosure is detailed in section 5.2.8 of this dissertation.

Figure 3.8: Left- ThermoCell from iThermo®. Right- Tire enclosure in operation on the Terramechnaics Rig controlling temperature.

3.1.5 Tekscan Pressure Mapping System

The pressure mapping system at the Advanced Vehicle Dynamics Laboratory is a commercially available system from Tekscan. The system consists of a MatScan® 3150 pressure pad and a handle to connect the pad to the computer, as seen in Figure 3.9. The system is employed to measure the pressure 2−D distribution in the tire contact patch. The Tekscan system also records images and videos of the pressure distribution in the contact patch.

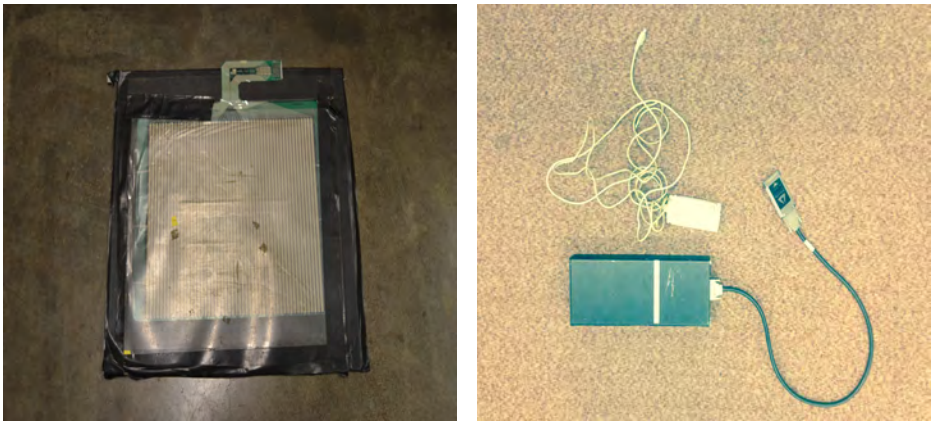

Figure 3.9: Left- Tekscan ® 3150 pressure pad. Right- Handle to connect the pressure pad to the computer.

The pressure pad is 20 in. X 19.65 in. with a sensor area of 14.52 in. X 17.16 in. and a resolution of 9.2 sensel/in^2 [43]. The pressure pad can measure a maximum pressure of 125 psi. The system also contains an equilibrator, as seen in Figure 3.10. Initially, the pressure pad is inserted in the equilibrator to ensure that every sensor of the pad measures an equal pressure. After this step, the pad is calibrated with a known load, and then it is ready to begin pressure distribution measurements.

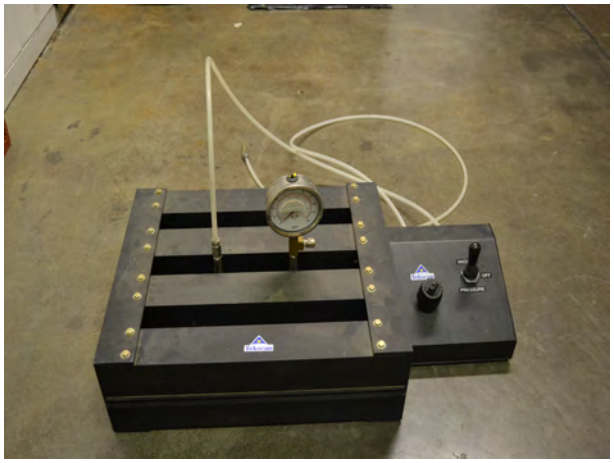

Figure 3.10: Tekscan ® equilibrator for the pressure pad.

3.1.6 Ice Resurfacing Tools

The ice surface on the Terramechnaics Rig has to be resurfaced between test tuns to ensure the same kind of ice surface, including the same static coefficient of friction, for all the test runs. A floor scrapper and water pusher, as shown in Figure 3.11, is used to remove a thin layer of ice and the ice flakes and traces of moisture, if any is removed by a water pusher. An absorbing cloth is also used to wipe off the ice surface to remove the traces of moisture, which cannot be removed by the water pusher. The detailed ice resurfacing procedure is described in section 5.1.3 of this dissertation.

3.1.7 American Slip Meter

The American Slip Meter® is a device used to measure the static coefficient friction of the floor. The device can be employed for measuring the friction coefficient of both, wet and dry friction, of a floor surface. The ASM−825A model, as shown in Figure 3.12, is initially calibrated, placed on the surface, and pulled using the nylon mono−filament attached to hook of the slip−meter. When the slip−meter starts sliding on the surface, the

Figure 3.11: Tools used for resurfacing the ice surface in the test chamber of the Terramechnaics Rig. L−floor scrapper and R−water squeegee.

static friction is displayed on the digital display of the device. The procedure is repeated in four perpendicular directions on the surface and the average value is the friction of the surface. The slip−meter was employed on ice, as seen in Figure 3.12, to measure the friction coefficient of the ice surface, in order to ensure repeatablity of the test results.

Figure 3.12: Slip meter employed to measure the static coefficient of friction of ice.

3.2 Outdoor Test Facility

This section describes the test facility at the Keweenaw Research Center (KRC) located in Calumet, Michigan, USA. The outdoor test program was conducted by Mobility Research Inc., Piedmont, South Carolina, USA at KRC. The test track and the traction truck are described in the following sections.

3.2.1 Test Track at Keweenaw Research Center

The ice test track is as seen in Figure 3.13. It is a split μ track, where the left wheels drive on asphalt and the right wheels on ice. Having one set of wheels drive on asphalt ensures sufficient traction levels during the test runs. The ice surface part on the test track is a pit when no ice exists. The pit is filled with water during the month of November−December and the water freezes naturally to form ice. The thickness of the ice surface is around 6 inches, the surface is resurfaced before the start of test program.

Figure 3.13: Test track at the Keweenaw Research Center used for studying tire−ice interaction.

3.2.2 Traction Truck - Mobility Research Inc.

The traction truck owned by Mobility Research Inc. as seen in Figure 3.14, was used to study the tire performance on the ice track at KRC. The test tire was fitted on the right−rear wheel. Additional details and specifications of the traction truck were not made available and they are proprietary information of Mobility Research Inc.

Figure 3.14: Mobility Research Inc.s' traction truck employed to evaluate tire performance on ice. Reprinted with permission from Mobility Research Inc.

3.3 Summary

In this chapter, the Terramechnaics Rig and all its allied systems used for indoor test program have been described. The ice track and publicly available details about the traction truck used for outdoor tests were also described in this chapter. The next chapters of this dissertation describe the design of experiment, the indoor test program, and the outdoor test program.

Chapter 4

Design of Experiment

This chapter has been adapted from [39, 40] by A.K. Bhoopalam, C. Sandu and S. Taheri. These papers are included in this dissertation with permission from Elsevier. Agreement attached.

The review of literature in Chapter 2 of this dissertation, gave a thorough understanding of different operational parameters that affect the tire performance on ice. The design of experiment was carried out with a goal to understand the effect of all operational parameters, during the operation of tires on icy roads. The following subsections of this chapter describe the tires used for this study and the test conditions.

4.1 P225 60/R16 97S Standard Reference Test Tire

The P225/60 R16 97S Standard Reference Test Tire (SRTT) [44] was chosen for this study. The SRTT is used as a control tire in the industry and as a reference tire for driving traction and braking traction on ice. The deviation in the between SRTTs are minimal, as

they are produced through a very controlled manufacturing process and thus used as control tires in test programs.

The SRTTs for this study were provided by Michelin; a buffed SRTT and a SRTT with full tread depth were used for this study. The SRTTs used for this study were brand new and were not broken-in. The tread patterns of the two SRTTs can be seen Figure 4.1. The reason for using a buffed and a treaded tire was to understand the effect of tread during tire operation on ice. The dimensions, weight, and the physical properties of the tread compound can be found in the standard ASTM-2493 [44].

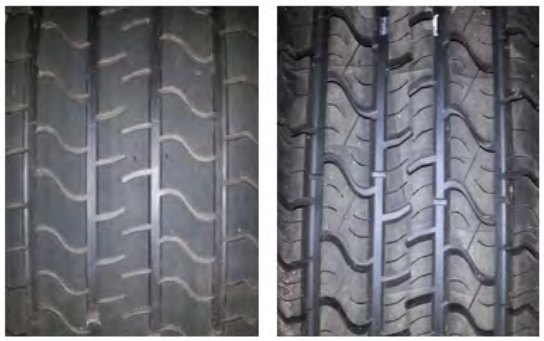

Figure 4.1: Tread pattern of the SRTTs. Left- Buffed SRTT with 1.6 mm tread depth. Right- Treaded SRTT with full tread depth of 7.97 mm.

4.1.1 Terminology

The tire with full tread depth of 7.97 mm is hereby referred to as *Treaded SRTT*. And the tire with reduced tread depth of 1.6 mm is hereby referred to as *Buffed SRTT*.

4.2 Indoor Test Program

Based on findings of the literature review and the capabilities of the the Terramechanics Rig, operational parameters of interest were chosen for the design of experiment. Three levels of normal load and inflation pressure were chosen: the nominal value, 60% of the nominal value, and 120% of the nominal value. The effect of wet friction and dry friction was understood by conducting tests on two ice temperatures: close to 0 °C and at −10 °C. Tests were also conducted at different ambient temperatures, toe angles, and camber angles. The design of experiment matrix with all testing conditions is as shown in Table 4.1. The levels of inflation pressure in Table 4.1 were chosen as an academic exercise to understand their substantial effect, during operation of tires on ice. In reality, operation with 60% or 120% of nominal inflation pressure is least possible. However, operation with 60% or 120% of the load index is very likely.

The slip ratios were split into three groups, with four slip ratios in each group. As the carriage moves from the home position and travels the length of test chamber, the slip ratio changes every 20 s. The toe and camber angle were initially set using the system of linkages described in section 3.1.1.

4.3 Outdoor Test Program

Outdoor testing was conducted for a reduced experiment matrix compared to the one presented in Table 4.1. The outdoor test program was conducted at an ambient temperature that prevailed in the evening at Calument, MI. All outdoor tests were conducted at 0° camber and toe, at an ice temperature of −13 °C, and an ambient temperature of −18 °C. The design of experiment matrix for the outdoor testing program is as shown in Table 4.2.

Table 4.1: Design of experiment matrix for the indoor test program

Operational Parameters	Number of Levels	Level 1	Level 2	Level 3	Level 4
Tires	2	Treaded SRTT	Buffed SRTT		
Ice Temperature	2	$-3\,^{\circ}\mathrm{C}$	$-10\,^{\circ}\mathrm{C}$		
Camber Angle	2	0°	2°		
Load on the Tire	3	60% Load Index 4000N	100% Load Index 7000N	120% Load Index 8500N	
Inflation Pressure	3	60% Inflation Pressure	100% Inflation Pressure	120% Inflation Pressure	
Toe Angle	4	0°	0.5°	1.5°	2°
Slip ratio	12	0% 15% 50%	3% 20% 60%	5% 25% 70%	10% 40% 80%

Table 4.2: Design of experiment matrix for the outdoor test program

Operational Parameters	Number of Levels	Level 1	Level 2	Level 3
Tires	2	Treaded SRTT	Buffed SRTT	
Load on the Tire	3	60% Load Index 4000N	100% Load Index 7000N	120% Load Index 8500N
Inflation Pressure	3	60% Inflation Pressure	100% Inflation Pressure	120% Inflation Pressure

Chapter 5

Indoor Test Program

This chapter has been adapted from [39] by A.K. Bhoopalam, C. Sandu and S. Taheri. This paper is included in this dissertation with permission from Elsevier. Agreement attached.

Indoor evaluation of tire performance on ice was carried out using the Terramechanics Rig at the Advanced Vehicle Dynamics Laboratory at Virginia Tech. The indoor testing program was carried out in two phases, to complete testing by varying different operational parameters. The two phases of testing were conducted in the winter of 2013 and of 2014 respectively, to take advantage low ambient temperatures in Blacksburg. The same test procedures and ice preparation methods were followed during both phases of testing. The following subsections describe the test procedure in detail.

5.1 AVDL Test Method

This section outlays the test method that is used to evaluate tractive tire performance on ice on the Terramechanics Rig at the Advanced Vehicle Dynamics Laboratory. The first

subsection details the ice preparation method, the next subsection details the initial test procedures carried out in between every test run and last subsection describes the test run procedures.

5.1.1 Terminology

The tire performance evaluated in the laboratory using the Terramechanics Rig is expressed in drawbar pull normalized with respect to normal load on the tire. The International Society of Terrain-Vehicle Systems (ISTVS) [45] defines drawbar pull as the force available for external work in a direction parallel to the horizontal surface over which the vehicle is moving. The results of the indoor test program are expressed using normalized drawbar pullslip ratio curves for the ice surface condition in the Terramechanics Rig. The friction coefficient refers to the static coefficient of friction of the ice surface measured on the Terramechanics Rig with the use of a slip meter.

5.1.2 Ice Preparation Procedure

The ice making process, as shown in Figure 5.1, begins with placing a layer of foam insulation on the false ceiling of the test chamber upon which two layers of plastic insulation are added, and the ends of the plastic sheets are taped to the test chamber. Finally, the ice mat is placed on the plastic sheet and connected to the outdoor refRigeration unit. The system is then charged with ethylene glycol, which acts as the coolant, until the system pressure reaches a constant value. Next, the desired ice temperature is input into the controller of the ice rink; this leads to formation of mist on the ice mat.

Once the mist is observed on the ice mat, water is spayed in layers of $1.5-2$ mm every 2 hours. The growth rate of less than 3 mm per hour was found to be optimal in previous

studies [9, 11] for uniformity and maximum compressive strength. Normal tap water was used; after 5 days of spraying water, the ice surface had reached a thickness of 3 inches. The ice growth rate of 2 mm / 2 hours led to formation of ice in layers, which ensured a uniform and smooth ice surface without any air bubbles. The ice was maintained at a temperature $-3\,^{\circ}\mathrm{C}$ for wet friction tests and at $-10\,^{\circ}\mathrm{C}$ for dry friction tests.

Figure 5.1: Steps involved in ice preparation on the Terramechanics Rig. (a) Laying of insulation and plastic sheets. (b) Placing the ice mat on the test chamber. (c) Water spayed in layers after 3 days. (d) 3 inches of ice after 5 days.

5.1.3 Initial Test Procedures

Initial preparation procedures were carried out using tools and equipment shown in Figure 3.6 and Figure 3.11. The procedure before every test run consisted of spraying a thin

layer of water, after which the ice surface was made even by scrapping a thin layer of ice with a metal scrapper (Figure 3.11). The ice flakes obtained as a result of scrapping were cleared of using a water squeegee (Figure 3.11). Next, the ice surface was wiped using an absorbing cloth, to ensure the surface is free from any traces of moisture or ice flakes. The final check to guarantee repeatability of the ice surface was to measure the static coefficient of friction using the slip meter, as per the guidelines laid out in ASTM C1028 [46]. The friction coefficient was tested between all the test runs for dry ice conditions with an ice surface temperature around $-10\,^{\circ}\mathrm{C}$ and its values lied between $0.15-0.18$.

The tire was placed in a Thermotron® chamber and cooled to a temperature lower than the ice temperature before every test run. Then, the tire was removed from the chamber and installed on the Rig; after installation, the tire reached a temperature equal to that of the ice surface. However, when testing was conducted towards the end of winter in 2013 and 2014, the tire would heat up faster and would not stay at the ice temperature.

5.1.4 Test Procedure

Once the surface is prepared, the tire installed on the Rig, and the enclosure placed on the tire, the testing is started and the force and moment data is collected. The tests run at each of the 12 slip ratios, as in table 4.1, for 20 s at steady-state value. As the carriage travels along the test chamber, the slip ratio changes after 20 s; the slip ratios are divided into groups of three: $0\%-3\%-5\%-10\%$; $15\%-20\%-25\%-40\%$; and $50\%-60\%-70\%-80\%$.

Testing was conducted on three parallel tracks, one for each of the slip ratio groups listed above; thus, the tire runs on fresh ice every time, with the carriage traveling at a speed on 0.2 km/h. On each track, four slip ratios are tested as per the groups; after testing on three tracks, the drawbar pull slip ratio curve is built. Each test condition is repeated

three times to ensure repeatability of the ice surface and the test results. The parameters controlled in the indoor test program are summarized in Table 5.1.

Table 5.1: Parameters controlled during the indoor test program on ice at AVDL.

Parameter	Control Method
Normal load	Normal load controller
Longitudinal slip ratio	Controlling motor speeds
Ice surface temperature	Ice rink: Set temperature option
Static friction coefficient of ice surface	Resurfacing procedures

Slip Ratio Calculation

The slip ratio is controlled by having the carriage move at a constant speed of 0.2 km/h and the torque to the wheel is varied for every 20 s intervals. The angular velocity input to the motor controller is based on the measurement of the deflected rolling radius of the tire. The defected rolling radius of the tire is measured using the *Wireless Internal Tire Sensors (WITS)* developed by Naranjo [42] at the Advanced Vehicle Dynamics Laboratory. The WITS system consists of infrared emitting diodes (IRED) mounted on the tire rim, the control program chooses the IRED approaching the contact patch and records the deflection data till the IRED passes over the contact patch. Then, the control program sets the next IRED into action of measuring the deflection.

The deflected rolling radius was measured using WITS at different normal load and inflation pressures for both, the buffed and the treaded SRTTs. Once the deflected rolling radius was known, and keeping the speed of the carriage constant for all runs, the tire angular velocity to achieve the desired slip ratio was calculated and inputted into the motor controller. The estimated effective rolling radius based on the deflected rolling radius was close to actual effective rolling radius, as the value of longitudinal force was measured closed

to zero. The estimated effective rolling radius with change in normal load was close to actual value, whereas the estimates with change in inflation pressure were not so close to the actual value, whereas the estimates with change in inflation pressure were not so close to the actual value.

$$Theoretical\,Slip\,Ratio = 1 - \frac{V_{carriage}}{R_{eff}.\omega} \tag{5.1}$$

The laboratory tests on the rig were based on the theoretical slip ratio formulation, as seen in Eqn. (5.1). Examining Eqn. (5.1), the first step was estimation of the effective rolling radius based on the deflected rolling radius from WITS. Knowing R_{eff}, the desired slip ratio to be achieved, and $V_{carriage}$ of the Terramechanics Rig set a constant value, the angular wheel velocity ω is calculated. $V_{carriage}$ and ω are now input into the motor controller of the Terramechanics Rig to achieve the desired slip ratio. The error associated with the estimation of the effective rolling radius R_{eff} of the tire led to observance of a small amount of drawbar pull even at 0% slip ratio.

Normal Load Control

The normal load on the tire was controlled using the Active Normal Load Control system developed by Naranjo [42] at the Advanced Vehicle Dynamics Laboratory. The system is a closed loop control system consisting of a pneumatic flow control valve. The pneumatic flow control valve regulates the amount of air flowing through the air springs based on the z−direction force feedback received from the KISTLER® sensor at the wheel hub. The voltage input to the pneumatic voltage is gradually increased, which in turn fills the air springs gradually. Once the KISTLER® sensor reads desired load level, the voltage input is held constant to the pneumatic valve. If any deviations from the desired normal

load occur during the test run, the control program adjust the voltage to pneumatic valve and corrects the normal load.

5.2 Test Results

The normalized drawbar pull−slip ratio curves were built for every test condition for slip ratio from 0% to 80%. The drawbar pull was normalized with respect to the normal force by averaging the longitudinal force in the x−direction for the 20 s steady−state slip ratio condition. A constant load on the tire was measured at the wheel hub by the KISTLER® sensor and a maximum variation of 50 N was observed in the longitudinal force. After comparing the results for three runs and ensuring minimal differences between the runs, the drawbar pull from the three runs were averaged. Additional test scenarios to study the effect of ambient temperature and aggregate application are also presented in this section.

5.2.1 Observations

As the tire rolled, a clear footprint impression was left on ice. The footprint path appeared smooth and polished compared to the rest of the ice surface, as shown in Figure 5.2; however the tire tread did not engrave the ice surface. Initially, when tests were conducted on ice that was a few weeks old, internal cracks were observed along the tire footprint, with a main crack and sub-cracks branching out as shown in Figure 5.3. A crackling noise was also heard during initial testing, as the tire rolled on ice. When tests were conducted on ice that was a few months old, no internal cracks were seen and the crackling noise was not heard.

When testing was conducted during late winter, a water film was seen on the tire

Figure 5.2: Smoothing and polishing of the ice surface by the tire footprint after testing on three parallel tracks.

Figure 5.3: Internal cracking of the ice in the Terramechanics Rig during the first few weeks of testing.

tread when being installed on the Rig, and was wiped off before every run. After installation of the tire enclosure, the condensation on the tire tread was eliminated. No prominent water film produced by frictional melting was seen by the naked eye when testing was observed.

5.2.2 Repeatability of Test Results

A good repeatability was observed with the normalized drawbar pull measured on the Terramechanics Rig for the treaded and the buffed SRTT between each of the three test runs. A maximum standard deviation of 0.11 was calculated, indicating that the normalized drawbar pull lied in a narrow band. Figure 5.4 shows the deviation between the three test runs for the treaded SRTT at 100% load and inflation pressure, a maximum deviation of 0.11 was observed at a slip ratio of 25%. The maximum standard deviation for the buffed SRTT for the case of 100% load and inflation pressure of 0.10 was observed at a slip ratio of 0%, as seen in Figure 5.5.

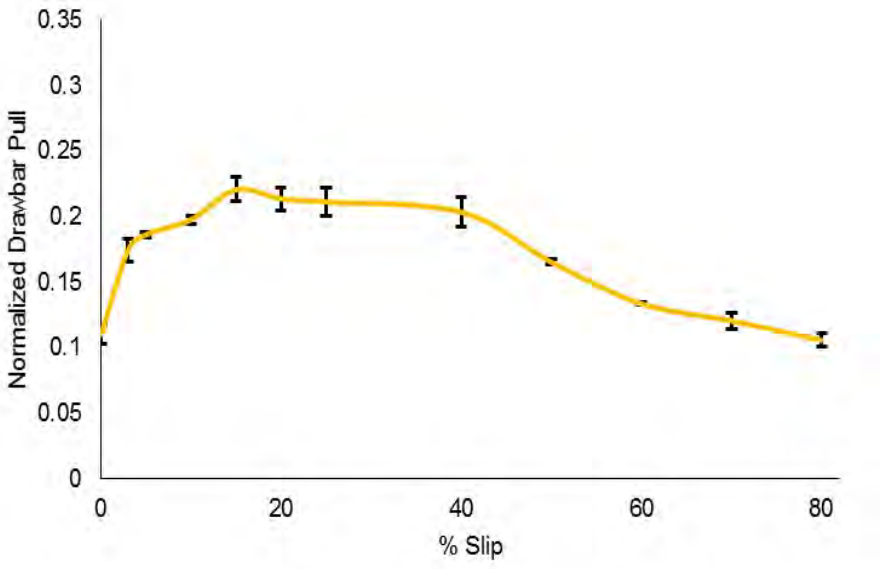

Figure 5.4: Variations of normalized drawbar pull from three test runs for the treaded SRTT. Ice surface temperature of $-10\,^{\circ}$C, 100% inflation pressure of 242 kPa, and 100% load of 7000 N.

Tests were also conducted to understand the repeatabilty of the measured drawbar bar pull with effect of longitudinal velocity of the carriage of the Terramechnaics Rig. 5 test runs were conducted at a slip ratio corresponding to the peak drawbar pull at nominal values

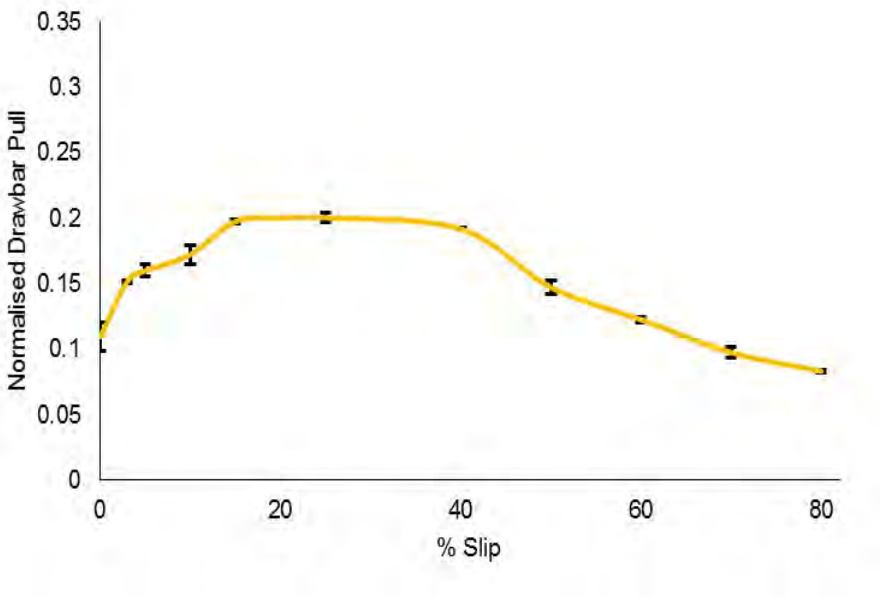

Figure 5.5: Variations of normalized drawbar pull from three test runs for the buffed SRTT. Ice surface temperature of $-10\,^{\circ}$C, 100% inflation pressure of 242 kPa, and 100% load of 7000 N.

of load and inflation pressure. The results are presented using bar plots for the treaded and the buffed SRTT, as seen in Figure 5.6 and Figure 5.7 and the metrics are tabulated in Table 5.2. A standard deviation of of 0.01 was observed for the buffed and treaded SRTTs. The ratio of standard deviation to mean also was found to be less than 5% for both the tires.

Table 5.2: Repeatabilty analysis of peak normalized drawbar pull.

	Treaded SRTT	Buffed SRTT
Run 1	0.27	0.21
Run 2	0.28	0.22
Run 3	0.28	0.22
Run 4	0.28	0.23
Run 2	0.28	0.22
Mean	0.28	0.22
σ	0.01	0.01
$\sigma/Mean$ (%)	2	3

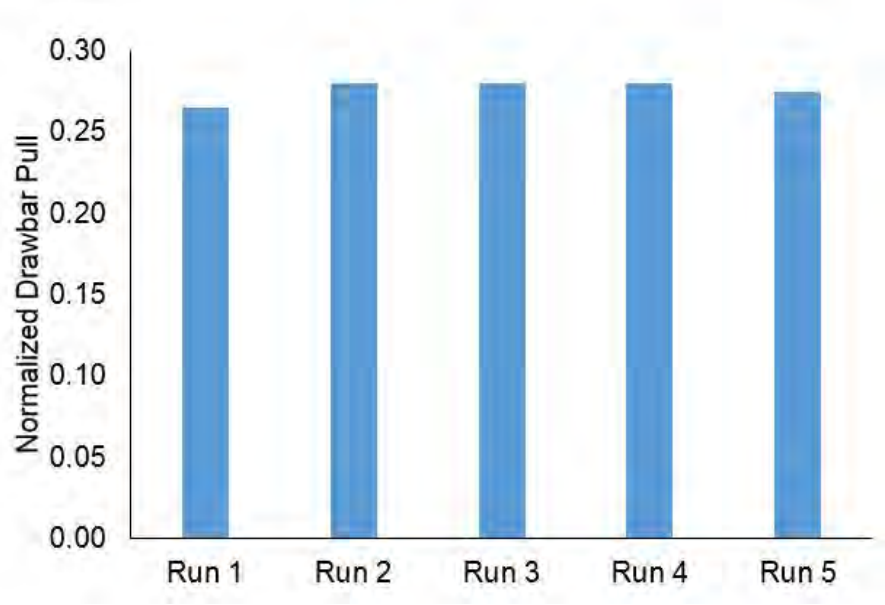

Figure 5.6: Variations of peak normalized drawbar pull from five test runs for the buffed SRTT. Ice surface temperature of $-10\,^{\circ}$C, 100% inflation pressure of 242 kPa, and 100% load of 7000 N.

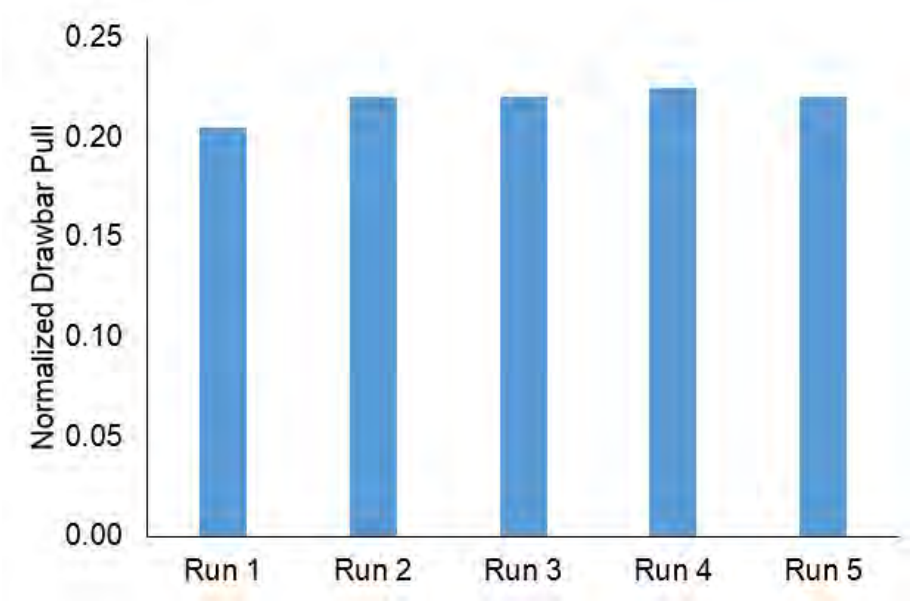

Figure 5.7: Variations of peak normalized drawbar pull from five test runs for the buffed SRTT. Ice surface temperature of $-10\,^{\circ}$C, 100% inflation pressure of 242 kPa, and 100% load of 7000 N.

5.2.3 Effect of Normal Load

The 16' SRTT has a load index of 97 which is 7161 N; tests were conducted at three normal loads of 4000 N, 7000 N, and 8500 N, which correspond to 60%, 100%, and 120% load index, respectively. A good repeatability was observed between the three runs and tests were conducted for dry friction on ice.

The treaded SRTT showed a decrease in the drawbar pull with increase in normal load, as seen in Figure 5.8. The peak drawbar pull occurred at 5% slip ratio with 60% load index and at 15% slip ratio with 100% and 120% load index. The buffed SRTT showed the same trend as the treaded SRTT until a slip ratio of 20%, as seen in Figure 5.9, after which a clear trend of the effect of the drawbar pull with change in normal load was not observed. The peak drawbar pull for the buffed SRTT occurred at 10% slip ratio with 60% load index and at 5% slip ratio with 100% and 120% load index.

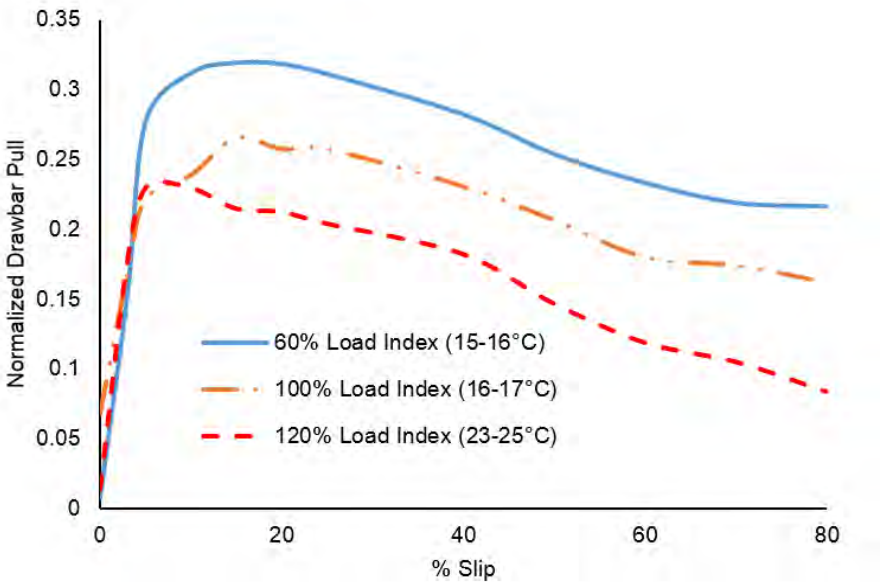

Figure 5.8: Effect of normal load on drawbar pull for the treaded SRTT on ice with dry friction. 100% inflation pressure of 242 kPa, the temperature indicated on plots is the laboratory temperature when testing was conducted.

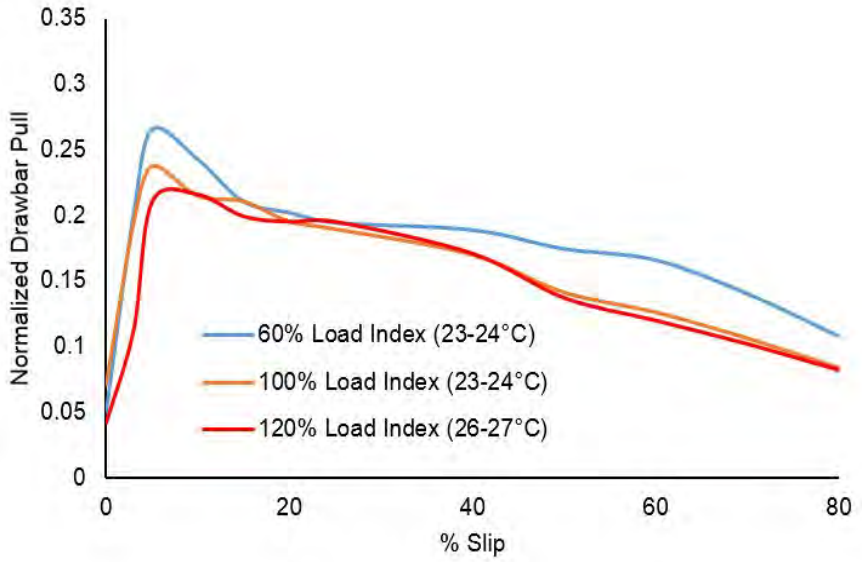

Figure 5.9: Effect of normal load on drawbar pull for the buffed SRTT on ice with dry friction. 100% inflation pressure of 242 kPa, the temperature indicated on plots is the laboratory temperature when testing was conducted.

The drawbar pull−slip ratio curves in this section and the following sections indicate a small amount of traction at zero slip ratio. This is due to the difficulty encountered in precisely collecting data at zero slip ratio on the Terramechanics Rig. The error in estimation of the effective rolling radius and the complexity of the rig lead to observance of a small amount of traction at zero slip ratio.

5.2.4 Effect of Inflation Pressure

The rated inflation pressure for 16 SRTT is 242 kPa. To understand the effect of inflation pressure on drawbar pull when running on ice, three levels of inflation pressure were chosen at 60%, 100%, and 120% of the rated pressure. Thus, tests were conducted at 145 kPa, 242 kPa, and 276 kPa.

An increase in the normalized peak drawbar pull with reduction in inflation pressure

was observed for the treaded SRTT as in Figure 5.10, at low slips all the three inflation pressures exhibited the same drawbar pull. Higher drawbar pull with a reduction in inflation pressure was observed from 20% to 50% slip ratio. At slip ratios above 50%, the 100% and 120% inflation pressure cases had almost the same drawbar pull. At high slip ratios and with 60% inflation pressure, the treaded SRTT showed a drop in drawbar pull. At high slip ratios and lower inflation pressures, an increased contact area and increased heat generated in the contact patch leads to reduction in the tractive forces.

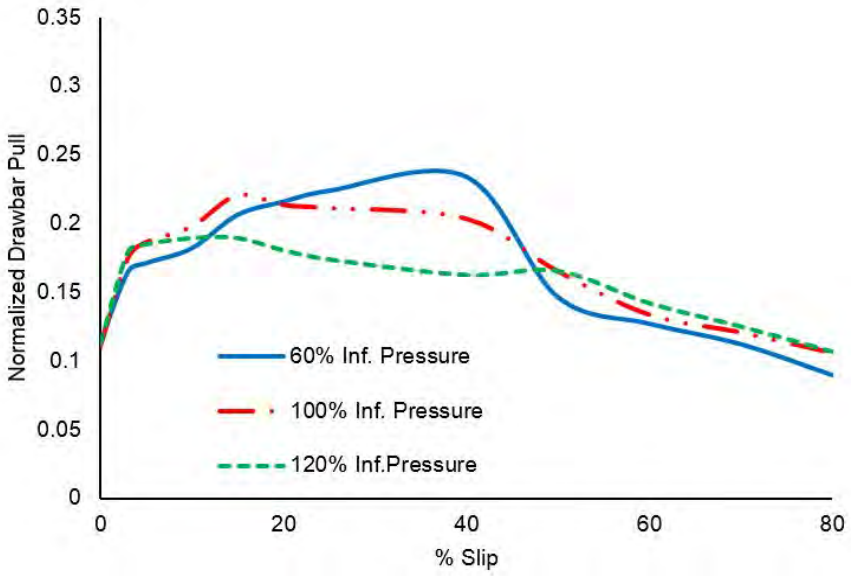

Figure 5.10: Effect of inflation pressure on drawbar pull for the treaded SRTT on ice with dry friction, with load of 100% the load index 7000N.

A clear trend of variation in drawbar pull with change in inflation pressure was not observed with the buffed SRTT, as in Figure 5.11. The 120% inflation pressure case experienced a maximum drawbar pull until 15% slip ratio; at higher slip ratios the 100% inflation pressure showed the highest drawbar pull. At 50% slip ratio a drop in drawbar pull was seen for all the three inflation pressures; an increase in heat generation in the contact patch leads to this drop.

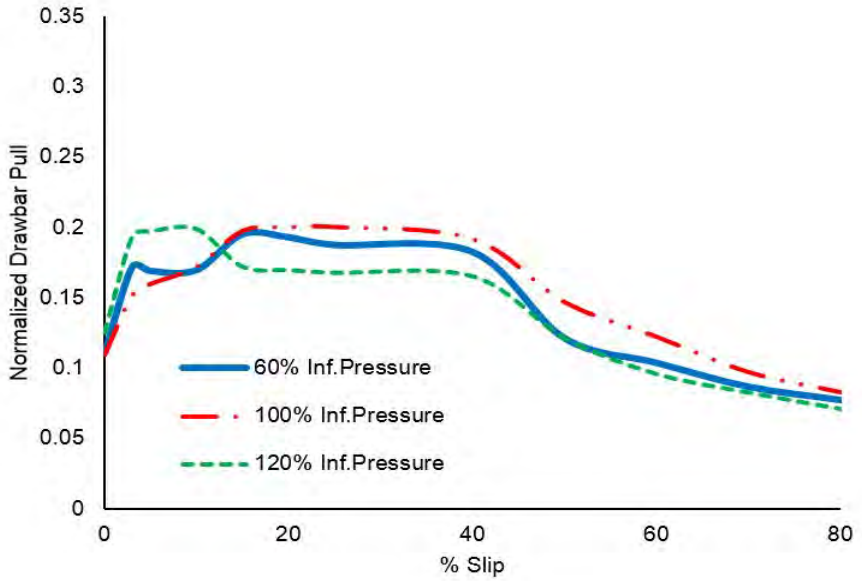

Figure 5.11: Effect of inflation pressure on drawbar pull for the buffed SRTT on ice with dry friction, with load of 100% the load index 7000N.

5.2.5 Effect of Tread Depth

This section compares the treaded SRTT and the buffed SRTT at three levels of normal load and inflation pressures. The effect of tread in increasing traction and safety can be clearly appreciated from Figure 5.12 and Figure 5.13, which compare the drawbar pull slip ratio curves when loaded with 60% and 120% of the load index. When tested with 60% load index, the peak drawbar pull occurred at 5% slip ratio for the buffed tire and at 15% slip ratio for the treaded tire; for 100% load index, the peak drawbar pull occurred at 5% slip ratio and at 15% slip ratio for the buffed tire and the treaded SRTT, respectively. When tested with 120% of the load index, the treaded tire performed better up to a slip ratio of around 55%, as seen in Figure 5.14, after which both, the treaded and the buffed tire, performed the same.

During operation with 60% inflation pressure, until 5% slip ratio, the buffed tire and the treaded tire perform the same; after 5% slip ratio, the treaded tire performs better than

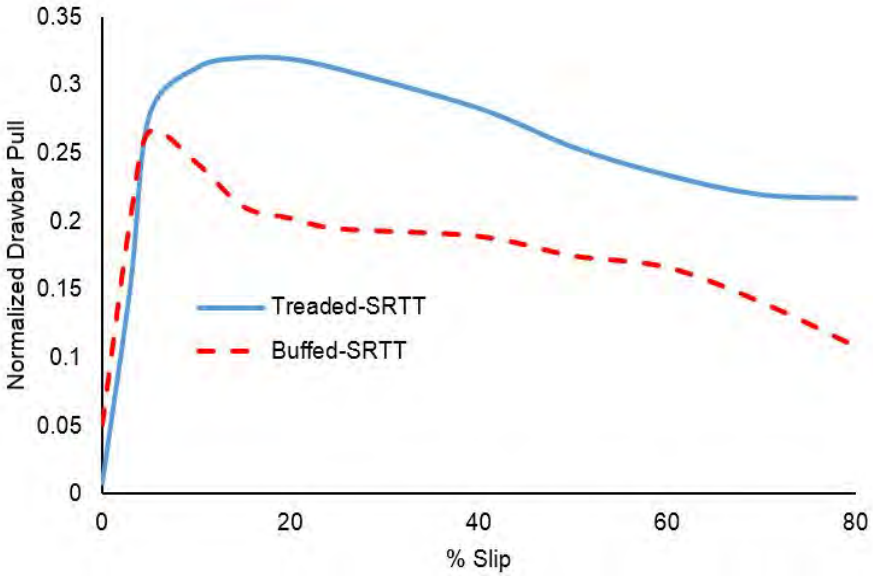

Figure 5.12: Comparison of drawbar pull slip ratio curves for the treaded and buffed SRTT at 60% load index (4000 N) with inflation pressure 242 kPa for dry friction condition.

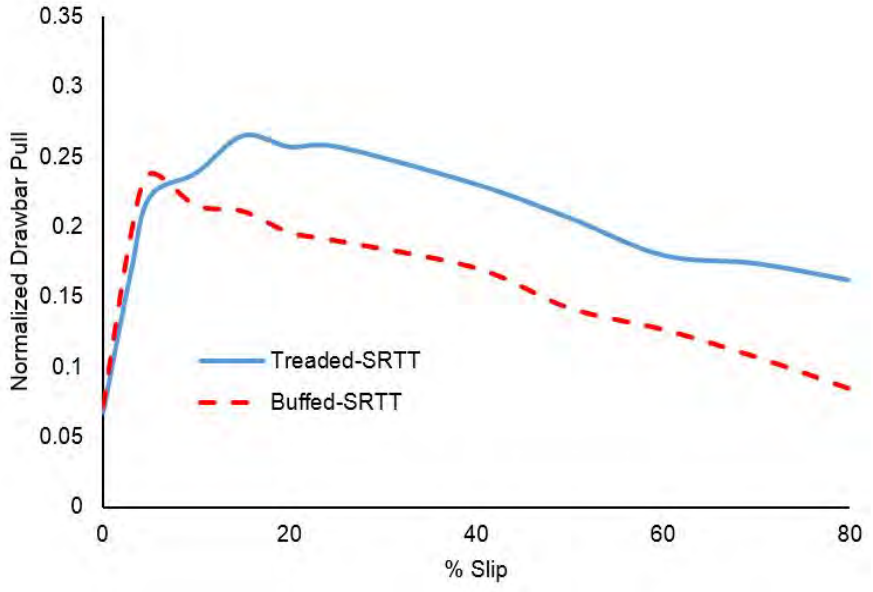

Figure 5.13: Comparison of drawbar pull slip ratio curves for the treaded and buffed SRTT at 100% load index (7000 N) with inflation pressure 242 kPa for dry friction condition.

the buffed tire, as seen Figure 5.15. When operating with nominal inflation pressure, the treaded tire exhibits higher drawbar pull compared to the buffed tire, for all slip ratios, as

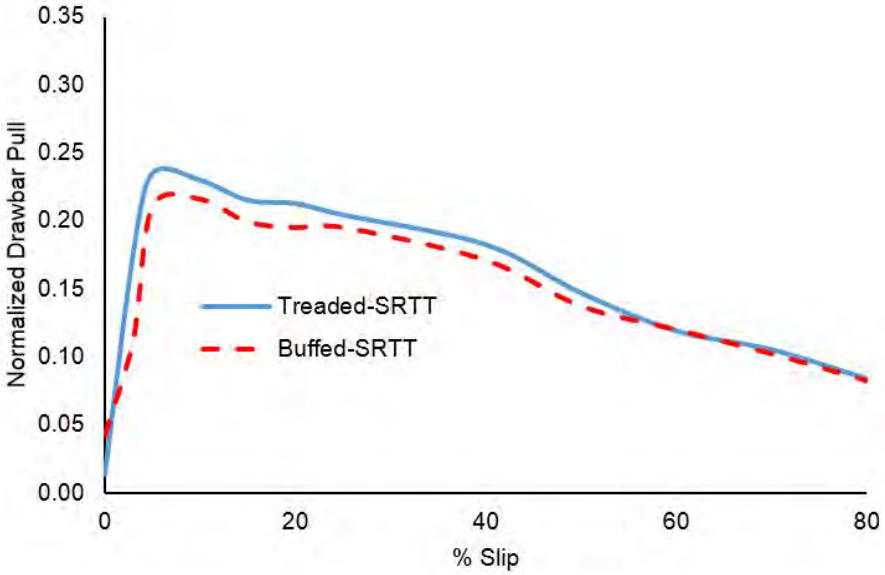

Figure 5.14: Comparison of drawbar pull slip ratio curves for the treaded and buffed SRTT at 120% load index (8500 N) with inflation pressure 242 kPa for dry friction condition.

seen in Figure 5.16. Figure 5.17 shows the comparison when operating with 120% of the rated inflation pressure; until 40% slip ratio a clear trend is not observed, but after 40% slip ratio the treaded tire shows an increased drawbar pull as compared to the buffed tire.

5.2.6 Effect of Toe Angle

Tests runs were conducted by varying the toe angle on ice at temperature close to 0 °C, with the treaded SRTT. The tire travelled along a straight line at different toe angles, thus, a variation in the lateral force was not seen, and the lateral force remained constant at different slip ratios. Variation in the longitudinal force with change in toe angle was observed; the decrease in drawbar pull was seen with increase in toe angle.

A prominent effect on the drawbar pull was not observed by variation of toe angle from 0° to 1.5°, as seen in Figure 5.18; a decrease in drawbar pull was seen with a 2° toe angle. A reduction in the peak drawbar pull was observed with increase in toe angle, as seen

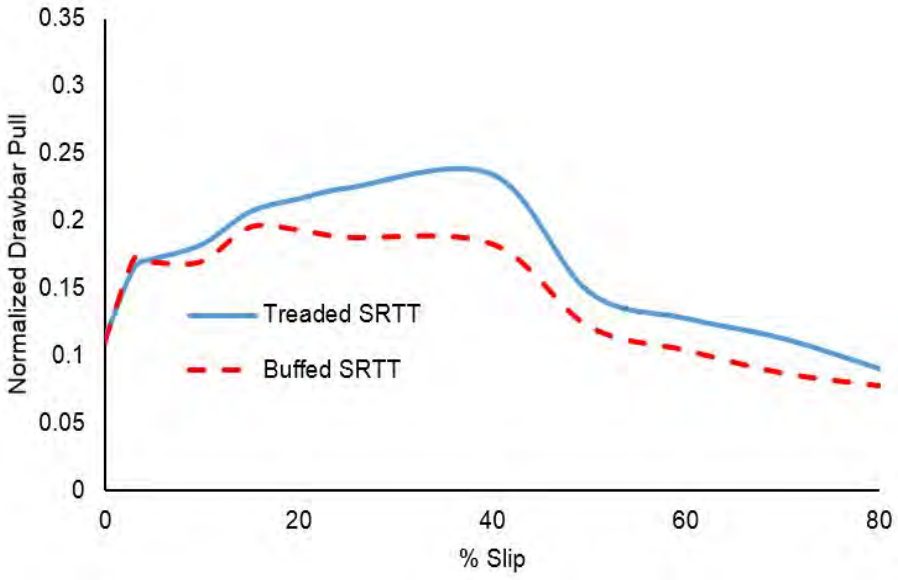

Figure 5.15: Comparison of drawbar pull slip ratio curves for the treaded and buffed SRTT with 60% inflation pressure of 145 kPa with normal load of 100% load index (7000 N) for dry friction condition.

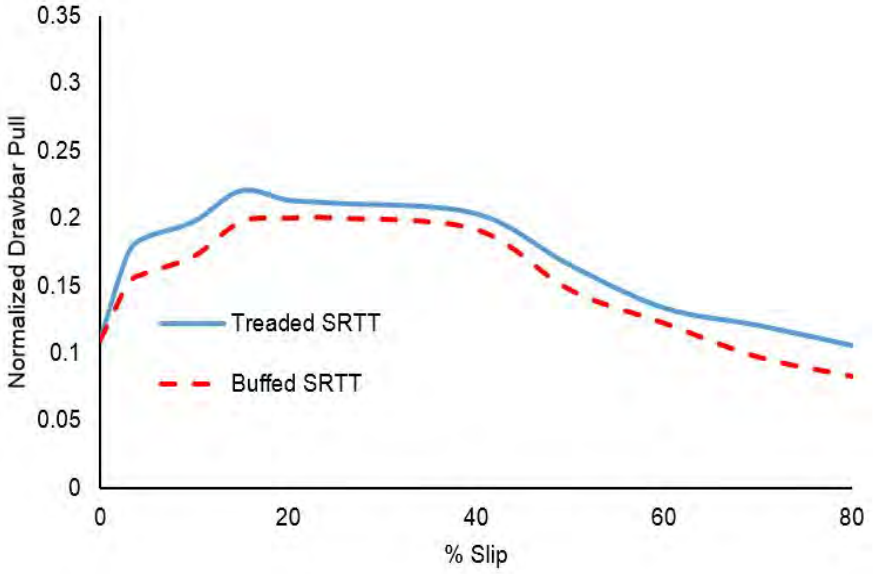

Figure 5.16: Comparison of drawbar pull slip ratio curves for the treaded and buffed SRTT with 100% inflation pressure of 242 kPa with normal load of 100% load index (7000 N) for dry friction condition.

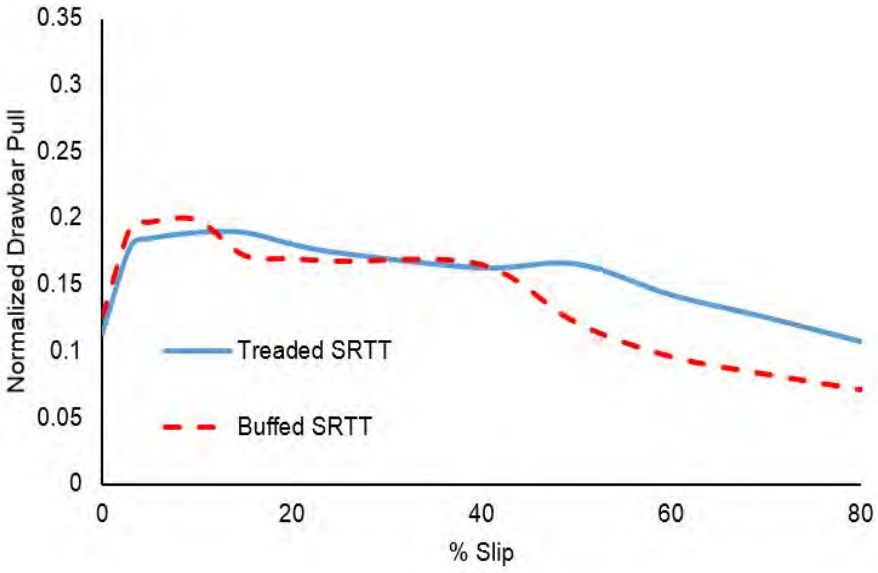

Figure 5.17: Comparison of drawbar pull slip ratio curves for the treaded and buffed SRTT with 120% inflation pressure of 276 kPa with normal load of 100% load index (7000 N) for dry friction condition.

in Figure 5.19; the reduction in the peak drawbar pull was marginal up to 1.5°, after which a sharp decrease was observed.

5.2.7 Effect of Camber Angle

The effect of the camber angle on the drawbar pull was studied at different slip ratios using the treaded SRTT during operation on ice with a temperature close to 0 °C. The tire travelled along a straight line with camber angles of 0° and 2°, the lateral force remained constant during the test runs. The drawbar pull variation with change in camber angle can be seen in Figure 5.20; until 5% slip ratio no difference was seen in the drawbar pull. After 5% slip ratio, a slight variation was seen in the drawbar pull levels; the drawbar pull for a 2° camber angle was slightly higher than for 2° camber angle.

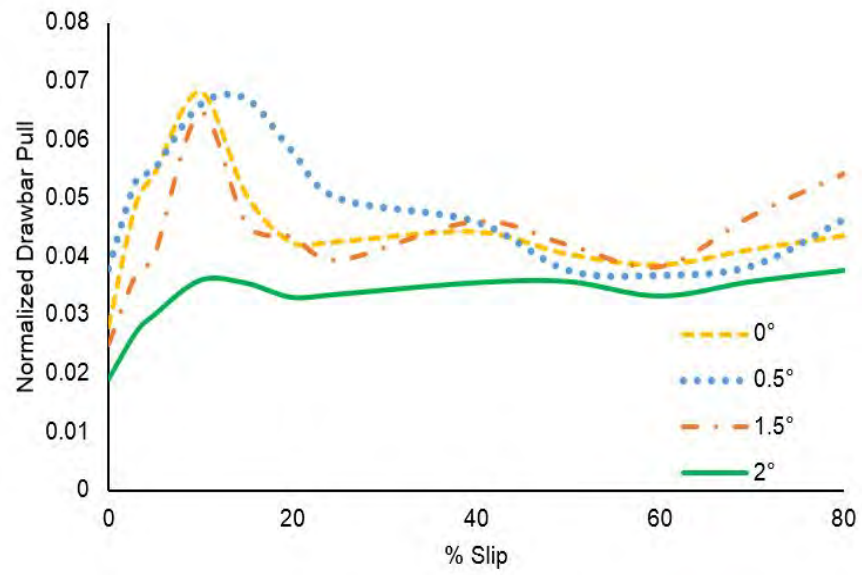

Figure 5.18: Comparison of drawbar pull slip ratio curves for the treaded SRTT with variation in toe angle. 100% inflation pressure of 242 kPa with normal load of 100% load index (7000 N), on ice with wet friction.

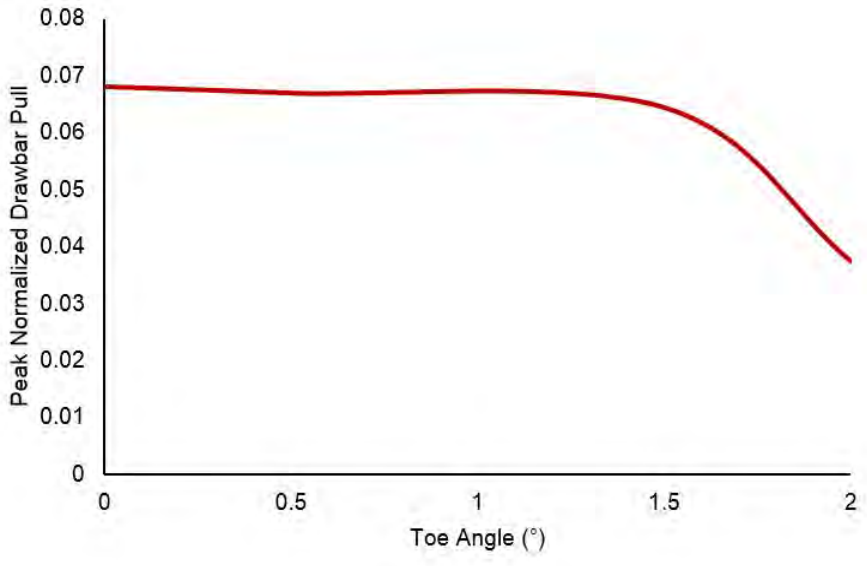

Figure 5.19: Variation of peak drawbar pull with toe angle for the treaded SRTT. 100% inflation pressure of 242 kPa with normal load of 100% load index (7000 N), on ice with wet friction.

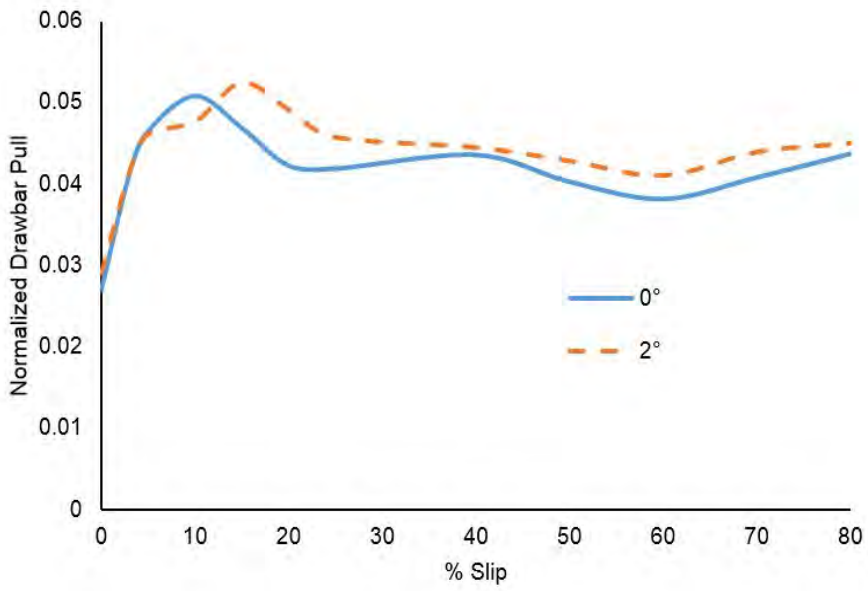

Figure 5.20: Comparison of drawbar pull slip ratio curves for the treaded SRTT with variation of camber angle. 100% inflation pressure of 242 kPa with normal load of 100% load index (7000 N), on ice with wet friction.

5.2.8 Effect of Ambient Temperature

To study the effect of ambient temperature on drawbar pull during operation on ice we conducted tests on different days with varying ambient temperature in the laboratory. The effect of the installation of the tire enclosure was also studied be comparing the drawbar pull vs. slip ratio curves of tests conducted at different laboratory temperatures.

A reduction in the drawbar pull with decrease in the ambient temperature was seen, as presented in Figure 5.22. The properties of the tread compound vary with temperature; the tread of the tire usually becomes harder with a reduction in temperature. A clear drop is thus seen in the drawbar pull with a decrease in the ambient temperature. The drawbar pull vs. slip ratio curves for the $-5\,^{\circ}\mathrm{C}$ case and for the case in which the tire enclosure was used are close, hence it can be concluded that the tire enclosure performs very well, maintaining a low temperature around the tire during the test runs.

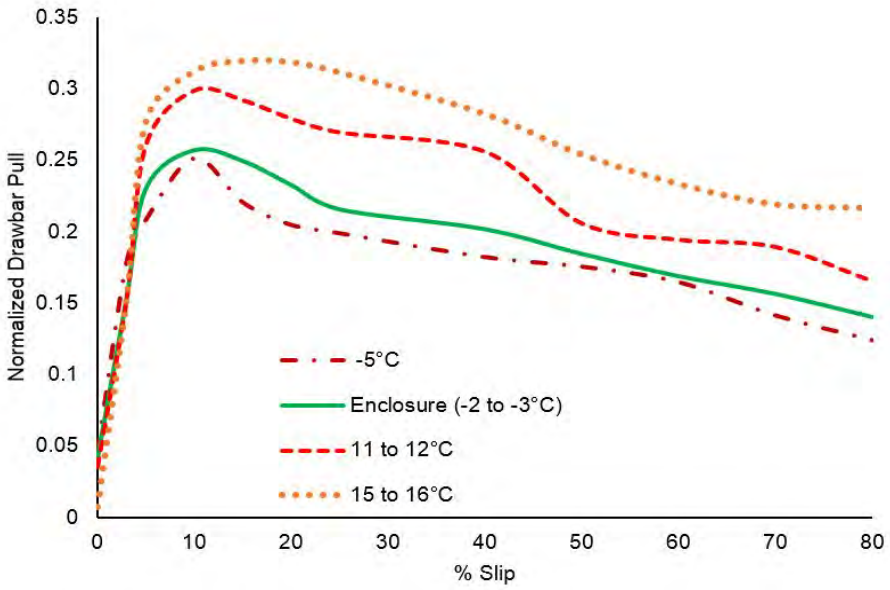

Figure 5.21: Comparison of drawbar pull slip ratio curves for the treaded SRTT with variation of ambient temperature. 100% inflation pressure of 242 kPa with normal load of 100% load index (7000 N), on ice with dry friction.

5.2.9 Effect of Ice Surface Temperature

The ice surface and the ambient temperature decide if the frictional phenomenon at the tire-ice interface is of dry or wet nature. At temperature close to 0 °C there is a formation of a water film in the contact patch due to frictional melting of the ice. Dry friction is predominant at temperatures of −10 °C and lower; the heat generated in the contact patch is not sufficient to melt the ice surface.

Both, the treaded SRTT and the buffed SRTT, were tested for wet and dry friction conditions. The treaded SRTT performed better than the buffed SRTT for both wet and dry friction conditions, as seen in Figure 5.22. A 32% decrease in the peak drawbar pull was observed between the wet and dry friction conditions for the treaded SRTT, and a 42% decrease in the peak drawbar pull was observed for the buffed tire.

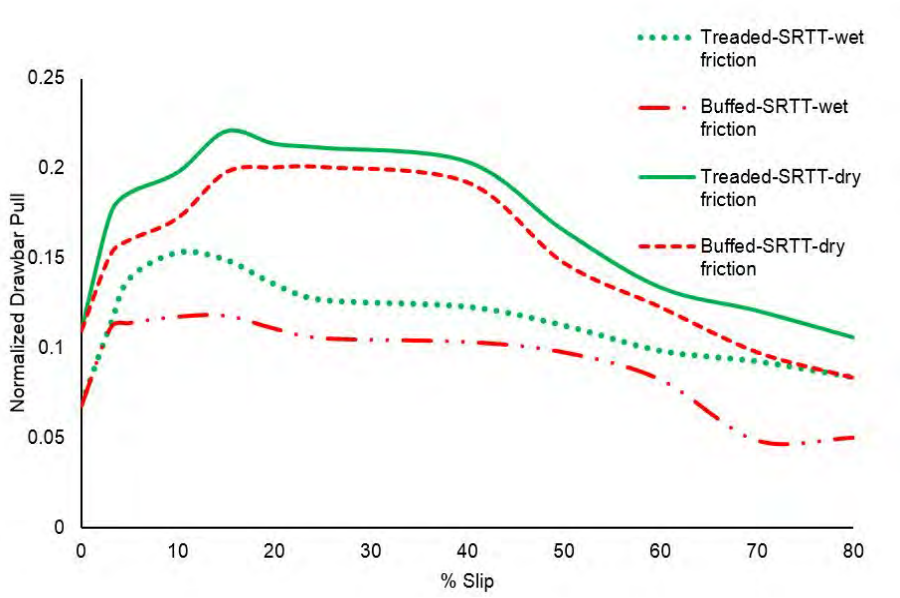

Figure 5.22: Comparison of drawbar pull slip ratio curves for the treaded and buffed SRTT at ice temperatures of $-3\,^{\circ}\mathrm{C}$ for wet friction and $-10\,^{\circ}\mathrm{C}$ for dry friction. 100% inflation pressure of 242 kPa with normal load of 100% load index (7000 N).

5.2.10 Effect of Aggregate Application on Ice Surface

Aggregate application on ice-covered roads is a common practice by the town or city administrations during winter months. Tests were conducted on the ice surface at a surface temperature of $-10\,^{\circ}\mathrm{C}$ covered with different friction modifiers, to understand the increase in traction levels by application of such aggregates on the ice surface.

A 300% increase is observed in the peak drawbar pull during operation on ice covered with soil and slush (shaved ice and water mix), compared to wet ice (ice covered with a thin layer of liquid water). The tire performance on ice surfaces covered with different aggregates can be seen in Figure 5.23. Slush with soil on ice provided the best traction, while wet ice provided the least friction. Tests runs were conducted with a uniform aggregate applied on the ice surface. Other factors, such as particle size of the aggregate and rate of application of the aggregate would also affect the tire performance characteristics; however, they were

not considered for this study.

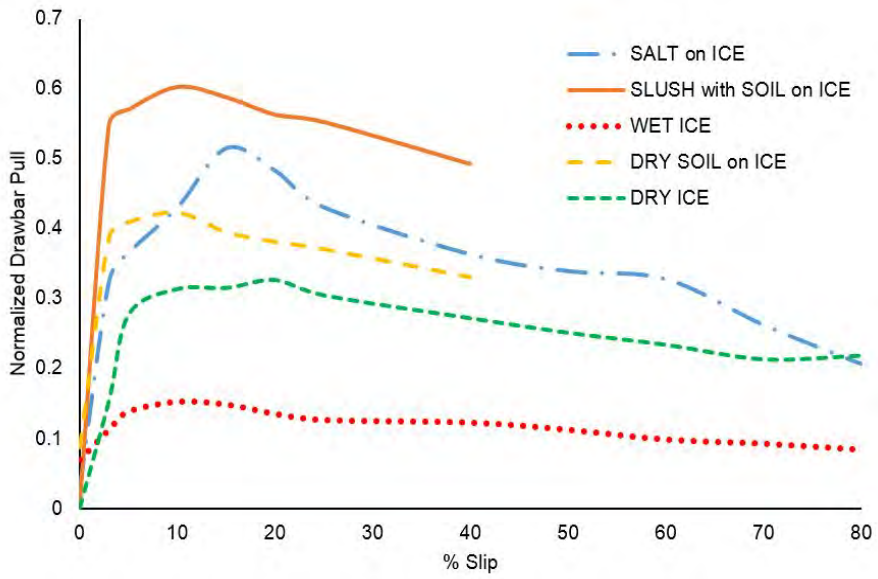

Figure 5.23: Comparison of drawbar pull slip ratio curves for the treaded SRTT on different ice surface conditions. 100% inflation pressure of 242 kPa with normal load of 60% load index (4000 N).

5.3 Summary and Conclusions

In this chapter, the effect of operational parameters, namely load on the tire, inflation pressure, toe angle, tread depth, camber angle, ice temperature, ambient temperature and type of ice surface were studied using the SRTT, during operation on ice using the Terramechanics Rig. A reduction in the drawbar pull with an increase in the normal load was seen for both, the buffed and the treaded SRTT, for the entire slip ratio range. An increase in the peak drawbar pull was seen with a reduction in the tire inflation pressure. When operating at lower inflation pressures, an increased contact area was observed that leads to increased friction levels at low slips. However, at high slips, with an increased contact area there is also an increased heat generation, which enhances frictional melting of the ice surface, thus

the friction levels are lower at higher slips. The variation of the toe angle until about 1.5° decreases the peak friction level minimally, after which a sharp decrease is noticed. The tread on the tire plays an important role in increasing the available friction during all conditions of load and inflation pressure, but at high slip ratios the effect of tread is also negligible. The aggregate application also plays a major role in increasing traction on icy roads; heavier particles are preferred, as they do not get thrown as the tire rolls on the ice surface.

Chapter 6

Outdoor Test Program

This chapter has been adapted from [40] by A.K. Bhoopalam, C. Sandu and S. Taheri. This paper is included in this dissertation with permission from Elsevier. Agreement attached.

Outdoor tests are an actual representation of the real world conditions, to understand the performance of the SRTTs outdoors, field tests were conducted at the Keweenaw Research Center in Calumet, Michigan, USA by Mobility Research Inc. The outdoor testing program included studying the performance of the two SRTTs on ice with dry friction, at three levels for normal load and inflation pressure, in February 2014. The tests were conducted using a traction truck, with the test tire on the right-rear wheel, as seen in Figure 3.14. Testing was conducted on split$-\mu$ track as seen in Figure 3.13, with the left wheels on asphalt and the right wheels on the ice surface. The test program commenced in the evening to have no effect of the solar load.

6.1 Test Conditions

Outdoor testing was conducted for a reduced experiment matrix compared to the one presented in Table 4.1; testing with different levels for the camber angle, toe angle, and ice temperature was not a part of the outdoor test program. All outdoor tests were conducted at 0° camber and toe, at an ice temperature of $-13\,^{\circ}\mathrm{C}$ and an ambient temperature of $-18\,^{\circ}\mathrm{C}$. The design of experiment matrix for the outdoor testing program is as shown in Table 4.2.

6.1.1 Terminology

The tire performance evaluated in the field at the Keweenaw Research Center (KRC) is expressed in terms of a driving coefficient. The outdoor test program was carried out as per the procedure ASTM-1805 [22]. ASTM-1805 defines the driving coefficient as the ratio of longitudinal force and vertical load. In the indoor test program of this study the results are expressed are expressed in terms of the normalized drawbar pull. According to the ISTVS standards [45], the drawbar pull refers to the force available for external work in a direction parallel to the horizontal surface over which the vehicle is moving, which refers to force the longitudinal force measured in the x−direction. Thus the normalized drawbar pull [45] is analogous to the driving coefficient [22]; in the interest of keeping the terminology as per ASTM- 1805, the results from the field testing are expressed using the expression driving coefficient.

6.2 ASTM−1805

Field testing was conducted as per ASTM-1805 [22], with the buffed and treaded tires as the candidate tires; the treaded SRTT was also used as the control tire. The control tire

was run every third condition, to follow the sequence of C (control), T1, T2, C, T3, T4, C, as specified in [22]. Initial test procedures before the test program included spraying a thin layer of water (using a water truck) on the ice surface; a wide tire is then used to polish the ice surface once the water layer is frozen.

Ten spin-ups were conducted for each test condition, as per Table 4.2, following the sequence of running the control tire every third test. Each spin-up lasted for about 3 s, during which the practical slip ratio was ramped up from 0% to 300% on the right rear wheel. The test vehicle was driven in a straight line maintaining a test speed of 8.0 0.8 km/h, as specified in [22]. A two-axis wheel force transducer at the right-rear wheel center measures the forces in the x and z directions. The ratio of the x−force and the z−force is defined as the coefficient of friction in ASTM F1805-06. The practical slip ratio formulation as seen in Eqn. (6.1), was used to report the findings from the outdoor test program.

$$Practical\ Slip\ Ratio = \frac{V_{tire}}{V_{vehicle}} - 1 \tag{6.1}$$

The velocity of the tire is measured with an encoder on the right-rear wheel. The results presented in next section have been converted in theoretical slip ratio to maintain uniformity between results, as presented for the indoor test program. A step jump is observed at very low slip ratios in field test results; this is due to the fact that the practical slip ratio is ramped up from 0% to 300% in a time period of 3−4 s. The range of the driving coefficient, as measured from the outdoor test program, is 0.054−0.19, as also reported by Martin et al. [18].

6.3 Test Results

The following sub−sections describes the effect of the normal load, the inflation pressure, and the tread depth during operation on ice, as obtained from outdoor testing.

6.3.1 Repeatabilty of Test Results

An acceptable repeatability of test data was observed for the field tests conducted at the Keweenaw Research Center (KRC). However, the variation of the measured driving coefficient was in a wider band when compared to the indoor test program. The curves for the 10 spin-ups can be seen in Figure 6.1 for the treaded SRTT with 100% load and inflation pressure; a standard deviation of 0.006 was calculated for the measured peak values. Figure 6.2 shows the measured curves for the buffed SRTT with 100% load and inflation pressure, a wider deviation was calculated for the at the peak value of 0.035 compared to the treaded SRTT.

6.3.2 Effect of Normal Load

Outdoor tests were conducted for three levels of normal load of 60%, 100%, and 120% of the load index. At low slip ratios, the higher the normal load, the lower the friction coefficients were seen for both, the buffed and treaded SRTT. The treaded SRTT exhibited this trend until a slip ratio of 30%, as seen in Figure 6.3, and for the buffed tire until 17% slip ratio, as seen in Figure 6.4. Above these slip ratios, both, the treaded and the buffed SRTT, exhibited the same behavior and no trend was seen with variation in the normal load.

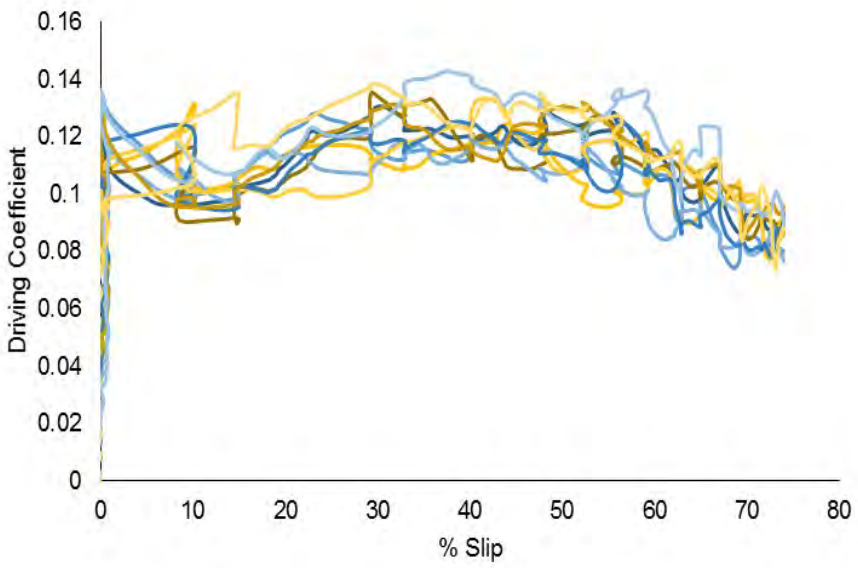

Figure 6.1: Variation in measured driving coefficient from 10 spin ups for the treaded SRTT. 100% inflation pressure of 242 kPa and 100% normal load of 7000 N.

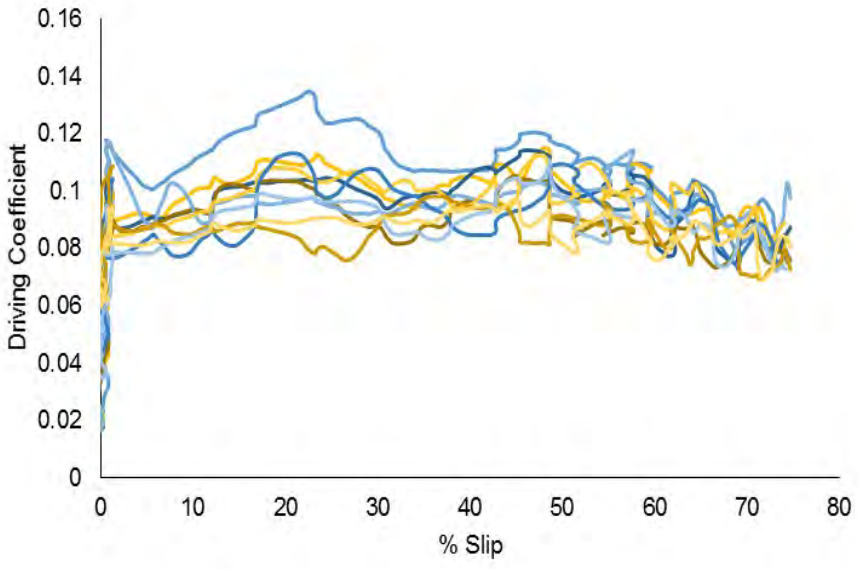

Figure 6.2: Variation in measured driving coefficient from 10 spin ups for the buffed SRTT. 100% inflation pressure of 242 kPa and 100% normal load of 7000 N.

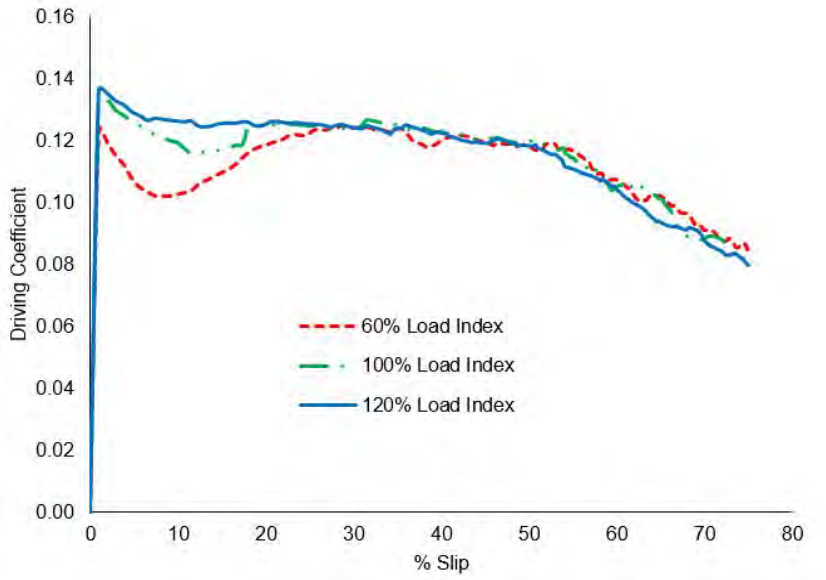

Figure 6.3: Effect of normal load on drawbar pull for the treaded SRTT on ice with 100% inflation pressure (242 kPa), from outdoor testing.

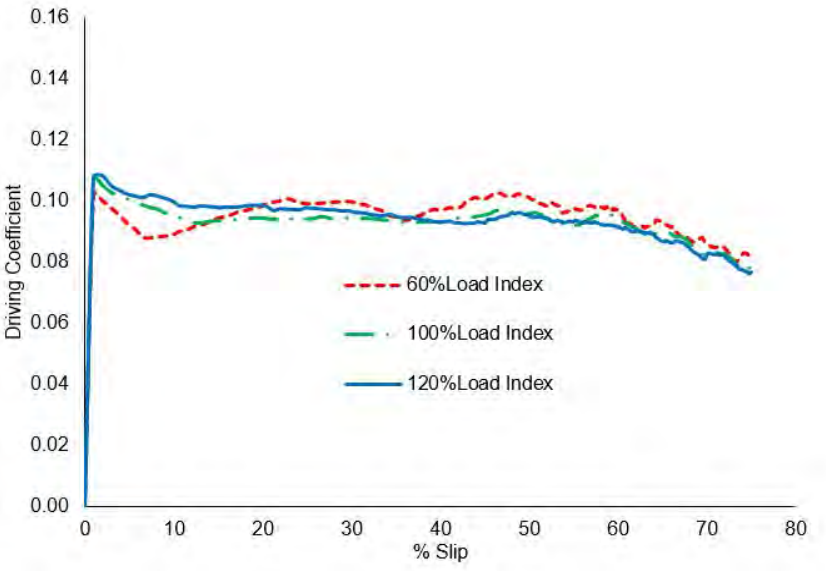

Figure 6.4: Effect of normal load on drawbar pull for the buffed SRTT on ice with 100% inflation pressure (242 kPa), from outdoor testing.

6.3.3 Effect of Inflation Pressure

The effect of the inflation pressure on the friction coefficient was also studied through field tests. As seen from Figure 6.5 and Figure 6.6, a variation in the friction levels was seen

at low slip ratios; however, a clear trend was observed. At higher slip ratios the effect of the inflation pressure was not noticed. For all levels of inflation pressure both, the treaded and the buffed SRTT, performed the same with friction vs. slip ratio curves overlapping.

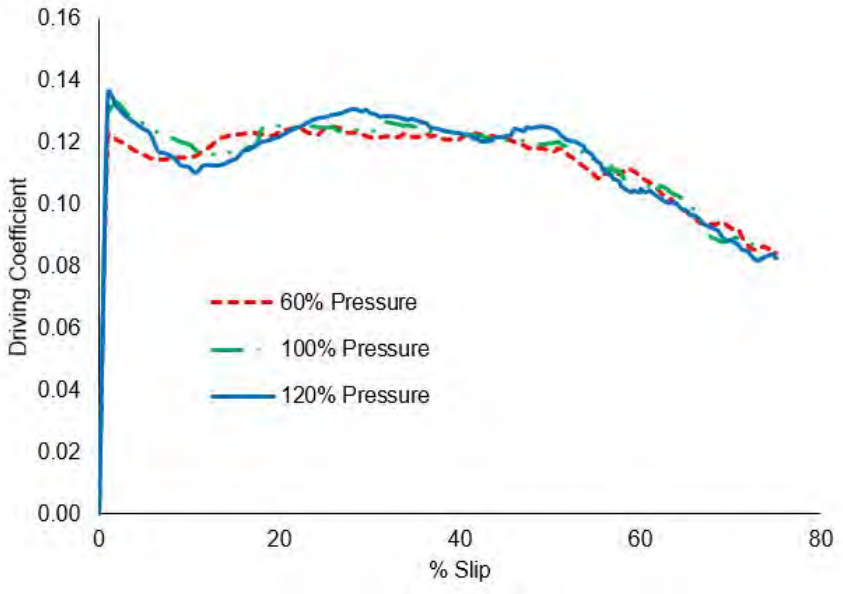

Figure 6.5: Effect of inflation pressure on drawbar pull for the treaded SRTT on ice with 100% normal load (7000N), from outdoor testing.

6.3.4 Effect of Tread Depth

Comparing the buffed and the treaded SRTT at three levels of inflation pressure and three levels of normal load, the treaded SRTT provided better friction levels compared to the buffed SRTT all the time. An increase of 35% in friction levels was seen from the buffed SRTT to the treaded SRTT operating with a 100% load index and at the nominal inflation pressure, as seen from Figure 6.7 and Figure 6.8. The effect of inflation pressure and normal load on the tire was not predominant at high slip ratios, all the friction levels were seen to overlap after a slip ratio of 65%. Hence, at high slip ratios, the SRTT performs similarly, irrespective of the tread depth, inflation pressure, and the load on the tire during operation

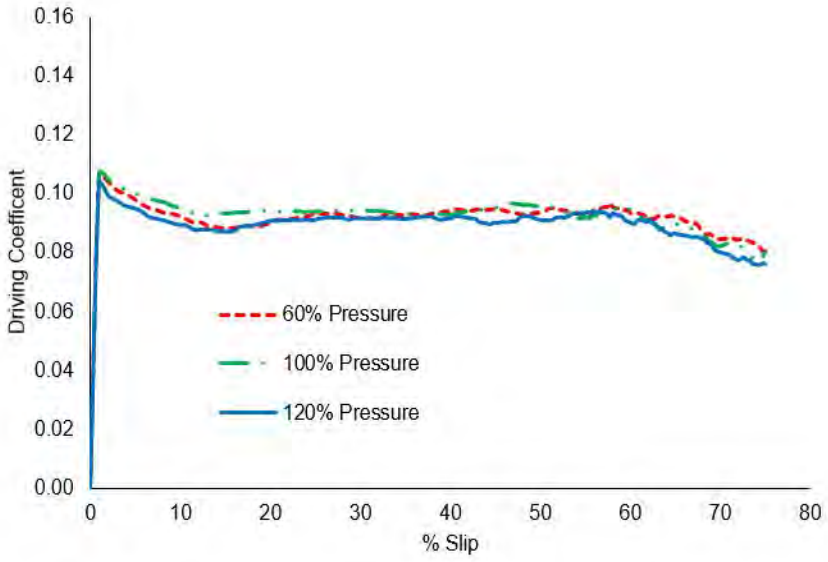

Figure 6.6: Effect of inflation pressure on drawbar pull for the buffed SRTT on ice with 100% normal load (7000N), from outdoor testing.

on ice.

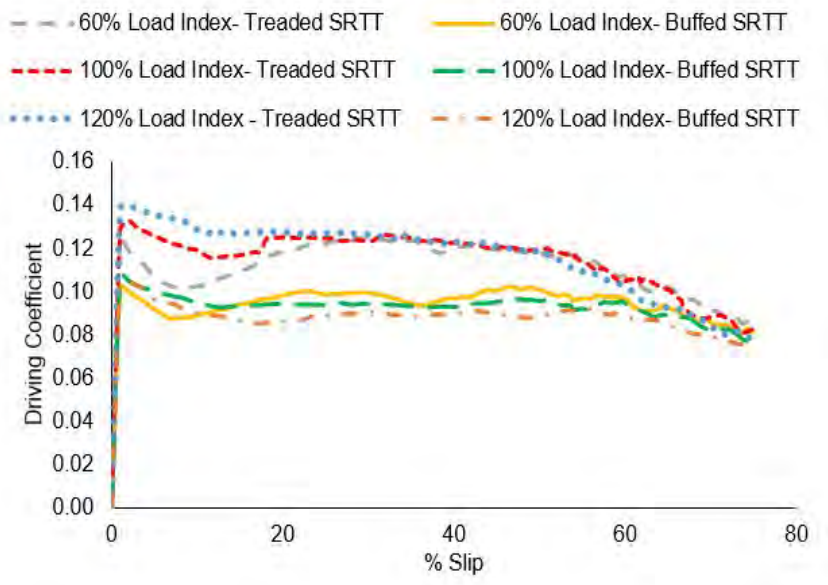

Figure 6.7: Comparison of friction slip ratio curves for the treaded and buffed SRTT with 100% inflation pressure of 242 kPa at different normal loads, from outdoor testing.

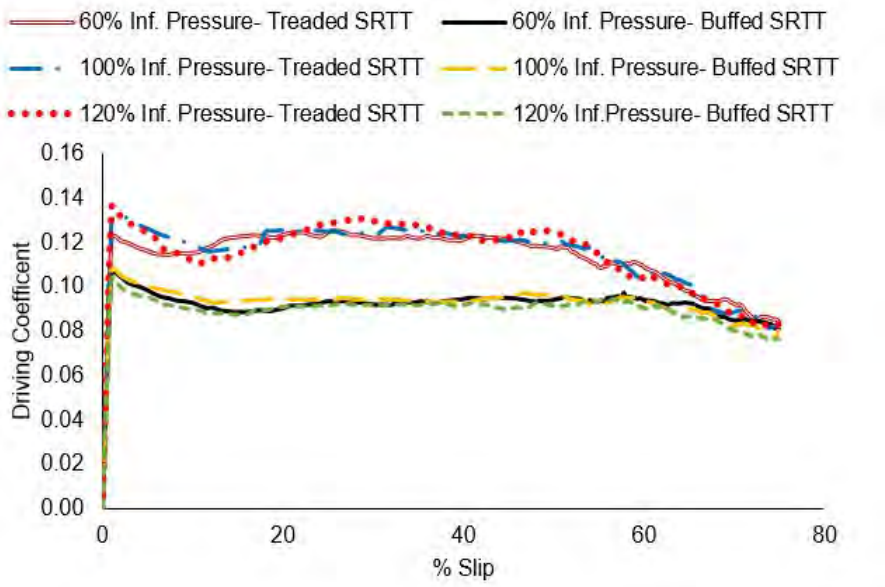

Figure 6.8: Comparison of friction slip ratio curves for the treaded and buffed SRTT with 100% normal load of 7000 N with different inflation pressures, from outdoor testing.

6.4 Summary and Conclusions

In this chapter, the results from field testing at the Keweenaw Research Center were presented. The outdoor testing program led to the understanding of the effect of inflation pressure, normal load, and tread depth during the operation of the SRTT on ice. The variations of friction levels with normal load were seen in an opposite trend compared to indoor testing at low slip ratios and at high slip ratios the effect of the normal load was not noticed. No increasing or decreasing trend of friction levels was observed with variation in the inflation pressure when tested as per ASTM−1805. However, the effect of the tread in clearly improving traction on icy surfaces was captured even with the outdoor testing program.

Chapter 7

Comparison of Indoor and Outdoor Test Programs

This chapter has been adapted from [40] by A.K. Bhoopalam, C. Sandu and S. Taheri. This paper is included in this dissertation with permission from Elsevier. Agreement attached.

This chapter compares the test results from the indoor and outdoor test programs. The effect of operational parameters, namely normal load and inflation pressure, as captured by the indoor and the outdoor programs, are explained in following sub-sections. The reasons for the differences in the performance measurements between the two test programs are explained in the next sections.

7.1 Effect of Normal Load

The effect of normal load during the operation of the treaded SRTT on ice as measured in the lab and on the field is shown in Figure 7.1. From the indoor experiments, the higher

the normal load, the lower the drawbar pull was measured. Whereas with higher normal loads, higher friction levels were measured in the field; this trend was observed until a slip ratio of 20%. Above 20% slip ratio, no clear trend was observed from the field tests and the curves for the three normal load cases were seen overlapping, as in Figure 7.1.

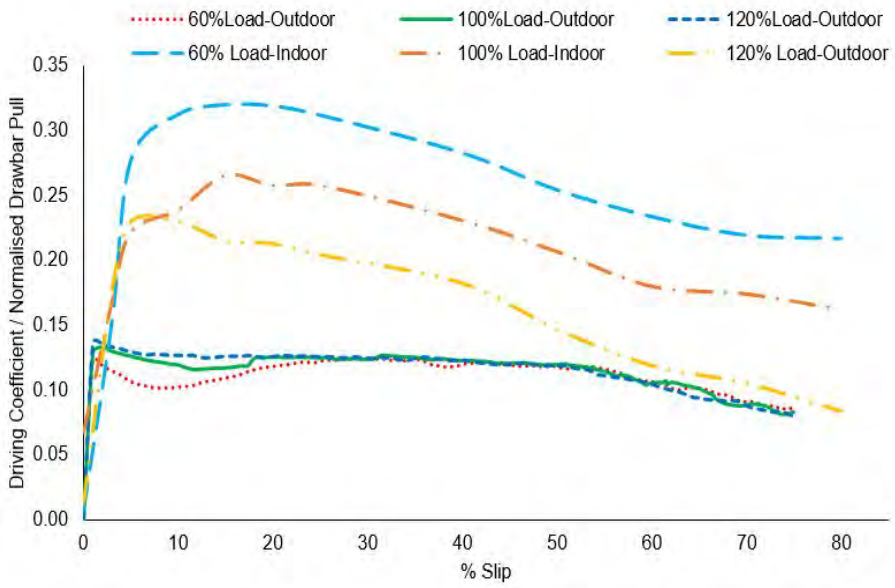

Figure 7.1: Comparison of drawbar pull/friction slip ratio curves for the treaded SRTT with 100% inflation pressure of 242 kPa at different normal loads, from outdoor and indoor test programs.

A comparison of the performance of the buffed SRTT on ice as measured on the terramechanics rig and on the outdoor ice track is shown in Figure 7.2. The buffed SRTT tire behaved the same as the treaded SRTT until a slip ratio of 15% when tested in the lab. At slip ratios of 15% and above no clear trend was observed with variation of normal load. From the field testing at the Keweenaw Research Center, at low slip ratios until 12% higher friction levels were measured with higher normal load, in the mid slip ratio range no clear trend was observed. High slip ratios above 40% the 60% load case yielded the maximum friction.

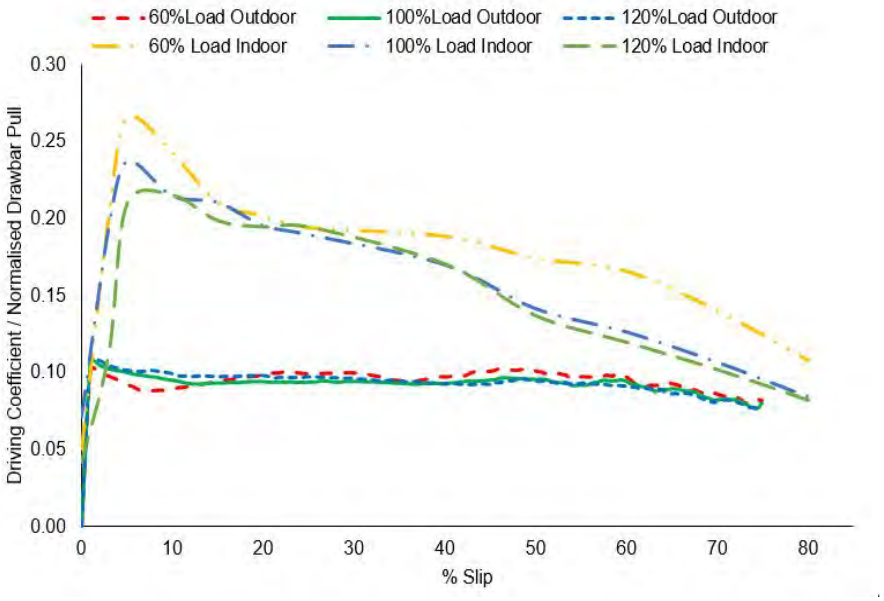

Figure 7.2: Comparison of drawbar pull/friction slip ratio curves for the buffed SRTT with 100% inflation pressure of 242 kPa at different normal loads, from outdoor and indoor test programs.

7.2 Effect of Inflation Pressure

Comparing the effect of inflation pressure as measured from the indoor and outdoor test program, from indoor studies for the treaded SRTT, after a slip ratio of 20%, with lower inflation pressure, a higher drawbar pull was measured, as seen in Figure 7.3. After a slip ratio of 50%, a reverse trend is seen due to effect of heat generation in the contact patch. The results from the field tests show a lower friction level with a lower inflation pressure up to a slip ratio of 9%, after which the effect of inflation pressure is not captured by the outdoor test procedure and curves for the three inflation pressure cases are seen overlapping.

The buffed tire exhibited no clear trend until a slip ratio of 15%, after which the tire with nominal inflation pressure showed the highest drawbar pull, as seen in Figure 7.4. Both 60% and 120% inflation pressure cases measured a lower drawbar pull compared to the 100% inflation pressure, from indoor testing. The field tests for the buffed tire did not capture any

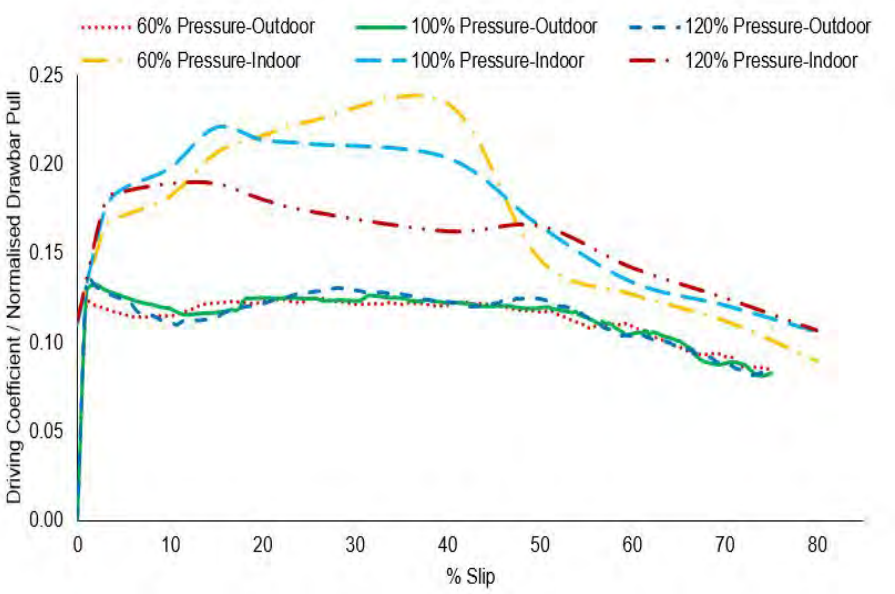

Figure 7.3: Comparison of drawbar pull/friction slip ratio curves for the treaded SRTT with 100% normal load of 7000 N with different inflation pressures, from outdoor and indoor test programs.

effect of the inflation pressure; from Figure 7.4 all the three curves are seen overlapping.

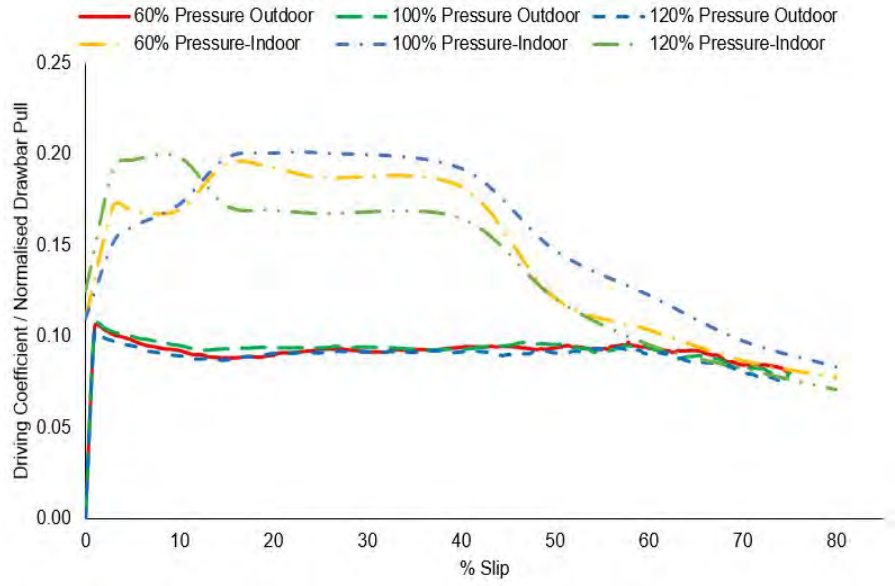

Figure 7.4: Comparison of drawbar pull/friction slip ratio curves for the buffed SRTT with 100% normal load of 7000 N with different inflation pressures, from outdoor and indoor test programs.

7.3 Reasons for Differences in Friction Measurement – Indoor versus Outdoor Test Methods

The previous section compares the friction measurements/tire performance from the indoor and the outdoor test programs. As one might have observed, the results from the two test programs are not similar. This section describes the investigations carried out to understand the reasons for the differences noticed in the friction measurements. Table 7.1, lists the differences in the calculation procedures and the test conditions.

Table 7.1: Design of experiment matrix for the outdoor test program

Parameter	AVDL	MRI
Slip ratio calculation	Theoretical Slip Ratio	Practical Slip Ratio
Water source	Town of Blacksburg	Underground well
Ice thickness	2.5 to 3 inches	6 inches
Ice temperature	-8 to −10 °C	−13 °C
Ambient temperature	-11 to −12 °C	−18 °C
Longitudinal velocity	0.218 km/h	8 km/h

A difference by 5 °C in the ice temperature and by 30 °C in the ambient temperature existed; such large differences in temperature alter the mechanical properties of the rubber compound of the SRTT and thus the performance of the SRTT (a later subsection describes the variation of tread hardness of the SRTT with temperature). A difference by 2 times in the ice thickness existed between the two test programs; however, 3 inches ice thickness in the lab would not likely cause a performance variation as compared to the tire performance

on ice thickness of 6 inches.

Ice in the lab was created using water from the Town of Blacksburg, which is fit for drinking. Whereas at the Keweenaw Research Center ice was created using water from an underground well; one can expect a high iron or copper content in this water due the old mines present in the town of Calumet, Michigan. The chemical content of the water sample used in ice creation also alters the performance levels of the tire; chapter 2 contains additional information about previous studies in this subject. There existed a difference of 40 times in the longitudinal velocity of the tire in the field versus the lab; an increased longitudinal velocity means increased heat generation in the contact patch, which definitely reduces the friction levels.

7.3.1 Ice Resurfacing Procedure

The ice preparation and resurfacing procedures are explained in section 5.1.3 and 6.2 for the indoor and outdoor test program, respectively. In the indoor investigations the tire runs on fresh ice for every test condition with resurfacing procedures followed between every test run. Whereas in outdoor tests, an initial water layer is sprayed on the ice after the water layer is frozen, a wide tire is used to polish the ice surface. After which the testing is conducted, with no resurfacing between the runs. The initial polishing and no resurfacing the ice between the runs leads to smoothing of ice surface and there by a reduction in the friction level.

7.3.2 Slip Ratio Control

Sections 5.1.4 and 6.2 describe the slip ratio control procedure followed while testing indoors and outdoors, respectively. For indoor tests the slip ratio is maintained at a steady-

state slip ratio of time period of 20 s; during field testing the slip ratio is ramped up from 0% to maximum in the 3 s to 4 s. This difference in slip ratio control leads to change in heat generation in the contact phenomenon. The ramp slip ratio control and 8 km/h longitudinal velocity during filed testing lead to shorter adhesion times and thus a reduced friction level is seen when compared to outdoor testing.

7.3.3 Tread Hardness versus Temperature

The hardness of the SRTT tread was measured using a durometer at different temperatures as in Figure 7.5, a 20% increase in tread hardness was observed from the indoor lab temperature to the outdoor test temperature. This measurement also confirms the findings in section 5.2.8, a reduced drawbar pull is seen with a reduction in ambient temperature. The increase in thread hardness is also a reason for the reduction in friction levels from indoor to outdoor testing.

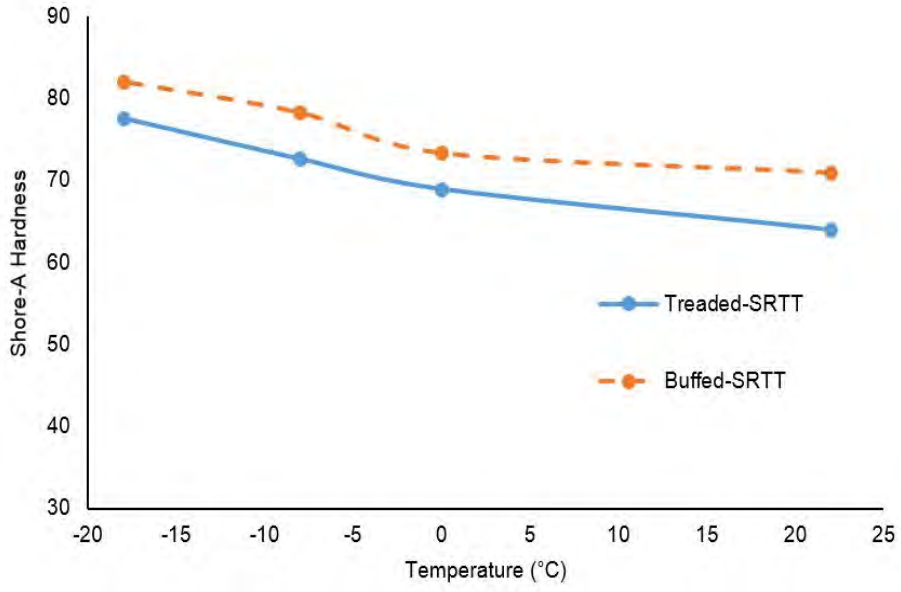

Figure 7.5: Variation of tread hardness with temperature for the SRTTs.

7.3.4 Normal Load Time Histories

The time histories of the normal load of the two test procedures were compared as seen in Figure 7.6. The Terramechanics Rig is equipped with an active normal load control system as described in section 5.1.4, which maintains a contents level of load throughout the entire run. On the other hand, a variation of 150 to 200 N was observed during the 3 s of slip ratio ramp-up during outdoor tests. A change in normal load means a change in effective rolling radius and a change in the slip ratio. Maintaining a constant normal load during filed testing is a challenge with the traction truck experiencing a certain amount of bounce. It is estimated that the variation in normal load is not a major, but a minor contributor to the difference friction levels measured in the lab and in the field.

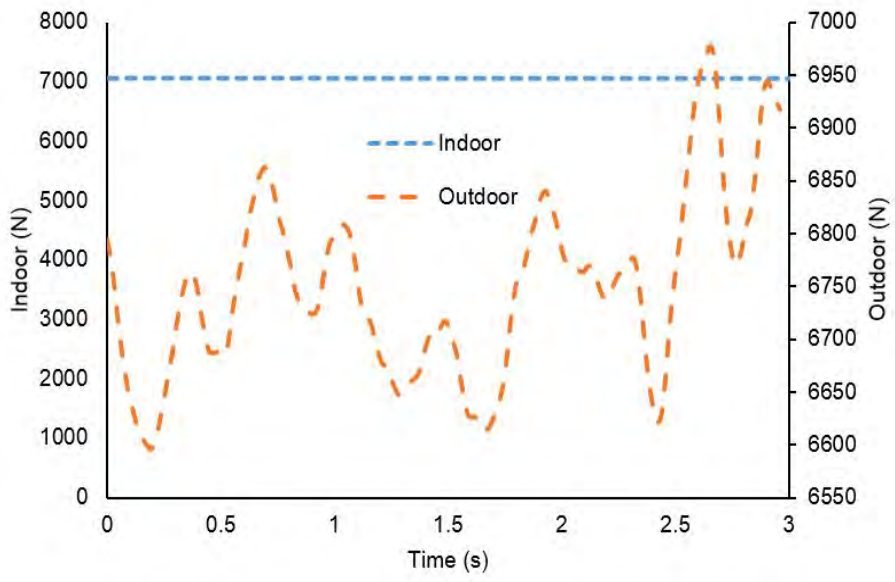

Figure 7.6: Variation of tread hardness with temperature for the SRTTs.

7.4 Summary and Conclusions

Outdoor testing as per ASTM−1805 is mainly used by the industry for relative performance analysis of different tires, rather than a method to study the effect of different operational parameters, which should be kept in mind. The reasons for differences in the recorded friction levels were investigated, with the temperature, change in tire properties and test setup being identified as major factors causing this discrepancy.

The uncertainties in the outdoor environment conditions could be due to the following: Variation in ambient temperature; variation in ice surface temperature; change of wind direction; effect of solar load; change in surface properties of ice due to temperature and wind; etc. Understanding the effect of each of the uncertainties would require outdoor testing with identical test conditions throughout the test program, where the value of the parameter of interest gets varied. Control of test conditions in outdoor test programs is not possible. Studying the effect of a change of a single parameter would require long wait periods to ensure suitable weather. This requires further investigations and is a potential topic for future research, but not feasible to be included in this study.

The design purpose of the test method should also be noted. The in-house developed indoor AVDL test method was successful in capturing the effect of different operational parameters, where ASTM−1805 was successful in capturing the effect normal load and inflation pressure. Certain test methods are widely to study the relative tire performance with respect to the SRTT and minimal procedures exist to study the absolute tire performance. Hence, the demand of the day is the establishment of standard test setups and standard test methods for uniform evaluation of tire performance on ice.

Chapter 8

Simulating Truck Performance on Ice using Experimental Data

The drawbar pull−slip ratio curves obtained from indoor testing were inputted into TruckSIM®, defining tire behavior for various ice scenarios and then simulating performance of trucks on ice. The TruckSIM® model and simulation results are presented in this chapter. The shortcomings of simulations in considering the effects of all the operational parameters which result in differences between findings of indoor testing and truck performance simulations are also presented in this chapter.

8.1 TruckSIM® Model

The indoor testing conducted on the terramechanics rig defines the longitudinal performance of the P225/R16 97S Standard Reference Test Tire for different configurations on ice. Utilizing the experimental data obtained and the modeling package TruckSIM®, a truck model was built, and longitudinal tractive and braking events were simulated while driving on ice. Taking advantage of the longitudinal force obtained at different slip ratios from indoor testing on ice, the longitudinal tire characteristics of the tire were defined, and TruckSIMs internal tire model was chosen to simulate the tractive and braking performance of a truck while driving on ice. The drawbar pull- slip ratio behaviors are assumed to be valid for both traction and braking events. All simulations were conducted using the value of the static coefficient of friction 0.15, measured in the terramechanics rig,as per ASTM C1028−07 [46], using a slip-meter.

The dimensions of the 16 SRTT were obtained from the ASTM-F2493-08 [44] standard, which contains the specifications of tire. Additional inputs required in TruckSIM to define the tire are vertical stiffness and effective rolling radius. The effective rolling radius was calculated using an in-house developed infrared measuring system mounted on the circumference of the rim, which measures the rolling radius in real time, as the tire rolls on the surface of interest in the rig. The vertical stiffness of the tire was calculated based on Rhyne's [48] vertical relationship for belted radial tires, which reads as in Eqn. (8.1). The relationship predicts vertical stiffness of the tire based on the outer diameter, contact patch width, and inflation pressure. The contact patch width for different cases was measured from tests conducted by running the tire on the Tekscan® pressure pad system.

$$K_z = 0.0274 \times P\sqrt{W \times (O.D)} + 3.38 \tag{8.1}$$

Where Kz is the vertical stiffness in kgf/mm, P is the inflation pressure in bar, W is the width of the contact patch in mm and OD is the outer diameter of the tire in mm.

8.2 Vehicle Description

A compact utility truck, as depicted in Figure 8.1, was chosen to study its tractive and braking performance. The simulations were carried out on a rear wheel drive configuration with a 175 kW diesel engine and 7-speed manual transmission. Both the front and rear axles contained a single pair of tires, with wheelbase of 1923 mm. Three drums, each weighing 2000 kg, were placed in the main vehicle. The vehicle was configured with a P225/60R16 97S Standard Reference Test Tire, the same tire for which indoor testing was conducted on ice using the Terramechanics Rig. A 10 kN-m hydraulic braking system configuration with ABS was selected for both the front and rear axle. The ratio of steering wheel torque (N-m) to total kingpin moment (N-m) was input as 1/25. The effects of aerodynamics were not considered for this simulation.

Figure 8.1: Compact utility truck model in TruckSIM® used for simulating tractive and braking performance on ice.

8.3 Simulation Results

This section describes the simulations results for longitudinal acceleration and braking events. Different scenarios were studied, which included simulations with varying inflation pressures and on different ice surfaces.

8.3.1 Braking Events

The braking performance was studied by simulating a spike brake application with a pressure of 10 MPa at time of 2 s, when the truck was traveling at a speed of 80 km/h. Simulations were conducted by inputting the different tire performance data collected from experiments conducted on the Terramechanics Rig for different scenarios on ice. The time for reduction in speed from 80 km/h and the stopping distance was computed for the various scenarios.

The time history of the longitudinal vehicle speed is shown in Figure 8.2. It is obtained from the braking simulation for a time period of 15 s. When driving on an ice surface with a mixture of slush and soil, the truck takes minimum time to reach a speed of 0 km/h, on the other hand the truck does not come to a complete stop even after 15 s, on wet ice. The highest peak drawbar-pull was observed while testing the SRTT on ice with a mixture of slush and sand. Analogous results are obtained from simulations and indoor testing, which can be seen by comparing Figure 5.23 and Figure 8.2. Therefore, there is a correlation between the peak drawbar pull and the stopping time, higher the peak drawbar pull, lesser is the stopping time on different surface conditions. The stopping distances are tabulated in Table 8.1 for different surface conditions, also show a similar trend. The wheel speed time history can be seen in Figure 8.3, the role of the ABS preventing wheel lock-up can be clearly seen. The ABS has a prominent effect while bringing the vehicle to complete stop

Table 8.1: Stopping distance of the truck traveling at speed of 80 km/h, on different ice surfaces as obtained from TruckSIM® simulations.

Surface Condition	Stopping Distance (m)
Wet−Ice	149.9, does not stop even after 15 s
Dry−Ice	67.6
Soil on Ice	56.3
Slush with Soil on Ice	37.8

when driving on surfaces of dry ice; soil on ice; and, slush and soil on ice. While driving on wet ice, the ABS still fails in bringing the vehicle to complete stop. Simulations with the ABS OFF, resulted in the truck never coming to complete stop even after 15 s, for all surface conditions.

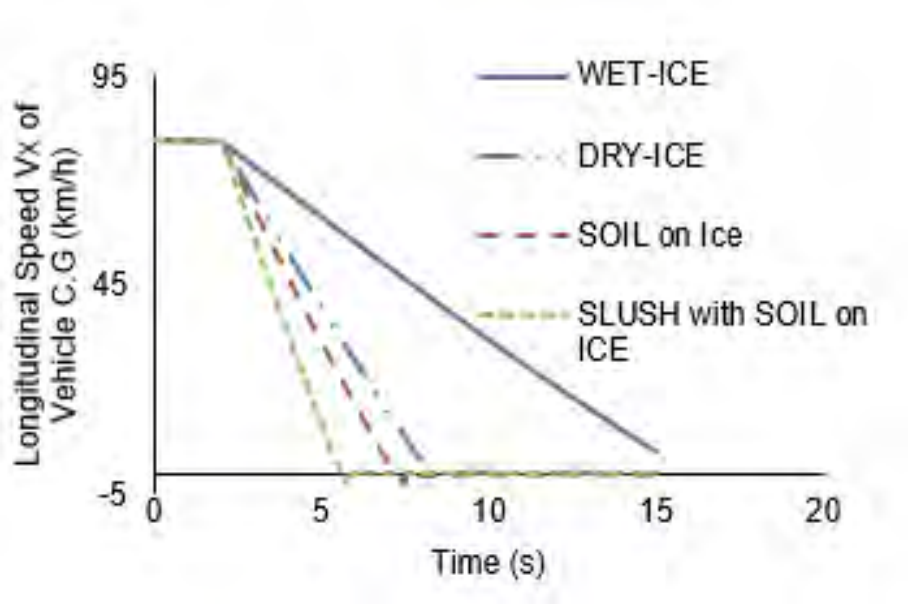

Figure 8.2: Time history of longitudinal speed (V_x) of the truck C.G traveling at speed of 80 km/h, spike braking at t = 2 sec, on different ice surfaces from TruckSIM® simulations.

The effect of tire inflation pressure on the braking performance of the compact utility truck was also studied by inputting longitudinal traction data obtained from indoor testing on ice into the TruckSIM® model. Figure 8.4 shows the time history of the longitudinal

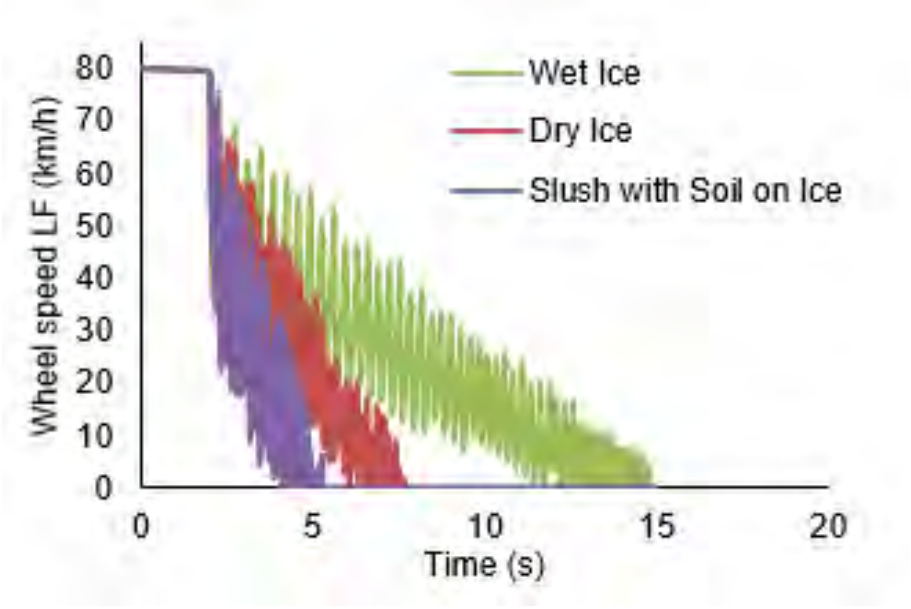

Figure 8.3: Time history of left front wheel speed, travelling at speed of 80 km/h, spike braking at t = 2 s, on different ice surfaces from TruckSIM® simulations.

velocity of the trucks center of gravity (C.G.) with the treaded SRTT. The time for complete stop, from 80 km/h was the minimum with 60% inflation pressure; the time for complete stop of the truck was found to increase with an increase in inflation pressure. On the contrary, for the buffed SRTT, the least time for complete stop of the truck was seen for the 100% inflation pressure case. Longer stopping times were observed from TruckSIM® simulations when the inflation pressure was changed from the nominal 100% value, as shown in Figure 8.5. Thus a tire with reduced tread depth exhibits higher braking traction levels at nominal inflation pressure. The simulation indicates the importance of maintaining the correct inflation pressure. The pneumatic stiffness together with the reduced tread stiffness seems to be optimal for braking at 100% inflation pressure. An extended experimental program that includes braking to validate the simulations would provide a better understanding of the braking performance.

It is evident from Figure 8.6 that the tread on the tire plays an important role in

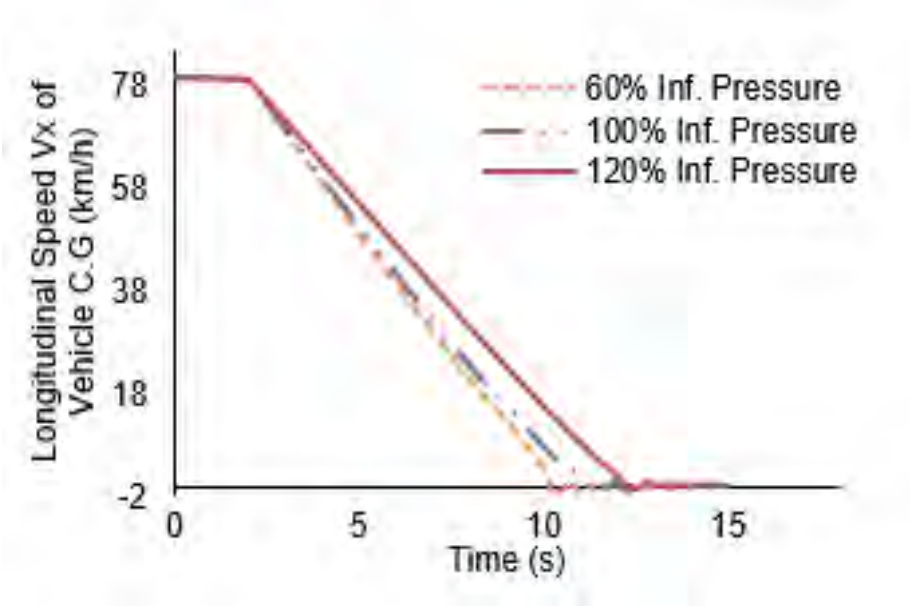

Figure 8.4: Time history of longitudinal speed (V_x) of the truck C.G traveling at speed of 80 km/h, spike braking at t = 2 sec, with different tire inflation pressures with full tread (treaded SRTT) on dry ice from TruckSIM® simulations.

reducing the stopping distance for all inflation pressure values. During operation of truck with full tread depth, reducing the inflation pressure resulted in a reduction of the stopping distance. The shortest stopping distance, when the truck was fitted with buffed tires, was seen at 100% inflation pressure. From Figure 8.6, both 60% and 120% buffed tire inflation pressures exhibited longer stopping distances.

8.3.2 Acceleration Events

The tractive performance of the compact utility truck on ice was studied by simulating an acceleration event with an open loop 50 sec. ramp throttle input. The time to complete 50 m on different ice surfaces and with different tire inflation pressures was simulated using TruckSIM®.

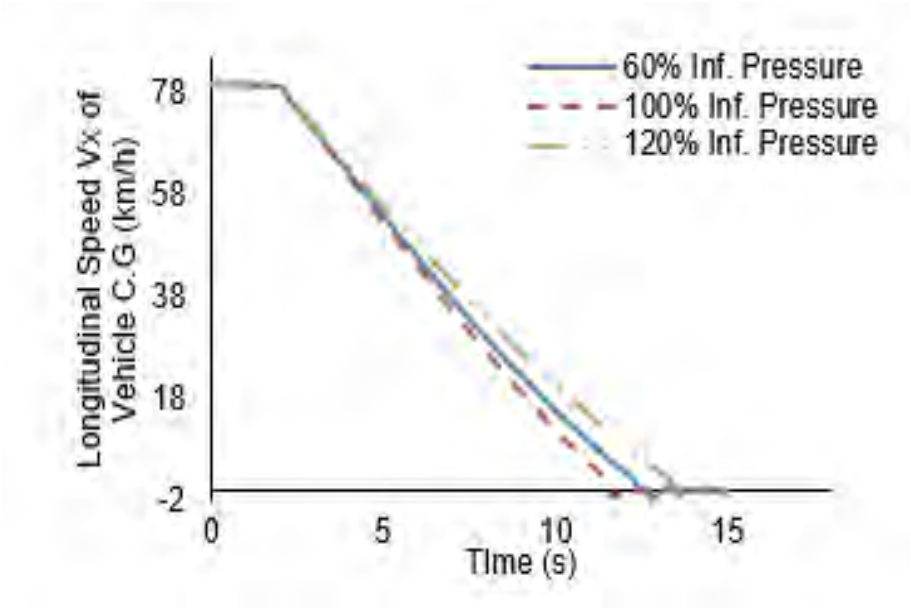

Figure 8.5: Time history of longitudinal speed (V_x) of the truck C.G traveling at speed of 80 km/h, spike braking at t = 2 sec, with different tire inflation pressures with tread depth of 1.6 mm (buffed SRTT) on dry ice from TruckSIM® simulations.

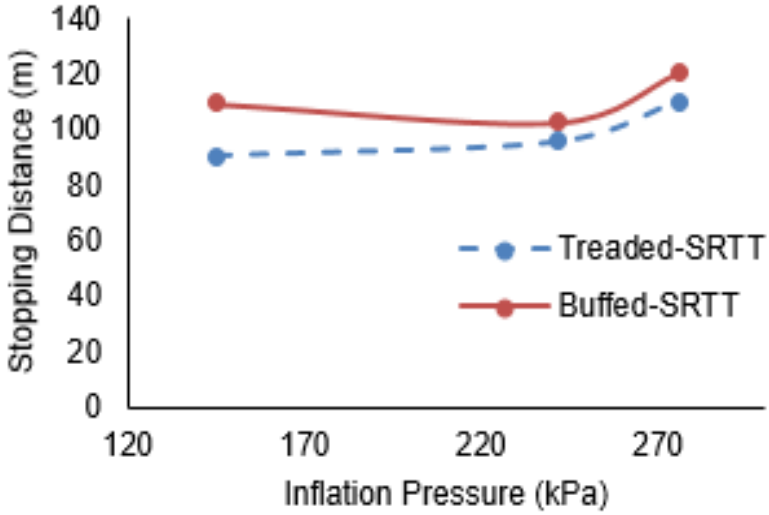

Figure 8.6: Effect of inflation pressure on stopping distance of the truck travelling at a speed of 80 km/h, spike braking at t = 2 sec, for the treaded and buffed SRTT on ice from TruckSIM® simulations.

Table 8.2: Time required by the compact utility truck to complete 50 m from rest on different ice surfaces from TruckSIM® simulations.

Surface Condition	Time to complete 50 m (s)
Slush with Soil on Ice	17.8
Dry−Ice	18.2
Soil on Ice	20.52
Wet−Ice	30

Table 8.2 shows the time required by the truck to complete 50 m on different ice surfaces. The truck takes the maximum time of 30 s on wet ice and the least time of 17.8 s on slush with soil on ice. Shorter completion times are obtained for surfaces with higher friction coefficients, with a discrepancy for the dry ice and soil on ice condition. The time for completion of 50 m with varying inflation pressures is shown in Figure 8.7; for treaded tire, the least time was obtained with 100% nominal inflation pressure, changing the inflation pressure from the 100% nominal inflation pressure resulted in increasing the time to completion of 50 m. The buffed tire showed a reverse trend, maximum completion time was seen with 100% inflation pressure and moving away from the 100% nominal value yielded shorter completion times. This behavior is due to the combined effect of the tread and pneumatic stiffness of the tire; further field tests with a compact utility truck will provide a clear understanding of the truck operation on ice with varying inflation pressure and tread depth.

8.4 Summary and Conclusions

This chapter presents tire behavior on ice through indoor experimental investigations conducted on the Terramechanics Rig at AVDL. The drawbar-pull versus slip ratio curves obtained experimentally for different scenarios are then input into TruckSIM® to define the

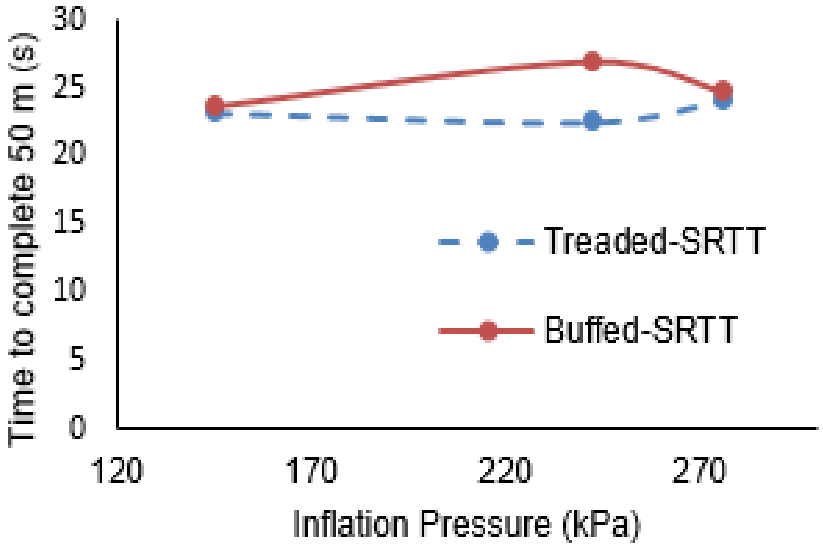

Figure 8.7: Effect of inflation pressure on time to complete 50 m from rest for the compact utility truck with treaded and buffed SRTTs on dry ice from TruckSIM® simulations.

longitudinal tire characteristics. Finally, a truck model from TruckSIMs® library is chosen, for which traction and braking events are simulated.

The prime advantage of this study is evaluation of longitudinal tire performance from experiments and simulation of braking and acceleration events with aid of TruckSIM®. Experimental evaluation of vehicle performance during braking and traction necessitates extensive testing programs; maintaining constant test conditions throughout the entire program is vital and heavily weather-dependent. However, the shortcomings of the simulations include accounting for the effect of temperature on the suspension, braking, and powertrain systems of the truck. The difference between longitudinal velocity during indoor testing on ice and longitudinal velocity of the truck in simulations, could also result in some error in the simulated results when compared to truck tests on ice. The assumption that the drawbar pull-slip ratio behavior for the traction and braking modes is the same is a simplification. The validity of the simulations can be ascertained only by conducting field tests

on ice, which was not part of the present study. Simulations must be run for the same field test conditions and the field test conditions should be maintained close to the conditions of indoor test program. Maintaining similar field and indoor test conditions necessary, as the simulations use experimental tire data. Maintaining similar indoor test conditions on the filed is really challenging. If such experiments would indicate that the braking simulations are off by a certain percent compared with our assumptions, a correlation can be developed to match the braking performance, which reduces the time and amount of effort involved with experimental studies. All-inclusive comprehensive models with all ice conditions and consideration of the effects of temperature on the truck systems are required for accurate simulation of the vehicle performance. Standard test methods for evaluation of tire and truck performance on ice are to be developed, which will allow an improved validation of tire and vehicle simulations on ice.

Chapter 9

Tire-Ice Model (TIM)

Increased traffic safety levels are of highest importance, especially when driving on icy roads. Experimental investigations for a detailed understanding of pneumatic tire performance on ice are expensive and time consuming. The changing ambient and ice conditions make it challenging to maintain repeatable test conditions during a test program. Although other studies discuss the operation of tires on ice through simulations and experimental studies ([9]; [2]; [38]; [36]), none of the previous simulation studies compute friction levels based on temperature rise in the tire footprint. The effects of operational parameters on the friction levels at the tire-ice interface and the effect of the test method are also not studied in detail in previous experimental studies. Chapter−2 documents the important aspects of tire performance on ice from previous experimental and modeling studies.

This chapter presents a tire-ice contact model (TIM) to simulate the friction levels between the tire and the ice surface during driving conditions. The model computes the temperature rise in the contact patch based on the pressure distribution in the contact patch and on the thermal properties of the tread compound and of the ice surface. The contact patch is next classified into wet and dry regions based on the ice surface temperature and

temperature rise simulations. The principle of thermal balance is applied to compute the friction level in the contact patch. The tire-ice contact model is validated for two parameters: temperature rise and friction levels. Temperature rise from simulations are validated against temperature measurements at the leading and trailing edges of the contact patch. Friction levels at different conditions of load, inflation pressure, and ice temperatures have been simulated using the tire-ice contact model and compared to the experimental findings.

9.1 Structure of Tire–Ice Model

The tire-ice model (TIM) is a modular structured model consisting of three main modules. The first module captures the pressure distribution in the contact patch; the second computes the temperature rise in the contact patch and classifies the contact patch into wet and dry regions. The third module computes the average friction values in the contact patch based on the principle of heat balance. The structure of the model-required inputs to simulate the friction levels at the tire-ice interface are shown in Figure 9.1. The three modules of the tire-ice model process the inputs and output the available friction levels in the tire footprint.

The flowchart of the TIM is shown in Figure 9.2. The first input into the model is a pressure map of the tire footprint. This is used in conjunction with Jaegers temperature rise formulation (Jaeger, 1942) and thermal properties of the tread compound and of the ice surface to simulate the temperature rise in the contact patch. The contact patch is then classified into wet and dry regions, based on the ambient temperature. Finally, a heat balance in the contact patch computes the average friction coefficient in the contact patch. This TIM has two validation parameters: i) temperature rise from simulations to be compared against temperature rise measurements at the leading and trailing edges of the

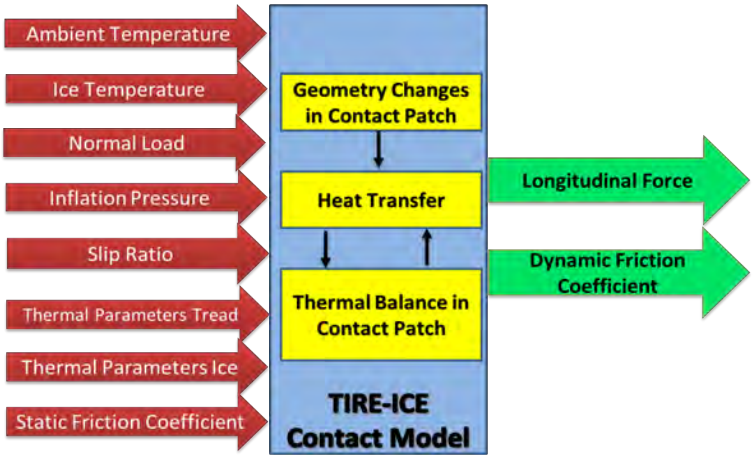

Figure 9.1: Structure of the tire-ice model (TIM).

footprint; ii) the friction computed from simulation compared against friction measured on the Terramechanics Rig (Chapter−5). The following sections of this paper detail the working principle of each of these modules and how the friction is finally computed in the tire-ice interface.

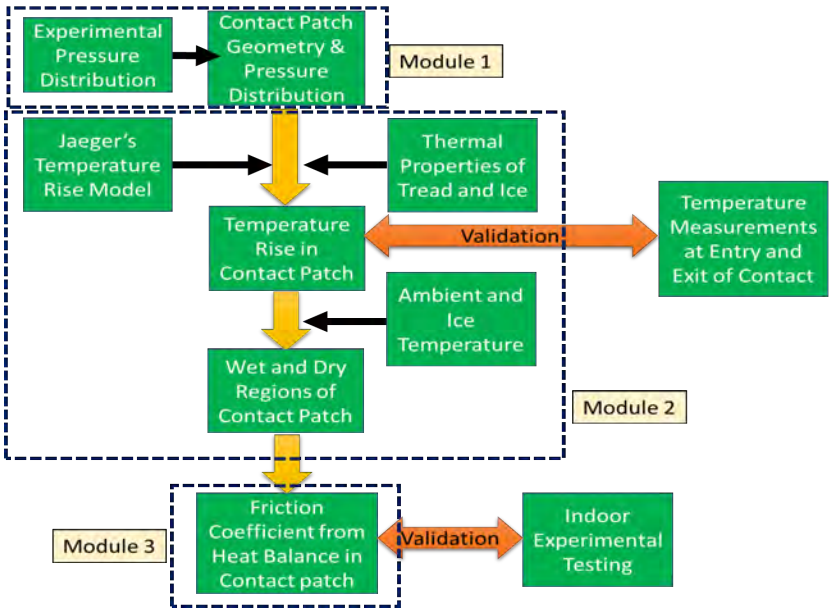

Figure 9.2: Flow chat of the tire-ice model (TIM).

9.2 Module 1: Experimental Pressure Distribution in the Contact Patch

The pressure distribution in the tire footprint is determined by the mechanical properties of the tire and the operation parameters, namely inflation pressure and normal load. The TIM presented in this paper does not compute the pressure distribution in the contact patch, but utilizes the footprint pressure map to determine with the goal of computing the friction levels at the tire-ice interface. The modular structure of this TIM allows users to input a footprint pressure map obtained through a method of their choice (analytically, experimental, or FEA) and simulate the friction levels at the tire-ice interface.

The model presented in this paper was developed using footprint pressure distribution images obtained experimentally. The model first reads the RGB value of the pressure map at each pixel and then it compares this value with the color bar of the map. This comparison allows computation of the numeric pressure value at every pixel. The footprint pressure images for different conditions were provided by Hankook Tire Ltd. for the 16 Standard Reference Test Tire (SRTT)[44], the same tire used in the experimental study (Chapter−5 and Chapter−6). This module also outputs the geometry of the contact patch: the dimensions and the shape. These parameters are then input into the temperature rise module, which computes the temperature rise in the footprint as the tire rolls on the ice surface.

9.3 Module 2: Temperature Rise in the Tire Contact

9.3.1 Constitutive Model

Jaegers [15] temperature rise formulation is chosen to compute the temperature rise at each of tread blocks as they contact the ice surface. The approach was employed by Fujikawa et al. [16]. In applying Jaegers [15] temperature rise, his formulation was modified for the purpose of simulating temperature rise at the tire-ice interface. Jaegers [15] temperature rise formulation computes the temperature rise at a point (x, y, z) due to heat source at another point (X, Y, Z), as is schematically shown in Figure 9.3. The governing equation to compute the temperature rise is shown in Eqn. (9.1).

$$\Delta T = \frac{Q\alpha}{8k\pi\alpha t^{\frac{3}{2}}} \times exp - \frac{(X-x)^2 + (Y-y)^2 + (Z-z)^2}{4\alpha t} \tag{9.1}$$

Eqn. (9.1) computes the temperature rise at (x, y, z) due to a heat source Q liberated at (X, Y, Z), as shown in Figure 9.3. Fujikawa et al. [16] apply the technique from [15] to compute tire tread temperatures in actual contact areas. The apparent contact area at the tire tread was observed using a video camera [16] and the temperature rise was computed in these actual contact areas by Fujikawa et al. [16]. The temperature rise in [16] is computed along the center line of the contact patch in the longitudinal direction with the assumption that the lateral slip of the tread is much greater than the longitudinal slip of the tread.

Based on the schematic presented in Figure 9.3, the footprint image of the tire is pixelated and the pressure value at each pixel is read. Jaegers formulation [15] as applied in (Fujikawa et al., 1994) is used for every row of pixels in the longitudinal direction. The schematic of the heat conduction model based on [16] for one tread block is also shown in Figure 9.3. The dimensions of each contact area (pixels of the pressure map) are ob-

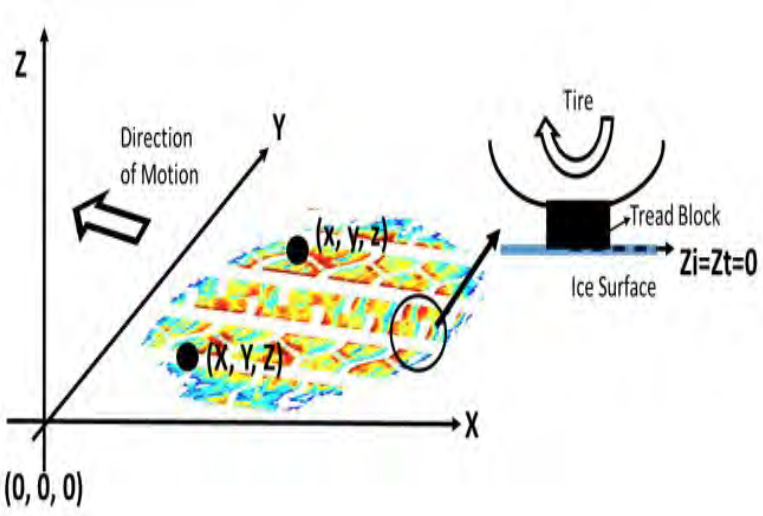

Figure 9.3: Schematic to represent Jaegers [15] temperature rise formulation, based on representation presented by Fujikawa et al. in [16].

tained through an iterative procedure comparing the simulations results and experimental temperature rise results. The following assumptions from [16] are used for this study:

1. The contact between the tread block and the ice surface occurs in the plane $z_t = z_i = 0$, as seen in Figure 9.3.

2. The frictional work equals the heat generated in the interface.

3. Heat is generated only at the interfaces where the thread blocks contact the ice surface and flows into the tread or the ice surface.

4. Generation of heat is uniformly distributed at the contact between the individual tread block and the ice surface.

5. Thermal resistance at the interface is neglected implying that the temperatures of the tread and of the ice surface are equal at the tire−ice interface.

6. Only the effects of two thread blocks (contact areas) are considered next to point of temperature computation in the contact patch.

7. The dimensions of the pixels of the contact patch are assumed to be uniform rectangles of length L along the x axis and of width B along the y axis.

The following additional assumptions are also made:

1. The ice surface is assumed to be perfectly flat. The ice surface is represented by the plane $z_i = 0$.
2. All the tread blocks of the tire in the contact patch are in complete contact with the ice surface.
3. There is no lateral slip of the tread; slippage of the tread occurs only in longitudinal direction.
4. The temperature effects between different longitudinal segments of the contact patch are only considered, with the lateral temperature effects neglected.

Application of Jaegers formulation of temperatures rise due a moving heat source as per Fujikawa et.al [16] is performed for every strip of the pressure map in the longitudinal direction at the pixel level, extending the uni-directional model in [16] to a two-dimensional formulation. Fujikawa et al. [16] compute temperature rise based on the average pressure value in the contact patch. The present study uses the pressure value at each pixel from the footprint pressure distribution to compute the temperature rise at the tire-ice interface. The tire and ice surface model from [16], as represented in Figure 9.4, along with finite difference formulation of Jaegers [15] formulation from [16] are employed in conjunction with the pressure value at each pixel to compute the temperature rise at the interface. Referring to Figure 9.4, the temperature rise at A is computed at time T due to two contact areas next to A at time t ($t < T$), as indicated in the figure. The dimensions of the contact areas and

other dimensions needed, per Figure 9.4, are obtained from the pressure distribution map (module-1).

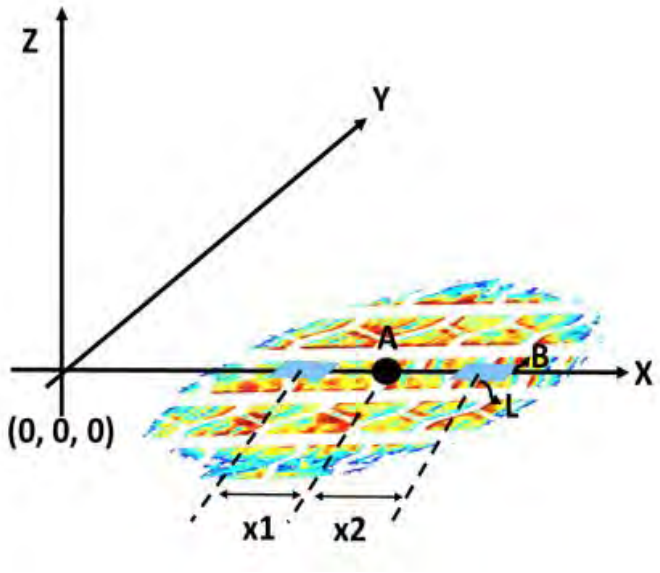

Figure 9.4: Schematic representation of tire-ice temperature rise prediction model, based on Fujikawa et al. [16]. The contact between the tread block and ice surface occurs at the plane $z_t = z_i = 0$.

The detailed finite difference formulation of [15] for a 1-D temperature rise simulation at the centerline of the contact patch is presented in [16]. The Q in Eqn.(9.1) in the TIM is computed as per Eqn.(9.2) along the same lines as presented in [9].

$$Q = \mu_{st}.p.V.S \tag{9.2}$$

The p in Eqn.(9.2) is passed from module-1 to the temperature rise module. Module-1 computes the pressure value at each pixel in the footprint and uses it to compute the heat rise for the respective pixel. Consistent with the assumptions made earlier, the boundary conditions, as per [16], used for this simulation are: i) the heat generated in the contact patch diffuses into the tire tread and the ice surface; ii) the temperature rise in plane $z_t = z_i = 0$ for

the tread and ice surface are equal, which is $\Delta T_t = \Delta T_i$. The tread and the ice parameters used are tabulated in Table 9.1.

Table 9.1: Thermal properties of the tread compound and ice surface used for the tire-ice model.

	Density (kg/m^3)	Thermal (W/mK)	Specific Heat $(kJ/kg-K)$
Tire Tread [16]	940	0.19	1.5
Ice [49]	917.5	2.22	2.02

9.3.2 Temperature Rise Simulations

The computed temperature rise in the tire contact patch of a rolling tire on an ice surface is as shown in Figure 9.5, for a 16 Standard Reference Test Tire (SRTT) [44] with a load of 100% of the load index (7000 N) and at a nominal inflation pressure of 242 kPa. The computed temperature rise distribution in the contact patch indicates a very negligible temperature rise towards at the leading edge of the contact patch. However, a significant temperature rise is observed towards the exit of the contact patch and at the trailing edge.

A gradual temperature rise from the leading edge towards the trailing edge was observed. A change in the numeric values of the operating parameters yielded in the same trend of temperature distribution in the tire-ice interface. The effect of normal load on the temperature distribution in shown in Figure 9.6. This effect of normal load on temperature distribution was studied by feeding in the pressure maps of the tire contact patch measured at three levels of load into module-1 of the tire-ice model.

The higher the normal load on the tire, the higher the temperature rise is observed in the contact patch towards the trailing edge. The simulation results, as shown in Figure 9.6,

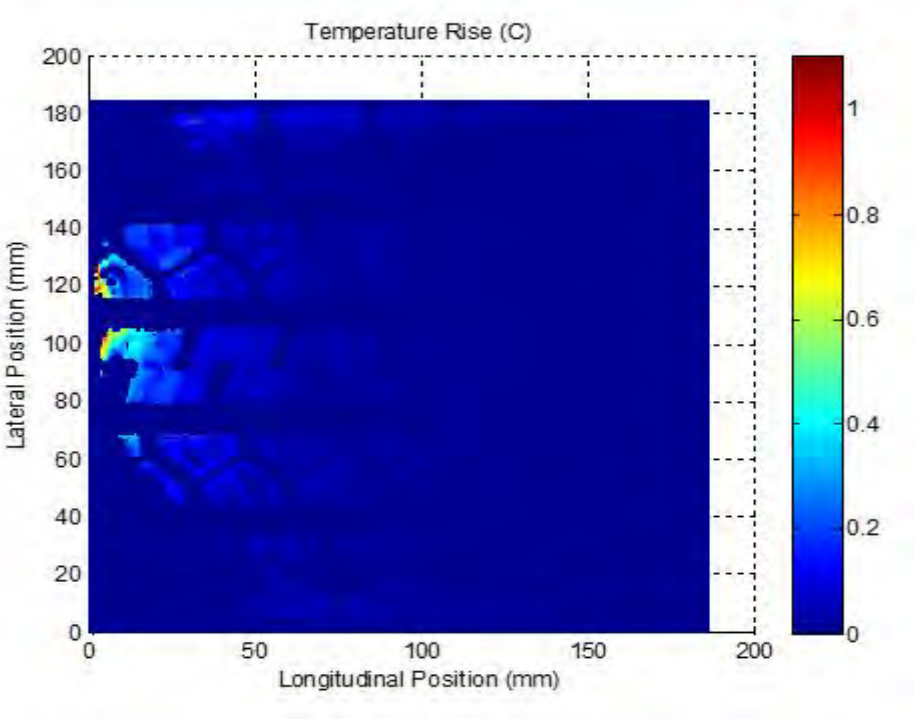

Figure 9.5: Temperature rise simulation from TIM for a 16" SRTT with nominal load and inflation pressure.

indicate a maximum temperature rise of 1.2°C was simulated for the 120% load case. The minimum rise of 0.25°C was simulated for the 60% load case and the simulation for the 100% load case resulted in a temperature rise of 0.9°C. The increase in load leads to an increase in the contact pressure in the tire-ice interface. A higher contact pressure in the interface leads to an increased heat generation leading to a higher temperature rise.

The effect of wheel torque on the temperature distribution in shown in Figure 9.7. This effect of wheel torque on temperature distribution was also studied by feeding in the pressure maps of the tire contact patch measured at three levels of wheel torques into module− of the tire-ice model.

An increase in wheel torque resulted in an increase in temperature rise, as seen from Figure 9.7(a) and Figure 9.7(b). The maximum temperature rise of 0.25°C and of 4.5°C

was predicted for wheels torques of 0 N-m and 445 N-m, respectively. A lower temperature rise of 1.6°C was observed for a wheel torque of 896 N-m compared to the 445 N-m case, which can be explained by the fact that a higher wheel torque means a given tire tread block spends less time on the ice surface. However, a higher temperature rise was observed when the wheel torque was increased from 0 N-m to 448 N-m. The increase in temperature rise with increase in wheel torque occurs to a particular value of wheel torque, after which a decrease in the temperature rise is simulated.

Experimental studies conducted to compare the temperature rise simulation are detailed in the following Chapter−10 of this dissertation.

9.4 Module 2: Contact Patch Classification

Once the temperature rise is simulated, the next step is the classification of the contact patch into wet and dry regions. This classification is done based on the ice surface temperature, which is an input to the tire−ice model. The classification process can be best explained by means of an example. Consider the ice surface to be at an initial temperature of -2°C; a temperature rise of 3°C means that the ice surface is now at a temperature of 1°C. A final temperature of more than 0°C indicates melting of the ice surface and formation of a water film leading to wet friction. On the other hand, if the initial temperature of the ice surface was -10°C and if the temperature rises by 3°C, the ice still remains dry. In this case, the temperature rise is not sufficient to melt the ice surface. Based on this principle, the contact patch is classified into three types, namely: completely wet contact patch; completely dry contact patch; wet and dry contact patch.

Figure 9.8 shows the classified contact patch obtained from simulations. The amount of wet and dry areas for the wet and dry case depends on the temperature rise simulated in

the previous step. The separation of the dry region and wet region in the combination case occurs when the temperature rises above 0°C. This model is developed considering −2°C as the melting point of ice due to the impurities present in the ice surface. The region of the contact patch below −2°C is modeled as dry, and above −2°C is modeled as wet.

9.5 Module 3: Thermal Balance in the Contact Patch

The principle of thermal balance (Figure 9.9) is employed here for the three classifications of the contact patch in order to compute the average friction coefficient in the tire contact patch, based on the works of [9, 2]. The heat generated in the contact patch due to the frictional mechanism at the tire-ice interface is divided into three parts. The first part is conducted through the ice surface, the second is conducted through tread, and the remaining heat diffuses through the water film, if present. The heat conducted through the water film is zero in case the contact patch is completely dry.

$$q_{generated} = \mu_{average}.p_{average}.V_{tire}.S.A_{total} \tag{9.3}$$

$$q_{ice} = \frac{k_{ice}.A}{d} \times \Delta T \tag{9.4}$$

$$q_{ice} = \frac{k_{tread}.A}{d} \times \Delta T \tag{9.5}$$

$$q_{generated} = q_{tread} + q_{ice} \tag{9.6}$$

Eqn.(9.3) represents the heat generated in the contact patch based on the average pressure in the contact patch. The heat conducted through the ice surface and through the tread is represented by Eqn.(9.4) and Eqn.(9.5). The depth of penetration was initially assumed to compute the average friction; the depth value was further modified to match the friction from simulation and from the indoor test program. The temperature rise (T) is obtained from the temperature rise simulations and then it is plugged into Eqn.4 and Eqn.(9.5). The heat balance in the dry contact patch is represented by Eqn.(9.6), with the only unknown being the average friction coefficient in the contact patch (μ_{av}).

$$q_{waterfilm} = \frac{k_{waterfilm}.A}{d} \times \Delta T \tag{9.7}$$

$$q_{tread} + q_{ice} + q_{waterfilm} = q_{generated} \tag{9.8}$$

$$(q_{tread} + q_{ice} + q_{waterfilm}) \times A_{wet} = q_{generated}.A_{total} - q_{dry}.A_{dry} \tag{9.9}$$

Eqn.(9.7) represents the heat conducted through the water film present in the contact patch for the completely wet contact patch case, as well as for the combination of the wet and dry contact patch. The heat is assumed to flow through the entire thickness of water film in the contact patch (assumed in this study to be 2 mm). Eqn.(9.8) represents the heat balance for the case of completely wet contact patch, with the only unknown being the average friction coefficient. The heat balance for the case of wet and dry contact patch is represented by Eqn.(9.9). The heat generated in the contact patch is assumed to melt the ice surface in part of the contact patch, thus leading to wet and dry regions in the contact patch [9]. In summary, Eqn.(9.6), Eqn.(9.8) and Eqn.(9.9) represent the heat balance for

the three contact patch classifications; from these equations the average friction coefficient in the contact patch is computed.

9.6 Summary

In this chapter, the developed tire−ice model is presented for the prediction of temperature rise and the average friction in the contact patch of tire−ice interaction. The model uses contact pressure distribution data, thermal properties of the tread compound and of the ice surface to predict the temperature rise. The contact patch is then classified into wet and dry regions based on the ice surface temperature. After the classification, a heat balance in the contact patch leads to prediction of the average friction coefficient. The effectiveness of the tire−ice model is presented in the next chapter.

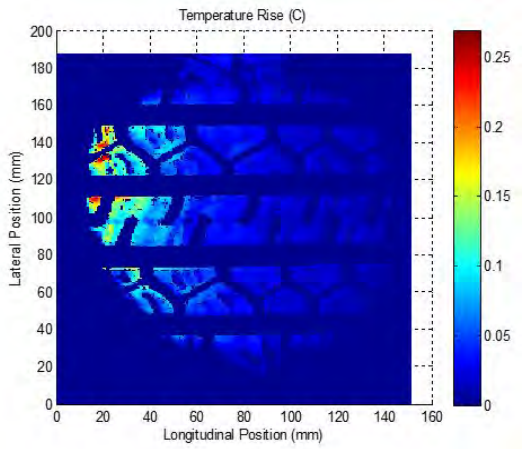

(a)

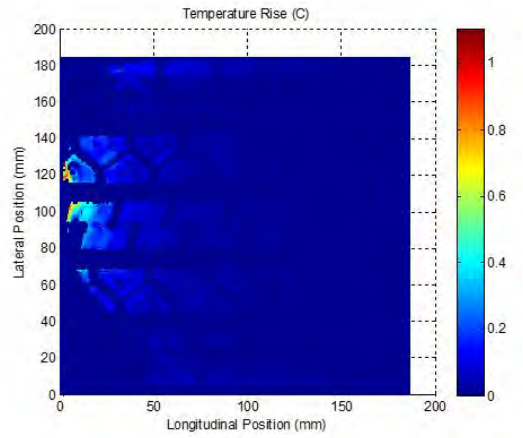

(b)

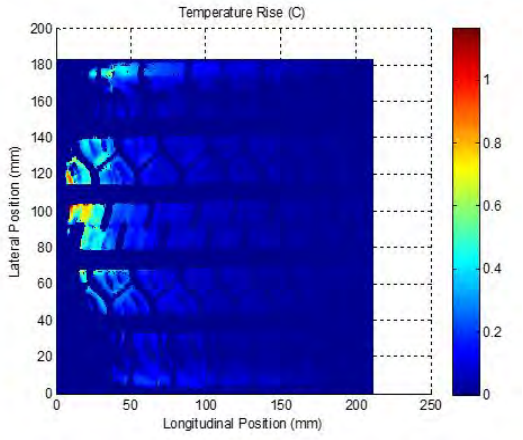

(c)

Figure 9.6: Temperature rise simulation for a 16" SRTT with, (a) 60% load index; (b) 100% load index; (c) 120% load index, Simulations parameters: inflation pressure of 35 psi and 0 N−m wheel torque. The right edge of the patch represents the entry and the left edge represents exit of the contact patch.

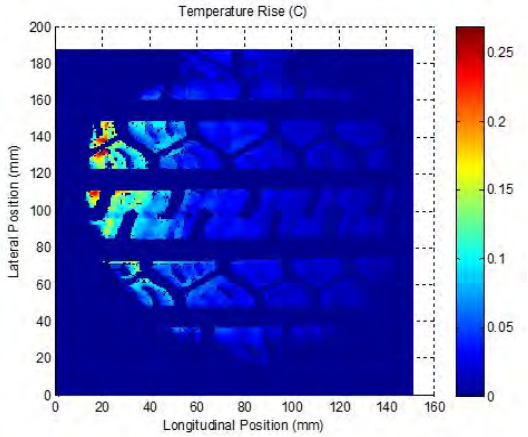

(a)

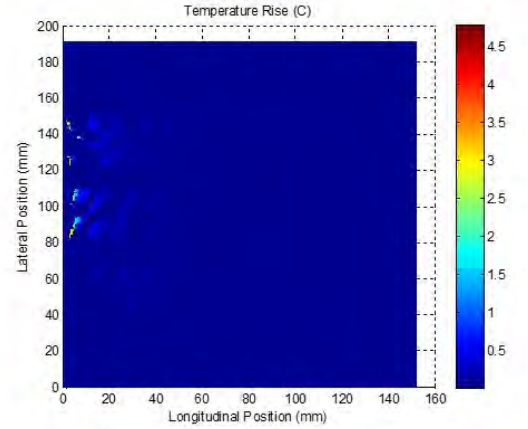

(b)

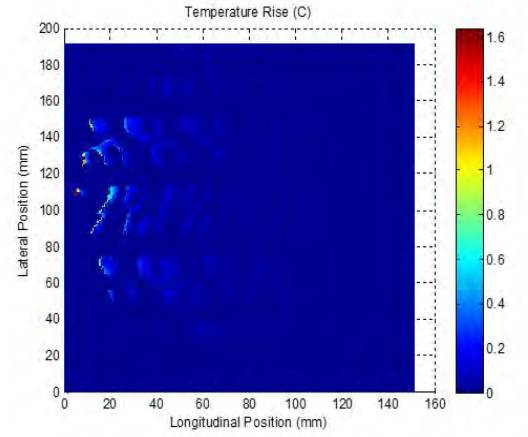

(c)

Figure 9.7: Temperature rise simulation from TIM for a 16" SRTT with wheel torque of (a) 0 N−m; (b) 448 N−m; (c) 896 N−m. Simulations parameters: inflation pressure of 35 psi and a normal load of 7000 N. The right edge of the patch represents the entry and the left edge represents exit of the contact patch.

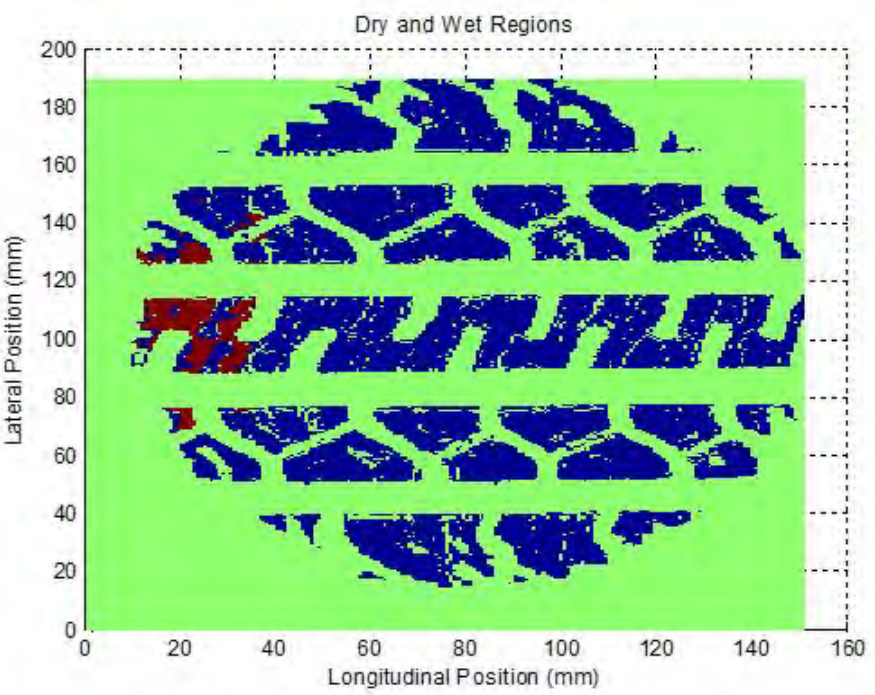

Figure 9.8: Contact path classification into wet and dry regions according to TIM. The red refers to the wet regions and the blue refers to the dry regions. The right edge of the patch represents the entry and the left edge represents exit of the contact patch.

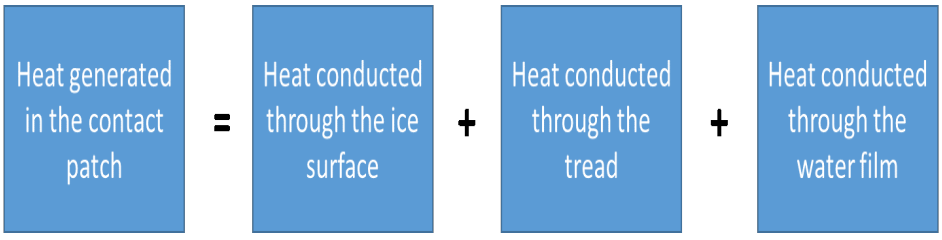

Figure 9.9: Heat balance principle employed in the tire-ice interface of TIM to compute the average friction in the contact patch.

Chapter 10

Validation TIM: Experimental versus Simulation

In this chapter, the validation studies to understand the effectiveness of the tire−model is presented. The developed tire−ice model has two validation parameters; i) temperature rise from simulations compared against temperature rise at the entry and exit of the contact patch; ii) friction from simulation compared against the measured friction on the Terramechanics Rig from the indoor test program.

10.1 Comparison of Temperature Rise

Standardized and complete procedures to measure the temperature distribution in the contact patch of a tire rolling on any terrain surface are still to be developed. In this study, the efficacy of the predicted temperature rise is evaluated versus the measurement of the temperature at the leading and trailing edges of the contact patch of a rolling tire on an ice surface. The temperature rise from the leading edge of the contact patch to the

trailing edge of the contact patch obtained from an infrared camera and the temperature rise obtained from the simulation with the TIM developed in this study were compared. The effectiveness and the accuracy of the predicted temperature distribution were assessed based on these comparisons.

10.1.1 Experimental Setup

The Terramechanics Rig [41] at the Advanced Vehicle Dynamics Laboratory was instrumented with a FLIR A655sc Infrared Camera, as shown in Figure 10.1. The thermal infrared camera has an accuracy of $\pm 2°C$ of the reading. The camera was mounted on the carriage of the rig and it moved along with the carriage, as the tire rolled on ice surface. The camera was pointed towards the side of the contact patch (perpendicular direction to the plane of the tire) to view the entry and exit of the rolling contact patch, as shown schematically in Figure 10.2. This positioning of the camera allowed simultaneous viewing of the ice surface, leading edge, and trailing edge of the contact path. These temperature measurements were conducted as per the same test procedure as presented in chapter-5, that was used to measure the tractive performance of tires on ice on the Terramechanics Rig. Same ice creation, ice resurfacing, slip ratio control, and measurement procedures were followed when the temperature was measured with the infrared camera.

10.1.2 Temperature Rise on Ice

The measurements obtained from the thermal camera are detailed in this section. The temperature measured in the trailing edge of the contact patch is higher than the one in the leading edge, for all loading cases, as shown in Figure 10.3. The higher the normal load, the higher the temperature difference (increase) is observed between the leading and the trailing

Figure 10.1: Infrared camera mounted onto the carriage of the Terramechanics Rig.

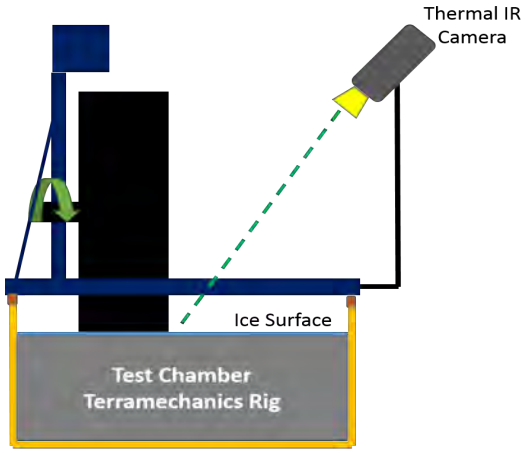

Figure 10.2: Schematic representation of infrared camera mounted onto the carriage of the Terramechanics Rig, pointing laterally towards the contact of the tire.

edge of the contact patch. The maximum temperature rise of 2.2°C was measured for the 120% LI load case and a minimum of 1°C for the 60% LI load case; the 100% LI load case saw an increase of 1.8°C. An increase of load on the tire results in an increase of pressure in the contact patch. Higher pressure in the contact patch produces larger heat generation in the contact patch leading to higher temperature rise between the entry and exit and entry of the contact patch, as seen in Figure 10.3.

The validity of the temperature rise simulations can be assessed by comparing Fig-

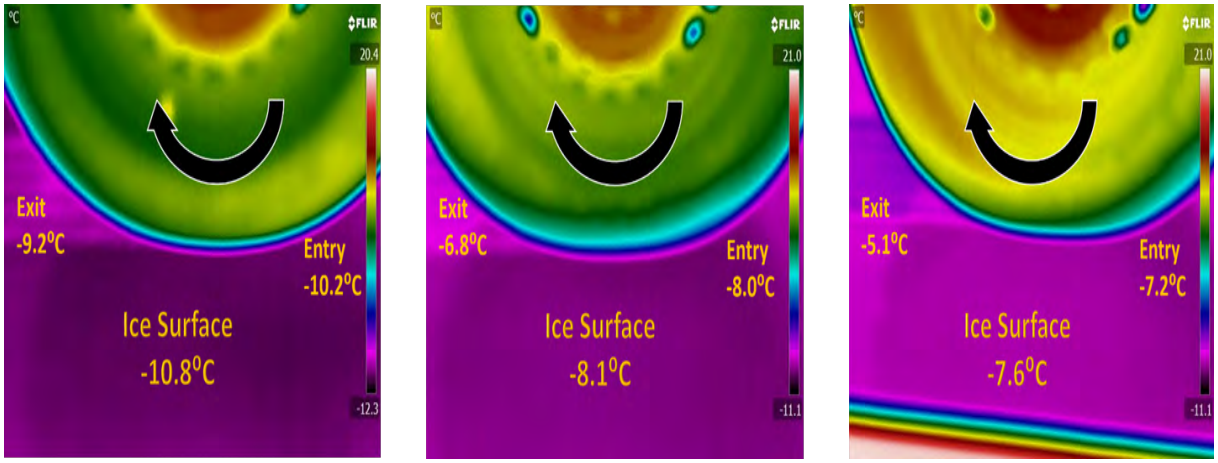

Figure 10.3: Snapshots from the thermal camera from testing conducted on the Terramechanics Rig with different normal loads: Left: 60% load index (LI); Middle: 100% load index (LI); Right: 120% load index (LI).

ure 9.6 and Figure 10.3. As stated earlier, measurement of temperature distribution in the rolling of a tire on ice still needs further investigation. In this study, the validity of the temperature rise simulations is investigated by comparing the temperature rise between the leading and trailing edge from measurements to simulations.

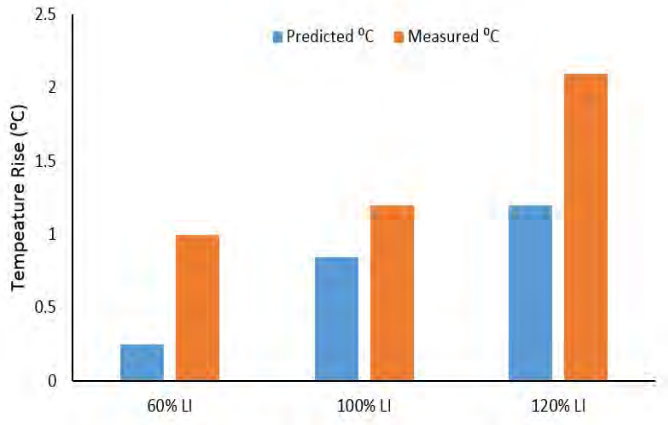

Figure 10.4: Comparison of temperature difference between leading edge and trailing edge of the contact patch, from measurements and simulations.

Figure 10.4 shows that the measured temperature rise is greater than the predicted temperature rise for the three cases of the load on the tire. The possible reasons for the

differences between the measured and the predicted values are: First, considering the accuracy of the infrared camera, a deviation of ±2°C must be accounted for the measured temperature. Second, differences may be due to the values of thermal properties used in the model. The thermal properties of the tread compound and ice surface, as shown in Table 9.1, were obtained from existing literature and their closeness to the actual values is not known. Third, the contact pressure distribution maps used for the development of this model were obtained from measurements made during testing where wheel torque has been applied to the tire. The data was provided by the project sponsors and the shearing mechanism in the contact patch is not captured in these tests, as they are not an actual representation of a slip ratio situation. However, similar trends are observed between the predicted and measured temperature rise between the leading and trailing edge of the contact patch. Furthermore, the pressure distribution thus collected could only be assimilate to the pressure distribution at lower slip ratio, thus making it very difficult to validate the temperature rise at high slip ratios. This topic is the subject of future investigations.

10.1.3 Applicability and Limitations of the Temperature Rise Model

The temperature rise in the contact patch is simulated based on the assumptions listed in section−9.3.1. The temperature rise measurements at the entry and exit of the contact patch with the aid of the infrared camera serve only as a comparison to the results from the simulation. The temperature rise measurements were conducted at certain experimental conditions and the temperature rise was simulated using generic parameters. The trend from both the temperature rise simulations and experiments match well. The effects of longitudinal velocity and humidity on temperature rise has also not taken into effect in the developed tire−ice model.

10.2 Validation of the Tire-Ice Model (TIM)

10.2.1 Friction from Experimental Studies

The indoor test program conducted on the Terramechanics Rig consisted of measuring the drawbar pull as the tire rolled on the ice surface. The indoor test program led to understanding of the effects of operational parameters on the friction levels at the tire-ice interface. The effects of load on the tire, inflation pressure, ice surface temperature, tread depth, toe angle, and camber angle on the friction levels was understood through the experimental study. Computation of the friction at the tire-ice interface from the measured drawbar pull was essential to validate the predicted friction against the measured friction. The drawbar pull is defined [45] as the difference between the tractive forces and the resistive forces. The tractive force is represented by Eqn.(10.1), where the torque on the wheel is measured on the Terramechanics Rig from testing with variation of different operational parameters and the effective rolling radius was estimated using the WITS (Wireless Internal Tire Sensors) [42]. The resistive forces are represented by Eqn.(10.2), the product of rolling friction coefficient and the load on the tire; the other contributions of the resistive forces for the development of this model have been neglected. Finally, Eqn.(10.3) represents the drawbar pull, and the rolling friction coefficient is computed from Eqn.(10.4).

$$Tractive force = \frac{T}{r_{eff}} \tag{10.1}$$

$$Resistive force = F_z.\mu_{rolling} \tag{10.2}$$

$$D.P = \frac{T}{r_{eff}} - (\mu_{rolling}.F_z) \tag{10.3}$$

$$\mu_{rolling} = \frac{-D.P + \frac{T}{r_{eff}}}{F_z} \tag{10.4}$$

10.2.2 Friction from Simulation and Experimental Studies

This section compares the predicted friction from the tire-ice model and the measured friction on the Terramechanics Rig. The correlation is between the predicted and the measured friction coefficient values for the low slip ratio range ($0-10\%$), for different operating parameters. The correlation plots for different normal loads are shown in Figure 10.5. The determinant coefficient R^2 is in the range of $0.7-0.9$, indicating an acceptable scatter around the 1:1 line. The linear fit line matches well with the 1:1 line; the regressions coefficients lie in the range $0.8-1.02$.

The validation results for wet friction conditions are shown in Figure 10.6, for testing with 0° and 2° camber angle. The determinant coefficients for the wet friction conditions are 0.72 and 0.83 for the 0° and 2° camber angle cases, respectively. The regression coefficients are 0.82 and 1.05 for the two camber angle cases, with different loads on the tire. The correlation plots in Figure 10.5 and Figure 10.6 back the argument that the predicted friction coefficient coincides well with the measured friction values. The TIM is thus validated by operational parameters, namely normal load, camber angle, and ice surface temperature (wet and dry ice). From Figure 10.5 and Figure 10.6, it can be said that the developed TIM was successful in predicting the friction levels in the tire-ice interface with minimal deviation.

10.3 Summary and Conclusions

The effectiveness of the tire-ice model was understood through the correlation plots with acceptable determinant and regression coefficients. The temperature rise prediction in the contact patch was the route to predict the average friction in the contact patch. Temperature rise simulations and measurements indicate a marginal temperature rise towards the entry of the contact patch and a significant temperature rise towards the exit of the contact patch. The comparison of the temperature rise simulations and measurements also indicate the need for further investigation of temperature rise patterns in the tire foot−print. The predicted friction values, along with change in normal load, camber angle, and wet/dry contact patch, were found to be very consistent with the values measured on the Terramechanics Rig. The predicted friction from the model has been validated only for low slip ratios, as the contact pressure distribution data used for the model development was an indirect representation of low slip ratios. However, the modularly structured tire-ice model allows the user to plug in their contact pressure distribution data, simulate the temperature rise, and compute the average friction in the contact patch.

The results validate the method proposed in this study, under the stated conditions, to assess the friction in the tire-ice interface. The modularly structured Tire−Ice Model (TIM) allows enhancing of different modules in the future, for example, tire companies may employ their own pressure distribution data and thermal properties for specific tires or interest. Although the model should be further enhanced and validated, it can be concluded that TIM can predict the friction levels in the contact between the tire and the ice surface in an adequate manner, especially in the low slip range. Furthermore, the model helps classify the contact into dry, wet, or dry and wet friction. This information could be employed in design of tires specialized for icy roads, vehicle safety systems, and possibly for accident reconstruction.

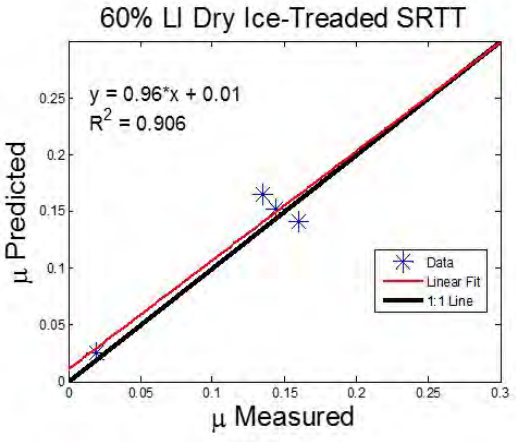

(a)

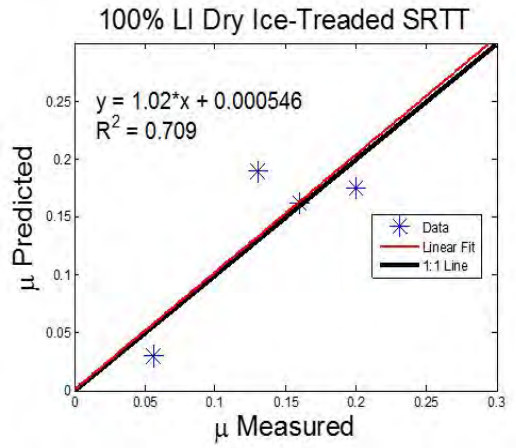

(b)

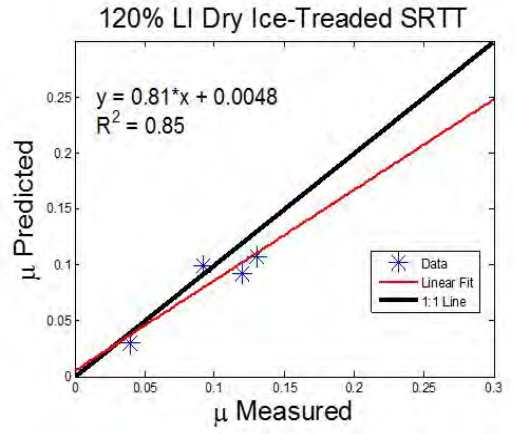

(c)

Figure 10.5: Comparison of the measured and friction vales predicted by TIM for three different loads on the tire: (a) 60% load index (LI); (b) 100% load index (LI); (c) 120% load index (LI). Inflation pressure of 242 kPa, camber angle of 0°, and dry friction conditions.

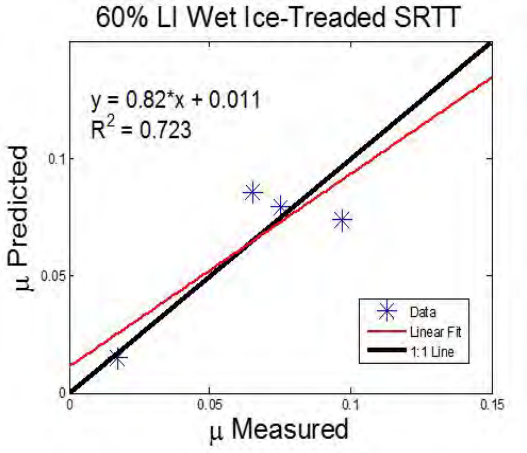

(a)

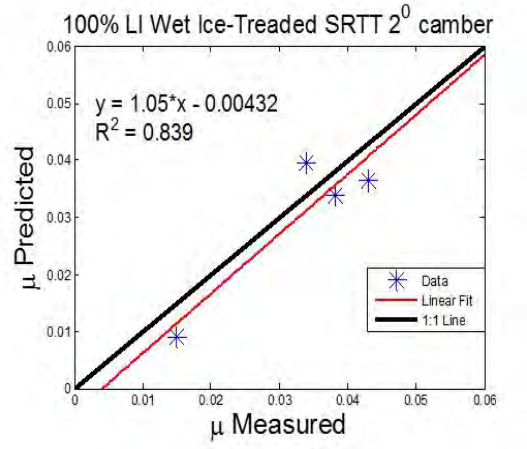

(b)

Figure 10.6: Comparison of the measured and friction vales predicted by TIM for wet friction conditions: (a) 60% load index and camber angle of 0° on wet friction; (b) 100% load index (LI) and camber angle of 2° on dry friction. Inflation pressure of 35 psi.

Chapter 11

Conclusions and Future Research Directions

This chapter presents a summary of the conducted research with the important results that were obtained. Directions for future research to be pursued are also presented in this chapter.

11.1 Summary of Research Outcomes

The experimental portion of this research consisting of an indoor test program and an outdoor test program, has led to a quantification of the effects of different operational parameters during operation of tires on ice.

The effect of the normal load as studied through the indoor test program indicates that the lower the load on the tire, the higher was the drawbar pull for the treaded SRTT. The trend was prominent throughout the entire slip ratio range. The buffed SRTT exhibited

the same trend at low slip ratios; at mid and high slip ratios no clear trend was observed. The outdoor test program indicated a reverse trend: the lower the load on the tire, lower was the friction level for the treaded SRTT. For the buffed tire tested in the field, the lower the load on the tire, lower was the friction level at low slip ratios until around 15%; in the mid slip ratio range, no clear trend was seen and the curves were seen overlapping. At high slip ratios, the lower the load on the tire, higher was the friction level.

Laboratory studies at different levels of inflation pressure showed no clear trend in the low slip ratio range until around 10% for the treaded SRTT. In the mid slip ratio range, the lower the inflation pressure, higher was the drawbar pull and a reverse trend was noticed at high slip ratios. The buffed SRTT showed no clear trend with varying inflation pressure in the low slip ratio range, after which for the nominal inflation pressure case exhibited the highest drawbar pull. The treaded SRTT tested in the field showed a reduction in the friction levels with a reduction in the inflation pressure at low slip ratios. At higher slip ratios, the effect of the inflation pressure could not be captured. The field tests could not also capture the effect of the inflation pressure for the buffed SRTT, over the entire slip ratio range.

The reasons for differences in the measured friction values from the indoor and the outdoor test procedures were identified; differences in ambient and ice temperature, longitudinal velocity, ice resurfacing procedures were the main causes. The variation in mechanical properties of the tire with varying temperature was also identified as a cause to exhibit different behavior.

The effect of tread depth was evident and the role of tread in enhancing the tractive performance of the tire was clearly seen. Higher friction levels were observed on dry ice compared to wet ice, with around 300% increase in the peak drawbar pull. Studies with varying camber angle did not indicate a major trend in the drawbar pull−slip ratio curves, except a slight variation in the peak drawbar pull and the occurrence of the peak. The effect

of toe angle studied in the lab indicated no clear trend with an initial variation of toe angle. With subsequent increase, a reduction in the drawbar pull was observed with an increase in toe angle. Testing with different aggregates on the ice surface indicated an increase in the friction levels with an increase in the weight and an increase in the adhesion capability of the particles to ice surface.

The modeling of the interface between the tire and the ice surface led to the simulation of the temperature rise and the average friction. Temperature rise and friction in the tire−ice contact patch were simulated based on the pressure distribution in the contact patch. The thermal properties of the tread compound and the ice surface are also inputs to compute the temperature rise at the interface. Based on the temperature rise in the contact patch and the initial ice surface temperature, the contact patch is classified into wet and dry regions. Then, a thermal balance in the contact patch leads to the computation of the average friction in the tire−ice interface.

The validity of the developed tire−ice model was justified by comparing two outputs from the model:

1. The simulated temperature rise in the contact patch compared against measured temperature difference between entry and exit of the contact patch.
2. Predicted friction from the tire−ice model compared against measured friction on the Terramechanics Rig.

The predicted temperature difference between the entry point and exit point of the contact patch match well qualitatively in terms of the general trend with the experimental results. However, there is an offset in terms of the magnitude of the temperature rise between the simulations and the measurements. The predicted friction values with changes in operating parameters match well with the measured values. The tire−ice model has been

validated only for low slip ratios, due to lack of availability of high slip ratio contact pressure data. The developed model is a modularly structured model which allows the user to plug in different contact pressure distribution data to simulate the friction in the tire−ice interface for a wider range of slip ratios. However, further investigation must be conducted to better capture the temperature rise in the contact patch in a mathematical model.

In conclusion, the comprehensive literature review helped identifying the areas to be investigated during the operation of tires on ice. An indoor and an outdoor experimental study were conducted, leading to the quantification of the effects of the operational parameters on the friction level at the tire−ice interface. A tire−ice contact model was developed to simulate the friction levels at the interface. Good correlations were obtained between the predicted friction and the measured friction, as well as between the simulated temperature rise and the measured temperature rise. Finally, the effects of operational parameters on friction levels at the tire−ice interface as studied from experiments and the tire−ice model matched closely.

There is a need to expand the experimental procedure due to uncertainties associated with the measured test data. Furthermore, based on the newly collected information, a refined tire−ice model should be developed. Other related are topics for future research are outlined in the section−11.3 of this dissertation.

11.2 Main Contributions of this Research

The main contributions of this research are itemized below:

- Investigated and summarized the state of the art in tire performance on ice from the past 50 years.

- Developed an experimental study to understand tire performance on ice.
- Conducted indoor studies using the Terramechanics Rig at AVDL. Designed and analyzed field tests conducted at the Keweenaw Research Center.
- Conducted a thorough analysis to understand the effects of operational parameters from lab and field tests.
- Simulation of truck performance on ice using experimental tire data with TruckSIM®.
- Developed a tire−ice contact model to predicts temperature rise in contact patch and average friction coefficient in tire-ice interface.
- Validated tire−ice model by comparing predicted friction against measured friction on the Terramechanics Rig.

11.2.1 Journals

1. Bhoopalam AK, Sandu C, and Taheri S, *"Experimental Investigation of Pneumatic Tire Performance on Ice: Part−1 Indoor Study"*, Journal of Terramechanics, 60: 43−54, 2015.
2. Bhoopalam AK, Sandu C, and Taheri S, *"Experimental Investigation of Pneumatic Tire Performance on Ice: Part−2 Outdoor Study"*, Journal of Terramechanics, 60: 55−62, 2015.
3. Bhoopalam AK, Sandu C, and Taheri S, *"Tire Traction of Commercial Vehicles on Icy Roads"*, SAE International Journal of Commercial Vehicles, 7(2): 357−365, 2014.
4. Bhoopalam AK and Sandu C, *"Review of the State of the Art in Experimental Studies and Mathematical Modeling of Tire Performance on Ice"*, Journal of Terramechanics,

53: 19−35, 2014.

5. Bhoopalam AK, Sandu C, and Taheri S, *"Development of a Tire-Ice Model (TIM)"*, Journal of Terramechanics - Under Review.

11.2.2 Peer Reviewed Conference Papers

1. Bhoopalam AK, Sandu C, and Taheri S, *"Development of a Tire-Ice Model (TIM)"*, 13th European Conference of the International Society for Terrain Vehicle Systems (ISTVS), October 21−23, 2015, Rome, Italy.

2. Bhoopalam AK, Sandu C, and Taheri S, *"Tire Traction of Commercial Vehicles on Icy Roads"*, SAE Technical Paper 2014−01−2292, 2014 SAE COMVEC Congress, October 7−9, 2014, Rosemont, IL.

3. Bhoopalam AK, Sandu C and Taheri S, *"A Comprehensive Study of Tire Traction on Ice Based on Laboratory and Field Tests"*, 18th International Conference of the International Society for Terrain Vehicle Systems (ISTVS), September 22−25, 2014, Seoul, Korea.

4. Bhoopalam AK and Sandu C, *"Experimental Study of Pneumatic Tire on Ice"*, Paper no. 78326, 7th Americas Regional Conference of the International Society for Terrain Vehicle Systems (ISTVS), November 4−7, 2013, Tampa, FL.

11.2.3 Oral Presentations

1. Bhoopalam AK, *A Comprehensive Study of Tire Traction on Ice: Experimental and Simulation Studies*, GSA Research Symposium: Virginia Tech, March 25^{th}, 2015.

2. Bhoopalam AK, Sandu C and Taheri S, *A Comparative Study of Indoor and Outdoor Tire Tractive Performance on Ice*, The 33rd Annual Meeting Conference on Tire Science Technology, September 8−10, 2014, Akron, OH.

3. Bhoopalam AK, Sandu C and Taheri S, *Experimental and Simulation Studies to Understand Tire Performance on Ice*, Tire Technology Expo 2015, February 10−12, Cologne, Germany.

11.2.4 Poster Presentations

1. Bhoopalam AK, Sandu C and Taheri S, *Pneumatic Tire Performance on Ice*, 2014 SAE COMVEC Congress, October 7−9, 2014, Rosemont, IL.

2. Bhoopalam AK, Sandu C and Taheri S, *Pneumatic Tire Performance on Ice*, 18th International Conference of the International Society for Terrain Vehicle Systems (ISTVS), September 22−25, 2014, Seoul, Korea.

3. Bhoopalam AK, Sandu C and Taheri S, *Pneumatic Tire Performance on Ice*, Torgersen Graduate Student Research Excellence Awards, College of Engineering, Virgina Tech, April 15^{th} 2014.

4. Bhoopalam AK, Sandu C and Taheri S, *Pneumatic Tire Performance on Ice*, 7th Americas Regional Conference of the International Society for Terrain Vehicle Systems (ISTVS), November 4−7, 2013, Tampa, FL.

11.3 Future Research Directions

Current regulations require the tire manufacturer to rate the braking performance of tires; thus experimental investigations to understand braking performance of tires on ice are necessary. Future directions could also include evaluation of cornering performance of tire on ice by varying operational parameters. Studying the effect of a change in a single parameter would require long wait periods to ensure suitable weather. Understanding the effect of uncertainties in the environmental conditions during testing on the measured friction is a potential topic for future research. A comparative experiential analysis of tires on ice would also help in better understanding the effects of material properties on the temperature rise and friction.

Shortcomings in simulation of truck performance on ice could be addressed by inclusion of the effects temperature and ambient conditions effects in the simulation. Validation of the truck simulation results by performing experimental studies on a truck in the field could also be pursued. Future directions for tire−ice model enhancement could include the development of another module to account for changes in the mechanical properties of the tire with temperature and the impact of these changes on the friction levels. The contact patch pressure distribution prediction could be part of the model, as well as its relation with the temperature. From the instrumentation perspective, there is a critical need to develop novel techniques need to be developed in the future to measure temperature rise in the tire−ice interface. Such sensors may lead to more accurate temperature rise simulations in the tire−ice contact. Further investigation is also necessary to understand the relationship between the pressure distribution and the temperature distribution in tire−ice interface.

Appendix A

Terramechanics Rig Operation Checklist for Safety

1. After switching ON the main breaker switches and powering all the electronics of the Terramecahnics Rig.
   (a) Switch ON the safety switch of the carriage motor and ensure the light turns ON.
   (b) Press the E-STOP button on the rig controller to make sure the emergency sound is heard. This is an indication of the system working fine.
2. Begin the calibration process of the KISTLER sensor.
   (a) Power ON the voltage controller of the normal load controller after opening the LABVIEW VI on the computer. Ensure the pneumatic flow control valve opens and the residual air from the air springs is released.
   (b) Ensure noise of air flow from the air springs is heard and open the value on the pneumatic line from the air compressor (orange line).

Figure A.1: Safety switch of the Terramechanics Rig

Figure A.2: Emergency Stop switch on controller of the Terramechanics Rig

(c) Wait till the completion of the calibration process to begin the next steps.

3. Once the calibration process is complete.

(a) Switch OFF the safety switch of the carriage motor.

(b) Input the desired slip ratios through PicPRO to the motor controller.

(c) Arm the LMS system with the desired settings.

(d) Lower the carriage of the Terramechanics Rig and ensure the tire is in contact with the test surface.

(e) Ensure enough slack exists in the belt of the lift winch and ensure the forces displayed on the KISTLER system read close to 0 N. Best option would be to disengage the winch once the tire is in complete contact with the test surface.

Figure A.3: Winch on the Terramechanics Rig

4. Normal load application on the tire

(a) Ensure the light on the NI DAQ pad is ON.

(b) Now begin applying load on the carriage of the Terramachanics Rig through the LABVIEW VI. Ensure the applied voltage through the slider matches with the multi-meter display.

Figure A.4: Light on NI DAQ pad.

(c) Now ON the safety switch of the carriage motor and start moving the carriage using the rig controller.

(d) Pay attention to the increase in noise of the motor when the change in slip ratio occurs at defined time periods.

(e) Once the rig reaches the home position, STOP the carriage using the rig controller and then immediately hit STOP on the LABVIEW VI to release the load on the tire. And send the carriage back to the home position.

Appendix B

Ice Rink Operation Manual

B.1 Terramechanics Rig Preparation

(a) Lay the C-channels on the top level of the test chamber of the Terramechanics Rig.

(b) After the channels are laid, place a layer of plastic tarp (BLUZ HAWK available at Lowes) over the entire the test surface (on top of the c-channel surface). Ensure enough tarp slacks on the edges of the test chamber.

(c) Next place a layer of pink foam insulation over the plastic tarp. The foam needs to be custom cut to shape to fit towards the end of the test chamber.

(d) All the joints on the pink foam layer needs to be sealed using gorilla tape.

(e) Now insert two layers of plastic tarp on the pink foam. Now place the ice mat and roll out the ice mat.

(f) Now tape all the plastic tarp hanging out from the test chamber to the edges of test chamber using gorilla tape. Ensure the tarp is not taped in the part of the test chamber.

(g) Connect the ice mat to the outdoor chiller unit. Place the wooden ramp on the rubber pipes next to the THERMOTRON chamber, so other people can walk over it.

Figure B.1: Wodden ramp on connecting hoses.

B.2 Ice Chiller Preparation

(a) Switch ON the breaker switch 27 in the breaker box and the mains on the chiller unit. Make sure the set point the controller is set to a high value around 99 °F. The system needs to be left ON for for 24 hours for warm up.

(b) Next fill in ethylene glycol in the expansion tank and turn on the pump to the ON position.

(c) Keep adding ethylene glycol to the tank if the glycol falls below the mark in the tank.

(d) Once the pressure has reached a constant value on the pressure scale of the chiller unit around 25-30 psi(shown in the figure), the air the system has been released

Figure B.2: Breaker switch for chiller system.

Figure B.3: Expansion tank of the ice making system.

and now the system is set for ice creation.

(e) Now place the temperature sensor on the ice mat and set the temperature to around a temperature of about 25 °F. Next, set the pump position to AUTO position. One should notice mist formation on the surface of the ice mat after

Figure B.4: Glycol from Aqua Solutions used in the ice making system.

Plate to be opened to view the pressure gauge of the ice making system.

about 30 minutes.

(f) Ensure there is no leakage of glycol in the ice mat and in the connecting mat.

(g) Place towels below the connecting pipes for absorption of frost condensation on the surface of the connecting pipes.

(h) Now start spraying water in test chamber in layers and once the desired ice thickness is reached testing can be started.

Figure B.5: Pressure gauge of the ice making system.

Temperature sensor of the ice making system.

B.3 Melting the Ice

(a) Switch OFF the chiller unit which leads to formation of a melt layer. Use the shop vacuum to remove the water periodically.

(b) Use the water pump to empty the filled shop vacuum into the sink by connecting the outlet of pump to the sink.

(c) When the ice layer becomes it could be broken using a chisel and hammer without damage to the ice pipes and the ice blocks can be thrown away.

Appendix C

Tire-Ice Model Documentation

C.1 Inputs to the tire−ice model

(a) Tire footprint pressure distribution image.

(b) Density of ice and tread compound.

(c) Temperature of ice surface.

(d) Thermal parameters of ice surface and tread compound.

   i. Specific heat

   ii. Thermal conductivity

(e) Operating parameters.

   i. Load on tire (effect captured in tire footprint pressure distribution image).

   ii. Slip ratio (effect captured in tire footprint pressure distribution image).

   iii. Inflation pressure (effect captured in tire footprint pressure distribution image).

   iv. Longitudinal velocity of tire.

C.2 Procedure to predict friction at tire−ice interface

(a) Open the MATLAB file tireice.m

(b) Feed in the required input parameters as per the comments provided in the script.

(c) Specify coordinates to crop the footprint pressure map and color−bar as per the comments provided in the script.

(d) Run the MATLAB script

C.3 Outputs from tire−ice model

(a) MATLAB Figure 1: Pressure distribution in the contact patch. Compare the figure to the experimental footprint pressure map to ensure the pressure distribution data has been read correctly. If not adjust the crop settings of the original tire footprint pressure distribution image and repeat the procedure.

(b) MATLAB Figure 2: Temperature rise in the contact patch.

(c) MATLAB Figure 3: Classification of contact patch into wet and dry regions.

(d) Average friction coefficient in the contact patch.

Bibliography

[1] A Topp, N Kendziorra, B Wies, and H Lange. Braking force transfer capabilities of tires on wet roads. In *17th EVU Annual Congress Proceedings*, pages 205–214, 2008.

[2] Martin Gießler, Frank Gauterin, K Wiese, and B Wies. Influence of friction heat on tire traction on ice and snow. *Tire Science and Technology*, 38(1):4–23, 2010.

[3] Ken-ichi Shimizu, Mitsuya Nihei, and François Dorémieux. Effect of texture of iced road surface on characteristics of ice and snow tires. Technical report, SAE Technical Paper 920018, 1992.

[4] AD Roberts. Rubber-ice adhesion and friction. *The Journal of Adhesion*, 13(1):77–86, 1981.

[5] A Schallamach. How does rubber slide? *Wear*, 17(4):301–312, 1971.

[6] John E Hunter. Reconstructing collisions involving ice and slippery surfaces. Technical report, SAE Technical Paper 930896, 1993.

[7] Henrik Åström and Romuald Banek. Wet ice friction of conventional m+ s tyres and of a retreaded m+ s tyre with hard granules in thread rubber. Technical report, Swedish Road and Transport Research Institute (VTI): SE-581 95., 2001.

[8] XD Peng, YB Xie, and KH Guo. A tire traction modeling for use in ice mobile. Technical report, SAE Technical Paper 1999-01-0478, 1999.

[9] XD Peng, YB Xie, and KH Guo. A new method for determining tire traction on ice. Technical report, SAE Technical Paper 2000-01-1640, 2000.

[10] Michael W Parker, Sally A Shoop, Barry A Coutermarsh, Kyle D Wesson, and Jesse M Stanley. Verification and validation of a winter driving simulator. *Journal of Terramechanics*, 46(4):127–139, 2009.

[11] Ken'ichi Shimizu and Chuuji Ikeya. Indoor test of ice and snow tires on iced drumdevelopment of tester and characteristics of coated ice for test. Technical report, SAE Technical Paper 890004, 1989.

[12] Karlsruhe Institue of Technology. *Testing Facilities: Institute of Vehicle System Technology.*, 2014 (accessed June 18, 2015). https://www.fast.kit.edu/download/DownloadsFahrzeugtechnik/140519-Testing_facilities_FAST_english.pdf.

[13] Barry A Coutermarsh and Sally A Shoop. Tire slip-angle force measurements on winter surfaces. *Journal of Terramechanics*, 46(4):157–163, 2009.

[14] GF Hayhoe and CG Shapley. Tire force generation on ice. Technical report, SAE Technical Paper 890028, 2013.

[15] J.C. Jaeger. Moving sources of heat and the temperature at sliding contacts. *Journal and Proceedings of the Royal Society of New South Wales*, 76:203 – 224, 1943.

[16] T. Fujikawa, A. Funazaki, and S. Yamazaki. Tire tread temperatures in actual contact areas. *Tire Science and Technology*, 22(1):19 – 41, 1994.

[17] Gerasimos Skouvaklis, Jane R Blackford, and Vasileios Koutsos. Friction of rubber on ice: A new machine, influence of rubber properties and sliding parameters. *Tribology International*, 49:44–52, 2012.

[18] Dennis P Martin and Gerard F Schaefer. Tire-road friction in winter conditions for accident reconstruction. Technical report, SAE Technical Paper 960657, 1996.

[19] Ross Eddie. Ice, abs, & temperature. *Stapp Car Crash Journal*, 2013:04–08, 1994.

[20] Francis Navin, Michael Macnabb, and Connie Nicolletti. Vehicle traction experiments on snow and ice. Technical report, SAE Technical Paper 960652, 2014.

[21] US-Department of Transportation. *Federal Highway Administration, Road and Weather Management Program.*, 2012 (accessed June 9, 2014). http://www.ops.fhwa.dot.gov/weather/q1_roadimpact.htm.

[22] *ASTM-1805 Test Method for Single Wheel Driving Traction in a Straight Line on Snow- and Ice-Covered Surfaces*, 2000. http://dx.doi.org/10.1520/f1805-00.

[23] Anudeep Kishore Bhoopalam and Corina Sandu. Review of the state of the art in experimental studies and mathematical modeling of tire performance on ice. *Journal of Terramechanics*, 53:19–35, 2014.

[24] Yukio Nakao, Hiroaki Kawasaki, and Douglas J Major. Estimation of friction levels between tire and road. Technical report, SAE Technical Paper 2002-01-1198, 2014.

[25] Tyre Safe. *Tyre Safety Month; 2011.*, 2011 (accessed June 9, 2014). http://www.tyresafe.org/campaigns/tyre-safety-month-2011.

[26] Tire Rack. *Testing on ice: winter/snow vs. all season vs. summer tires;2008.*, 2008 (accessed June 9, 2014). http://www.tirerack.com/tires/tests/videoDisplay.jsp?ttid=116.

[27] Tire Rack. *Why Gamble With Winter Tire Selection When Four of a Kind Always Beats Two Pair?*, 2008 (accessed June 9, 2014). http://www.tirerack.com/tires/tests/testDisplay.jsp?ttid=153.

[28] Tire Rack. *All- vs. Rear-Wheel Drive on Ice*, 2008 (accessed June 9, 2014). http://www.tirerack.com/tires/tests/TireTestServlet?perfType=LTPW_1.

[29] S Shoop. Electric vehicle traction and rolling resistance in winter. *Tire Science and Technology*, 26(2):64–83, 1998.

[30] Michael J Macnabb, Randolph Baerg, Scott Sanderson, Barry Chafe, et al. Tire/ice friction values. 1996.

[31] Olle Nordström. The vti flat bed tyre test facility-a new tool for testing commercial tyre characteristics. Technical report, SAE Technical Paper 933006, 1993.

[32] S Ripka, H Lind, M Wangenheim, J Wallaschek, K Wiese, and B Wies. Investigation of friction mechanisms of siped tire tread blocks on snowy and icy surfaces. *Tire Science and Technology*, 40(1):1–24, 2012.

[33] Sally A Shoop. Vehicle bearing capacity of frozen ground over a soft substrate. *Canadian geotechnical journal*, 32(3):552–556, 1995.

[34] Deborah Diemand and James H Lever. Cold regions issues for off-road autonomous vehicles. Technical report, DTIC Document, 2004.

[35] *ASTM-1572 Test Methods for Tire Performance Testing on Snow and Ice Surfaces*, 2005. http://dx.doi.org/10.1520/f1572-99r05.

[36] S Shoop, B Young, R Alger, and J Davis. Effect of test method on winter traction measurements. *Journal of terramechanics*, 31(3):153–161, 1994.

[37] S Shoop, B Young, R Alger, and J Davis. Winter traction testing.. *Automotive Engineering*, 1994.

[38] Marion G Pottinger, James E McIntyre, Alan J Kempainen, and Wolfgang Pelz. Truck tire force and moment in cornering- braking- driving on ice, snow, and dry surfaces. Technical report, SAE Technical Paper 2000-01-3431, 2012.

[39] Anudeep K. Bhoopalam, Corina Sandu, and Saied Taheri. Experimental investigation of pneumatic tire performance on ice: Part 1 indoor study. *Journal of Terramechanics*, 60(0):43 – 54, 2015.

[40] Anudeep K. Bhoopalam, Corina Sandu, and Saied Taheri. Experimental investigation of pneumatic tire performance on ice: Part 2 outdoor study. *Journal of Terramechanics*, 60(0):55 – 62, 2015.

[41] Corina Sandu, B Taylor, J Biggans, and M Ahmadian. Building an infrastructure for indoor terramechanics studies: the development of a terramechanics rig at virginia tech. In *Proceedings of 16th ISTVS international conference, Turin, Italy*, pages 177–85, 2008.

[42] S Naranjo. Experimental investigation of the tractive performance of an instrumented off road tire on a soft soil terrain. Master's thesis, Virginia Tech, Blacksburg, 2013.

[43] Tekscan. *Sensor Model/ Map 3150*, Accessed Septemebr 2, 2014. http://www.tekscan.com/3150-pressure-sensor.

[44] *"ASTM-2493 Specification for P225/60R16 97S Radial Standard Reference Test Tire"*, 2008. http://dx.doi.org/10.1520/f2493.

[45] International society for terrain-vehicle systems standards. *Journal of Terramechanics*, 14(3):153 – 182, 1977.

[46] *"ASTM-1028 Test Method for Determining the Static Coefficient of Friction of Ceramic Tile and Other Like Surfaces by the Horizontal Dynamometer Pull-Meter Method"*, 2007. http://dx.doi.org/10.1520/c1028-07.

[47] Anudeep K Bhoopalam, Corina Sandu, and Saied Taheri. Tire traction of commercial vehicles on icy roads. *SAE International Journal of Commercial Vehicles*, 7(2014-01-2292):357–365, 2014.

[48] TB Rhyne. Development of a vertical stiffness relationship for belted radial tires. *Tire Science and Technology*, 33(3):136–155, 2005.

[49] *The Engineering ToolBox.*, Accessed June 10, 2015). http://www.engineeringtoolbox.com/ice-thermal-properties-d_576.html.